



저작자표시-비영리-변경금지 2.0 대한민국

이용자는 아래의 조건을 따르는 경우에 한하여 자유롭게

- 이 저작물을 복제, 배포, 전송, 전시, 공연 및 방송할 수 있습니다.

다음과 같은 조건을 따라야 합니다:



저작자표시. 귀하는 원저작자를 표시하여야 합니다.



비영리. 귀하는 이 저작물을 영리 목적으로 이용할 수 없습니다.



변경금지. 귀하는 이 저작물을 개작, 변형 또는 가공할 수 없습니다.

- 귀하는, 이 저작물의 재이용이나 배포의 경우, 이 저작물에 적용된 이용허락조건을 명확하게 나타내어야 합니다.
- 저작권자로부터 별도의 허가를 받으면 이러한 조건들은 적용되지 않습니다.

저작권법에 따른 이용자의 권리는 위의 내용에 의하여 영향을 받지 않습니다.

이것은 [이용허락규약\(Legal Code\)](#)을 이해하기 쉽게 요약한 것입니다.

[Disclaimer](#)

Doctor of Philosophy

**Modification of Polysaccharide through Graft
Copolymerization as Adhesion Binder for High
Capacity Anode of Lithium Ion Battery**

The Graduate School of the University of Ulsan

Department of Chemical Engineering

Bolormaa Gendensuren

**Modification of Polysaccharide through Graft
Copolymerization as Adhesion Binder for High
Capacity Anode of Lithium Ion Battery**

Supervisor Professor Eun-Suok Oh

A Dissertation

Submitted to

The Graduate School of the University of Ulsan

In partial Fulfillment of Requirements for the Degree of Doctor of Philosophy

By

Bolormaa Gendensuren

Department of Chemical Engineering and Bioengineering

December 2019

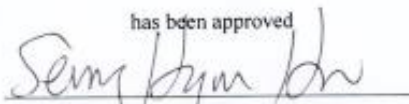
Modification of Polysaccharide through Graft Copolymerization
as Adhesion Binder for High Capacity Anode of Lithium Ion
Battery

Thesis for the degree of Doctor of Philosophy

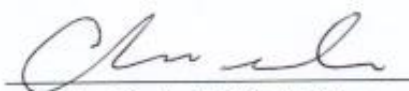
by

Bolormaa Gendensuren

has been approved



Committee Chair Prof. Seung Hyun Hur



Committee Member Prof. Jin Suk Chung



Committee Member Prof. Won Mook Choi



Committee Member Prof. Jung Kyo Lee



Committee Member Prof. Eun-Suok Oh

Department of Chemical Engineering and Bioengineering

University of Ulsan

December 2019

ABSTRACT

Silicon demonstrates a next generation anode material for lithium ion battery due to an energy storage capacitor greater than that of commercial graphitic carbon. But, Si based electrode is not still came to nearly commercial market because its high capacity could not remain stable in long-term cycles that result from suffering from repeated volume change of Si during reversible charging and discharging. To further enhance the durability of Si electrode, more researches have been attempted innovative composition and architectures polymer binders to increase storage capacities and improve stability. Polymer binders maintain adhesion between the electrode and current collector, cohesion within the electrode. In addition, the binder serves ensuring the stability of solid electrolyte layer that form on the surface of silicon, and some cases providing electronic and ionic conductivity.

To replace the organic solvent binder including polyvinylidene difluoride (PVdF), environmental-friendly water soluble polysaccharide (PS) and other polymers are considered to be a good choice of binders for Si-based anode due to their robust mechanical ability and lower electrolyte-uptake properties while compared with commercial PVDF. However, the mechanical property of PS is still several limited their applications because of its poor mechanical ability. Although, highest brittle PS might be not sustainable condition during slurry preparation with high loading of active material and thus it does not provide structural stability of electrode film. The modification of PS trough graft copolymerization and crosslinking provides tool in the hands of researchers to incorporate targeted properties in backbones for specialized application. That knowledge has already practiced a development new binder system in various batteries, as the result as the branched and single or dual crosslinked designed binder provides to better adhesion modest and structural stability of electrode film compared with pure linear polysaccharides.

In our first study, water-treated dual-crosslinked binder systems will be introduced for a high capacity silicon/graphite electrode. And so, maintaining central role play to improve mechanical properties and preserve memory initial state three common PS trough graft copolymerization and dual-crosslinking method. The PS is firstly graft copolymerized with polyacrylamide (PAAm) to product new graft copolymer of PS-*graft*-PAAm (PS-*g*-PAAm). In furthermore, PS-*g*-PAAm is crosslinked with ionic and chemical crosslinker agents to subsequently perform dual-crosslinked PS-*g*-PAAm network. In addition, both ionic and covalent crosslinkings in the binder maintain their intrinsic good binding properties and additionally enhance lithium ion diffusion. Three types of PS, sodium-alginate (Alg), sodium-carboxymethyl cellulose (CMC), and pectin (Pec), will be employed and compared for their performance as a binder material for high-capacity macroparticles silicon and graphite (Si/C) anodes. A variety of characterization tools will used to examine the electrochemical performance of the electrodes containing the dual-crosslinking binder systems. In summarize, the newly designed saccharide based polymer binder through grafting and dual-crosslinking (PS-*g*-PAAm and *c*-PS-*g*-PAAm) gives better adhesion to active

material and current collector, it is still required to enhance the ionic conductivity for high powered electrodes.

In another study, our group developed one-step process to prepare sulfonated polysaccharide backbone to provide high ionic conductivity compared to pure polysaccharide. In last chapter, we synthesis sulfonated alginate-graft-polyacrylamide (SAlg-g-PAAm) from pure alginate (Alg) by two in-situ step methods. Herein, sulfonated group propose to increase ionic conductivity and PAAm unite in graft copolymer improves an adhesion ability on poor mechanic ability of Alg. The SAlg-g-PAAm which high ionic conductivity and adhesion polymeric binder is constructed to Si/C anode of LIB, leading to highly stable electrochemical performance compared to natural Alg and non-functionalized graft copolymer.

ACKNOWLEDGEMENT

The work presented in this thesis would have been impossible for me to accomplish without the help of several people. Here I would like to thank everybody, who supported me and contributed to the presented work.

First of all I would like to thank Prof. Eun-Suok Oh, my supervisor, for giving me the great opportunity to work in his group, and guiding me into the exciting field of lithium ion batteries. Specially, I am very grateful to him for giving me the opportunity to present my work at international conferences and symposia, many fruitful discussions, ideas and comments.

I express my sincere gratitude to my old lab member Dr. Kwang-Hyan Kim and Dr. Minh Hien Thi Nguyen whose are introduced me to the scientific life during first my PhD studying year, for giving me invaluable advice and suggestions for beginning of my research work, and for the fruitful discussions. Further, I would like to thank all my co-members in Nano-Energy laboratory for being very friendly and extremely supportive, and for being always available for answering questions.

I am very grateful to my committee members, Professor Seung Hyun Hur, Professor Jin Suk Chung, Professor Won Mook Choi, and Professor Jung Kyoo Lee for all the supports for my PhD work. I am so proud that I have been their student in the past five years. It would be also impossible for me to write this thesis without their valuable help and corrections.

I am grateful to all the people from School of Chemical Engineering at the University Of Ulsan for the supply of materials and devices, and for giving the opportunity to work in their laboratory. Particularly, I would like to thank Kyong Jo Lim, who lab technician of our school, and all other members who helped me. My special thanks go to Dr. Tam Van Tran for his advice, and being always available for discussions.

I have received endless support and love from my family, my friends, and my teacher whose Prof. Battsengel Baatar during my PhD study. I would like to thank them that they were always being there to accompany and encourage me to stand up from frustration and share the happiness with me.

Finally, I would like to cordially acknowledge financial support from BK21 plus project for my PhD study. I am also very grateful to all those coordinators of BK21 plus project, for being very helpful, supportive and friendly. Furthermore, I would like to cordially acknowledge financial support and the international scientific conferences by BK21, and by other project.

Table of Contents

ABSTRACT.....	i
ACKNOWLEDGEMENT	iii
Table of Contents.....	1
Overview of dissertation	4
List of tables.....	7
List of figures.....	8
1 Background of Battery	9
1.1 History of battery timeline	9
1.2 Classification of battery	10
1.3 Present market for battery	10
2 Lithium-ion Cell Materials in Practice	12
2.1 Lithium ion batteries components and materials.....	12
2.1.1 Cathode active materials.....	13
2.1.2 Anode active materials.....	14
2.1.3 Electrodes: Conductive agent and Binders	15
2.1.4 Electrolyte Solutions.....	16
2.1.5 Porous Separator.....	16
2.2 The binder for lithium ion battery	17
2.3 Polysaccharide based graft copolymer and its cross-linked network	19
2.3.1 Polysaccharide	19
2.3.2 Graft copolymers	20
2.3.3 Polysaccharide-based copolymer hydrogel.....	21
2.4 Study object.....	22
3 Experimental Method.....	24
3.1 Fabrication of new polymeric binder	24
3.1.1 Synthesis of polyacrylamide grafted onto polysaccharide	24
3.1.2 Preparation of crosslinked binder	25
3.1.3 Preparation of sulfonated alginate backbone	26
3.1.4 Synthesis of sulfonated alginate grafted with polyacrylamide	26

3.2	Preparation of the slurry film	27
3.3	Fabrication of 2032 coin half cells	27
3.4	Physical characterization.....	27
3.4.1	Fourier transform infrared spectroscopy (FT-IR)	27
3.4.2	Thermal analysis	28
3.4.3	Electrolyte uptake	28
3.4.4	Contact angle measurement	28
3.4.5	Tensile test.....	28
3.4.6	Adhesion strength	28
3.4.7	Ionic conductivity of polymeric membrane	29
3.4.8	Morphology analysis as scanning electron microscopy.....	29
3.5	Electrochemical properties.....	29
3.5.1	Galvanostatic charge-discharge test.....	29
3.5.2	Voltammetry and Impedance analysis	29
3.5.3	Electrochemical dilatometer (ECD).....	30
4	Dual crosslinked Alginate grafted Polyacrylamide for high capacity electrode.....	31
4.1	Introduction.....	31
4.2	Result and Discussion	32
4.2.1	Confirmation of dual-crosslinking.....	32
4.2.2	Physical characterization of binder and electrode.....	34
4.2.3	Electrochemical characterization	35
4.3	Conclusion	41
5	Dual crosslinked CMC grafted Polyacrylamide for high capacity electrode	42
5.1	Introduction.....	42
5.2	Result and Discussion	43
5.2.1	Confirmation of dual-crosslinking.....	43
5.2.2	Physical characterization of binder and electrode.....	45
5.2.3	Electrochemical characterization	46
5.3	Conclusion	49
6	Dual crosslinked Pectin grafted Polyacrylamide for high capacity electrode	50
6.1	Introduction.....	50

6.2	Result and Discussion	51
6.2.1	Confirmation of dual-crosslinked binder	51
6.2.2	Physical characterization of polymer	53
6.2.3	Electrochemical characterization	55
6.3	Conclusion	57
7	Comparison study of Dual crosslinked binders	59
7.1	Introduction	59
7.2	Result and Discussion	60
7.2.1	Physical characterization of binder and electrode.....	60
7.2.2	Electrochemical characterization	62
7.3	Conclusion	64
8	Sulfonated alginate-graft-polyacrylamide	65
8.1	Introduction	65
8.2	Result and Discussion	66
8.2.1	Confirmation of sulfonated functionalized copolymer binder	66
8.2.2	Physical characterization of polymer	68
8.2.3	Electrochemical characterization	70
8.3	Conclusion	74
	Summary	75
	Reference	77
	List of Publication or Curriculum Vitae	81

Overview of dissertation

This dissertation is focused on developing a new water-soluble polymeric binder material for high-capacity silicon and graphite (Si/C) with 1/3 ratio anode in lithium ion batteries (LIBs). Herein, this dissertation is structured as follows:

Chapter 1 covers the introduction of lithium battery technology, key issues around lithium ion marketing nowadays. LIBs may start to take over some lead-acid applications if the price can be lowered and the service life prolonged. On one of responsibly to the LIB demand is driven by cell phones and tablets. Forever, we consider only the design of the LIB, especially, new architectures of polymer binders aimed at increasing storage capacities and improving stability of polymer part of lithium ion battery.

Chapter 2 describes about lithium ion cell materials and main roles that is indicated, lithium-ion electrode materials are divide into “active materials” that are capable of reversibly intercalating lithium ions into their structure, “conductive materials” that assist in electron conduction within electrode, current collecting foils, as well a binder that assure adhesion to current collector and cohesion within the active materials. Continuously, we introduce a basic information about a modification of the polysaccharide trough grafting and crosslinking progress to prepare target polymeric binder system for Si/C anode in LIBs.

Chapter 3 detail an all experimental parts including maintaining a synthesis steps of polymer, an electrode fabrication process by slurry casting, sample preparation with various methods for chemical and physical characterization tests , and a technical information for all using analysis instruments.

Chapter 4 describes the electrochemical performance improvement of high capacity Si/C composite electrode by employing new synthetic dual-crosslinked binder system. The performance of Si/C electrode is comparatively examined with four alginate based binders, namely pure alginate (Alg), ionic crosslinked Alg (*c*-Alg), alginate-*graft*-polyacrylamide (Alg-*g*-PAAm), dual-crosslinked Alg-*g*-PAAm (*c*-Alg-*g*-PAAm). The PAAm provides strong adhesion in the electrode with resistance to the penetration of the organic electrolyte. Both ionic and covalent crosslinkings in the binder maintain their intrinsic good binding properties and additionally enhance lithium ion diffusion. More interestingly, an in-situ electrochemical dilatometer study indicates that the dual-crosslinked binder is considerably helpful to prevent volume expansion beyond the inevitable value caused by active materials in electrodes during the cycle. After 100 charge and discharge, the nanoparticles Si/C electrode with *c*-Alg-*g*-PAAm retains nearly 900 mAh g⁻¹ high capacity even after one hundred cycles with excellent cyclic ability.

Chapter 5 reports the modification of commercial oldest polysaccharide binder as sodium-carboxymethyl cellulose (CMC) in the electrode to solve improvement of the slurry preparation condition and cyclic performance of high capacity anode. Herein, the modified CMC through grafting and crosslinking progress investigates as the candidate binder system for the huge volume change Si based electrode

compared with pure CMC. The modification process is followed the graft copolymerization of acrylamide monomer saccharide backbone as CMC and then a graft product as CMC-*g*-PAAm is linked by two different crosslinked agents. Besides, the modified CMC through the graft copolymer and dual-crosslinking are much effective in better preparation of electrode slurry without peel-out during drying process than the Si/C electrode with CMC. That indicated to an increase binding contact with active materials and good adhering to the current collector by the PAAm side chain on the polysaccharide backbone and cross-linker agents. As the result, Si/C electrode contained with single crosslinked *s*-CMC-*g*-PAAm are yielded 800 mAh g⁻¹ after 200 cycles while maintained high discharge capacity and high columbic efficiency compared to that electrode based on nature CMC binder.

Chapter 6 reprints that modification of pectin polysaccharide through grafting with polyacrylamide and crosslinking is newly proposed as a powerful candidate for water-soluble binder of high capacity Si anodes in lithium ion batteries. The pectin-*grafted*-polyacrylamide (Pec-*g*-PAAm) significantly enhances adhesion in electrode, a basic characteristic of binder, due to its multipoint functional groups. A strong carbonyl dipole in polyacrylamide also contributes to good electrolyte wettability of carbonate electrolyte. In present study, dual-crosslinking of the Pec-*g*-PAAm is achieved by ionic crosslinking of pectin with divalent calcium ions and chemical crosslinking of polyacrylamide with a bisacrylamide. The dual crosslinking in binder provides good contribution on integrity of electrode and ease movement of lithium ions through electrodes. Therefore, the dual-crosslinked binder shows further improvement cycling performance of the Si/C composite anode with the loading of 1.2 mg cm⁻², which remains the specific capacity of 690 mAh g⁻¹ at 100th cycles.

Chapter 7 mainly focuses the comparison study of dual-crosslinked binders for high capacity Si/C electrode. In previous three chapters, we are explained for preparation of dual-crosslinked binder systems from three different polysaccharides (PS) through grafted with polyacrylamide (PAAm) and crosslinked progress: alginate based, carboxymethyl cellulose based and pectin based. As result, these dual-crosslinked PS-*g*-PAAm (*c*-PS-*g*-PAAm) binder systems shows superior cyclic stability for Si/C electrode at high current rate compared to their parents such as pure PS and Ps-*g*-PAAm. At this current chapter, we have examined a comparison study of the dual-crosslinked *c*-PS-*g*-PAAm binders including *c*-Alg-*g*-PAAm, *c*-Pec-*g*-PAAm and *c*-CMC-*g*-PAAm. That comparison study proposes the determining of optimizing which PS dual-crosslinked binders to improve electrochemical performance of high capacity anode. Compared to highly stiffness CMC based dual-crosslinked binder, both *c*-Pec-*g*-PAAm and *c*-Alg-*g*-PAAm obtain a suitable electrolyte uptake, high ionic conductive and better mechanical ability after swollen in the electrolyte solvents for application as the binder for Si-based anode, resulting in the improvement of the cycling performance.

Chapter 8 describes a new finding whereby the ionic conductivity properties could be endowed to polysaccharide-graft-polyacrylamide (PS-*g*-PAAm) binder samples by a simple sulfonated conjunction into saccharide backbone. A new modified PS-*g*-PAAm as sulfonnic-alginate-graft-polyacrylamide

(SAIg-g-PAAm) is candidate by the high-performance binder for silicon and graphite composite anodes to increase ionic conductivity and adhesion ability, and to improve electrochemical properties compared to alginate and non-functionalized graft copolymer. While modification of Alg through sulfonated and graft copolymer, its ionic ability and high adhesion, the surface of Si/C electrodes shows a preserved porous structure and a relatively stability SEI layer appearance. Increase of sulfonated content in graft copolymer decreased multiple-cracking on the surface.

List of tables

Table 2-1 Electrochemical reaction for Li-ion cell	12
Table 2-2 The most common organic solvents in lithium ion electrolyte.....	16
Table 2-3 Various structured polymer as binder system for Si-based anode electrodes.....	18
Table 2-4 Structure of three polysaccharides.....	23
Table 5-1 Impedance parameters of Si/C anodes with CMC based binders	47
Table 7-1 Impedance parameters of Si/C anodes with various <i>c</i> -PS- <i>g</i> -PAAm binders.....	63
Table 8-1 Ingredient of graft copolymerization (g)	67
Table 8-2 Impedance parameters of Si/C anodes with various binder.....	72

List of figures

Figure 1-1 History of battery development progress	9
Figure 1-2 Design of Li-ion battery for portable devise	9
Figure 1-3 World battery marked.....	10
Figure 2-1 Schematic of a Lithium ion battery	12
Figure 2-2 Radar diagram with performance characterization of common positive electrode materials .	13
Figure 2-3 Volume exchange of insertion electrode materials in lithium cells	14
Figure 2-4 Schematic drawing of electrode components.....	15
Figure 2-5 Synthesis step of graft copolymerization between vinyl monomers and polysaccharide	21
Figure 2-6 Preparation of grafted copolymer hydrogel based on polysaccharide.....	21
Figure 2-7 Chemical structure of selecting three polysaccharides.....	23
Figure 3-1 Schematic diagram of preparation of dual-crosslinked <i>c</i> -Pec- <i>g</i> -PAAm.	24
Figure 3-2 Schematic of dissolving of hydrogel in water; and a formation of hydrogel slurry sample....	26
Figure 3-3 Electrode preparation	27
Figure 3-4 Equivalent circuit edition for impedance analysis.	30
Figure 4-1 Synthesis of (a) Alg- <i>g</i> -PAAm and (b) <i>c</i> -Alg- <i>g</i> -PAAm.....	31
Figure 4-2 Spectrometry analysis of aliginat based polymers and Si slurry	33
Figure 4-3 Adhesion and swelling ability of alginate based binders	34
Figure 4-4 Cyclic voltammograms of Si/C electrodes with alginate based binders	36
Figure 4-5 Galvanostatic charge/discharge performance of Si/C electrode with alginate based binders .	37
Figure 4-6 Change in the thickness of Si/C electrodes during discharge and charge process at 0.05C....	39
Figure 4-7 Morphology and FTIR study of cycled Si/C electrode	40
Figure 4-8 Morphology of the Si/C electrode after ECD and after 100 cycling	41
Figure 5-1 Preparation of synthetic CMC based polymer	42
Figure 5-2 Chemical structure analysis of dual crosslinked CMC- <i>g</i> -PAAm sample.....	45
Figure 5-3 Physical characterization of CMC based polymer binders.....	46
Figure 5-4 Electrochemical performance of Si/C electrode with CMC based binders	48
Figure 5-5 Si/C slurry films with pure CMC (left hand) and CMC- <i>g</i> -PAAm binders (right hand)	48
Figure 6-1 Synthesis of (a) Pectin- <i>g</i> -PAAm and (b) <i>c</i> -Pectin- <i>g</i> -PAAm.....	50
Figure 6-2 Spectrometry and thermogravimetric analysis of Pectin based polymeric binders.....	52
Figure 6-3 The effect of modifying Pec based binders for adhesion ability and swelling performance...	54
Figure 6-4 Electrochemical performance of Si/C electrode with binders.....	56
Figure 6-5 Top-viewed SEM-image of Si/C electrodes.....	57
Figure 7-1 Physical characterization of various dual crosslinked copolymers	61
Figure 7-2 CV and Nyquist plots of Si/C electrode with various <i>c</i> -Ps- <i>g</i> -PAAm binders	62
Figure 7-3 Electrochemical performance of Si/C with various <i>c</i> -Ps- <i>g</i> -PAAm binders anodes	64
Figure 8-1 Synthesis schema of sulfoanted graft copolymer	66
Figure 8-2 Spectrometer and thermal analysis of sulfonated graft copolymer	68
Figure 8-3 Mechanical and ionic conductivity properties of binder films.	69
Figure 8-4 Adhesion and sheet resistance of Si/C slurry film.	70
Figure 8-5 Voltammeter and impedance curve of Si/C electrode with various binders	71
Figure 8-6 Galvanostatic performance of Si/C electrode.....	73
Figure 8-7 Top-view SEM analysis of Si/C electrode with four binders.....	74

1 Background of Battery

Increased penetration of smart electric device and electric vehicles across the global has rapid demanded for battery worldwide, with a high density or a high power and an eco-friendly since the past few years. For instance, there is one major reason why you are able to carry around a powerful microchip in wherever. Today's battery device can satisfy most revolutionizing telecommunication and transportation, enabling the increase of smartphone an electric car.

1.1 History of battery timeline

Figure 1-1 shows batteries timeline whereas basic battery construction has remained unchanged from the earliest development battery in Baghdad that the jars contained sheets of copper rolled up with an iron rod. In general, the battery consists of a group interconnected electrochemical cells that all batteries consist of two electrodes (herein, anodes and cathode), immersed in an electrolyte and separated by a membrane. For instance, Figure 1-2 illustrates one design of lithium ion battery (LIB) used as portable device.

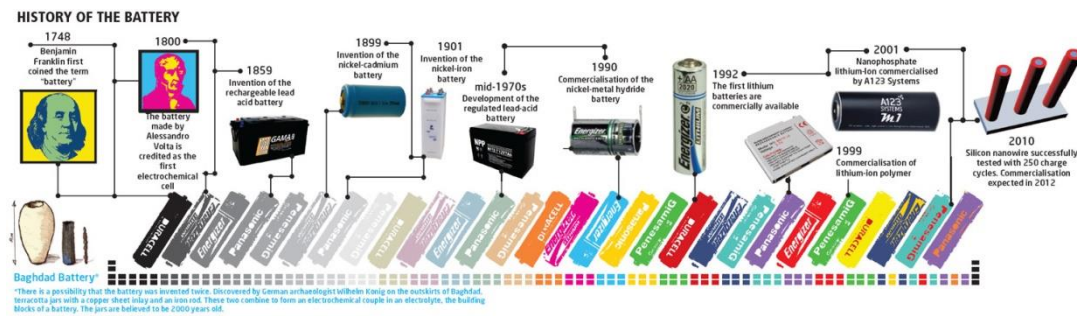


Figure 1-1 History of battery development progress

The battery is one of the most important man-made inventions all throughout history. Today, it is generally used as a portable source of power, but in the past, batteries were our only source of electricity. Without its conception, modern comforts such as computers, vehicles and communication devices may not have been possible

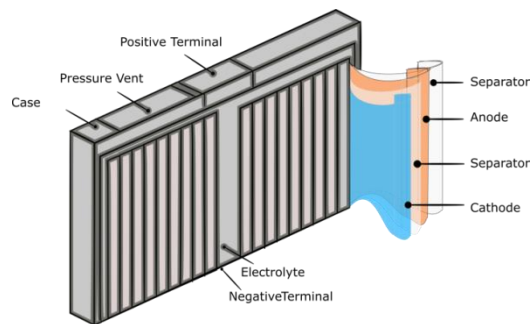


Figure 1-2 Design of Li-ion battery for portable devise

However, it is surprising that their development has progressed much more slowly that other areas of electronics. Volta discovered in 1800 that certain fluids would generate a continuous flow of electrical power when used as a conductor. This discovery led to the invention of the first voltaic cell, more commonly known as battery. After over 50 years, in 1859, the French physician Gaston Planté invented the first rechargeable battery based on lead acid, a system that is still used today. Until then, all batteries

were primary, meaning they could not be recharged. Most research activities today revolve around improving lithium-based systems, the lithium ion battery was conceived and developed in Japan by Asahi Kasei Col. and first commercialized by Sony in 1991.

1.2 Classification of battery

On the based battery developing progress, batteries are classified into two types: single-used (primary) and multiple-used (secondary) or common called by non-rechargeable and rechargeable battery. Primary batteries are designed to be used until exhausted of energy then discarded. Their chemical reactions are generally not reversible, so they cannot be recharged. When the supply of reactants in the battery is exhausted, the battery stops producing current and is useless. These batteries are used in day-today devices such as watches, electronic keys, remote, controls, toys, flashlights, beacons, and military devices in combat.

Secondary batteries can be recharged; that is, they can have their chemical reactions reversed by applying electric current to the cell. This regenerates the original chemical reactants, so they can be used, recharged, and used again multiple times. Besides powering cellular phones, laptops, digital cameras, power tools and medical devices, especially Li-ion is also used for electric vehicles and satellites. The battery has a number of benefits, most notably its high specific energy, simple charging, low maintenance and being environmentally benign.

1.3 Present market for battery

According to The Freedonia Group, a Cleveland-based industry research firm, the world demand for primary and secondary batteries is forecasted to grow by 7.7 percent annually, amounting to USA\$120 billion in nearly years. Alkaline will dominate the primary battery marked compared primary other batteries that is illustrated in Figure 1-3(a), and Frost & Sullivan predicated a 7.4 percent decline by 2015.

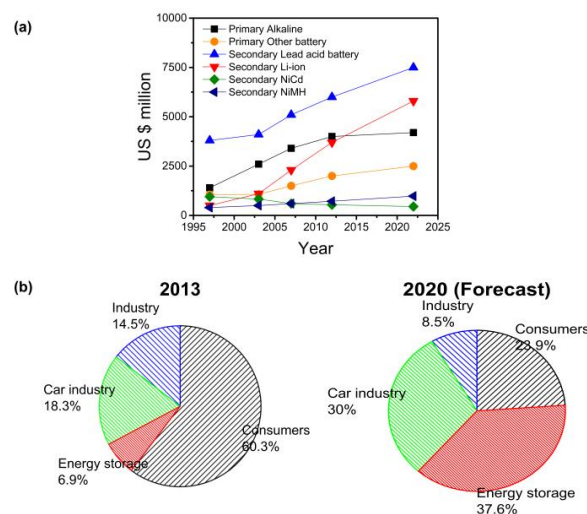


Figure 1-3 World battery market

(a) primary and secondary batteries statistic and (b) global demands for Li-ion battery

However, the analysts forecast the global primary market to grow by 4.27 percent during the period 2018-2220. The real growth lies in secondary battery and according to Frost & Sullivan secondary batteries account for 76.4 percent of the global market, a number that is expected to increase to 82.6 percent in 2015. Lead-acid was account for half the demand of rechargeable. This battery is mainly used for automotive and stand-by applications. Because of low cost and dependable service in adverse environmental conditions, lead-acid remains a steady increase through to the year 2012.

Lithium-based batteries may start to take over some lead-acid applications if the price can be lowered and the service life prolonged. On one of responsibly to the LIBs demand is driven by cell phones and tablets. Nowadays, it is estimated that lithium batteries for consumer electronic currently account for 60 percent of the world market with about 18 percent for electric car cell and less than seven percent for energy storage as show in Figure 1-3 (b). Furthermore, a global statistic for lithium ion batteries is expected to reach \$70 billion by 2020, according to experts from Frost & Sullivan, that rapidly big percent will be especially accounted for high power electric demand such smart electric grid and storage product and electric car. However, this increase of the specific application depends upon the battery configuration and consistent to improve battery performance and power density. Forever, we consider only the design of the lithium ion based battery, especially, new architectures of polymer binders aimed at increasing storage capacities and improving stability of polymer part of LIB.

2 Lithium-ion Cell Materials in Practice

In this chapter, I will discuss the background of several important concepts starting with a brief introduction of lithium ion battery cell materials including electrode composite, electrolyte and a polymer separator. Herein it is especially focused on an electrochemical inactivity polymer material of electrode manufacturing that is namely a binder. Finally, I will introduce our study objects of this thesis.

2.1 Lithium ion batteries components and materials

In response to the need for best battery, the lithium ion battery (LIB) was put on the market by Sony in 1991, owes its name to the reversible insertion (intercalation) of lithium ions between the graphite (Li_xC_6) anode and a layered-oxide ($\text{Li}_{1-x}\text{MO}_2$) cathode, respectively.¹⁻⁶ The LIB was immediately commercialized because of its high energy density, good performance, and no memory effect as occurred with other secondary batteries such as nickel-cadmium (Ni-Cd) or nickel hybrid (Ni-MH) batteries. LIBs are being used mainly to power devices ranging from consumer electronics (e.g. cell phone, and laptop) to electric car with a practical range. However, nowadays technology is still limited by each distinct battery design option, for intensity, many mobile phones cannot be used it through a day without being recharged. Appropriate selection of battery materials that are best for the application is made and systematic process of optimization of materials' performance in a battery begins.

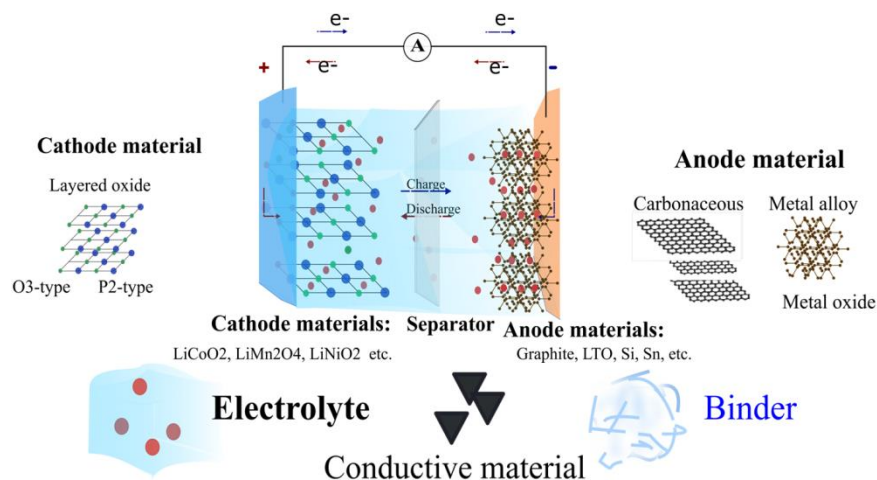


Figure 2-1 Schematic of a Lithium ion battery

The anode (graphite etc.) and the cathode (LiCoO_2 etc.) are separated by a separator with liquid electrolyte

Table 2-1 Electrochemical reaction for Li-ion cell

Site	Charge	Discharge
Cathode	$\text{LiMO}_2 \rightarrow \text{Li}_{1-x}\text{MO}_2 + x \text{Li}^+ + x e^-$	$\text{Li}_{1-x}\text{MO}_2 + x \text{Li}^+ + x e^- \rightarrow \text{LiMO}_2$
Anode	$\text{C} + y \text{Li}^+ + y e^- \rightarrow \text{Li}_y\text{C}$	$\text{Li}_y\text{C} \rightarrow \text{C} + y \text{Li}^+ + y e^-$
Overall	$\text{LiMO}_2 + x/y \text{C} \rightarrow x/y \text{Li}_y\text{C} + \text{Li}_{1-x}\text{MO}_2$	$x/y \text{Li}_y\text{C} + \text{Li}_{1-x}\text{MO}_2 \rightarrow \text{LiMO}_2 + x/y \text{C}$

LIB (Figure 2-1) are composed of a cathode and anode active materials electronically separated by a microporous polymer membrane and connected by an organic liquid electrolyte dissolving an inorganic lithium salt, in which the lithium ion reversibility inserts and extracts, therefore there major four

elements packaged in the case.² When active material in an electrode inserts lithium ions, it becomes electrochemically reduced without undergoing a substantial structural change other than the unit volume change. During discharge, lithium ion moves from the anode to cathode and the reverse occurs with lithium ion during charge. The following equations exemplify the chemistry as shown in Table 2-1.

Both negative and positive electrodes are prepared by casting slurry onto a metallic current collector foil. The slurry contains active material, conductive material, and binder in a solvent, as shown in Figure 2-1. Active materials constitute about 90 percent of dry mass of both electrodes; and conductive agents and binders are comprised balanced range. The function of conductive material is to enhance electronic conductivity of active materials and facilitates electronic transport between active material particles and toward the current collecting foil. The polymeric binder both binds all the constituents of electrode together and attaches them to the current collector.^{5,7,8}

2.1.1 Cathode active materials

Multiple cathode materials are currently used in commercial lithium-ion cells. Many of the lithium battery cathode materials have a layered structure, which enables the two-dimensional diffusion of the lithium ion or a spinel structure (Figure 2.1). Nowadays, the most current active materials are already commercialized in battery global market, for example: there are focused on mean five active materials, at first, first Li-cobalt cathode active material is commonly applied in mobile phones, tablets, laptops, cameras. Currently, its derivative Ni additive cathode is used more power device such as medical devices, industrial, electric powertrain (Tesla) due to high capacity, safety compared to Li-cobalt. The radar chart graphic (Figure 2-2) summarizes the performance of most common cathode active materials in terms of specific energy or capacity that relates to runtime; specific power or the ability to deliver high current; safety; performance at hot and cold temperatures; life span reflecting cycle life and longevity; and cost.^{1,9,10}

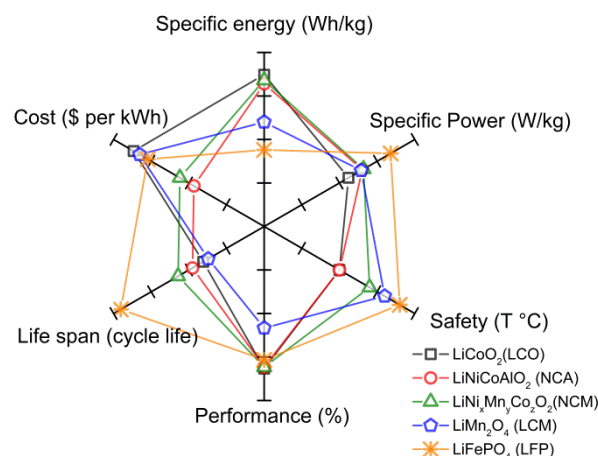


Figure 2-2 Radar diagram with performance characterization of common positive electrode materials

Herein, the Li-cobalt (LCO) electrode is extremely high specific energy but offers only moderate performance power safety and life span. The LCO is losing favor to Li-manganese (LCM) but especially

NMC and NCA due to high cost of cobalt and improved performance by blending compared with other active cathode materials. On the other hand, Li-phosphate (LFP) excels on high current rating, long cycle life, and good thermal stability but moderate specific energy and elevated self-discharge. However, researches are performed or modified on these main active materials and their derivatives and increased attention to new structure intercalation materials. During a successful cathode materials and its development, following designing criterions are often considered: (1) energy density; (2) rate capability; (3) cycling performance; (4) safety or environmentally; (5) cost. The energy density is determined by the material's reversible capacity and operating voltages, which are mostly determined by the material intrinsic chemistry such as the effective redox couples and maximum lithium concentration in active materials. For rate capability and cycling performance, electronic and ionic mobility are key determining factors though particle morphologies are also important factors due to nature of the structures.

2.1.2 Anode active materials

Since the commercialized of lithium-ion cell in end 1989 and early 1991 by Sony many kinds of anode materials have been investigated as illustrated in Figure 2-3. Theoretically, lithium metal has the highest possible specific capacity and lower voltage value of all possible anodes herein (as shown Figure 2-3(a)). In practice, the problem are the lithium dendrite which is grown into the polymer separator and electrical short circuit and relating safety hazard in Li-ion cell during repeated cycling lithium.^{2,3,5,10-12} Accordingly, most of researchers are directed toward the replacement of metallic lithium by lithium insertion compounds such as carbon, transition metal oxide, alloy to improve both cycle life and safety but at the expense of cell voltage, specific charge and rate capability. The anodic reaction usually reports reversible according to scheme shown in Figure 2-3 (b).

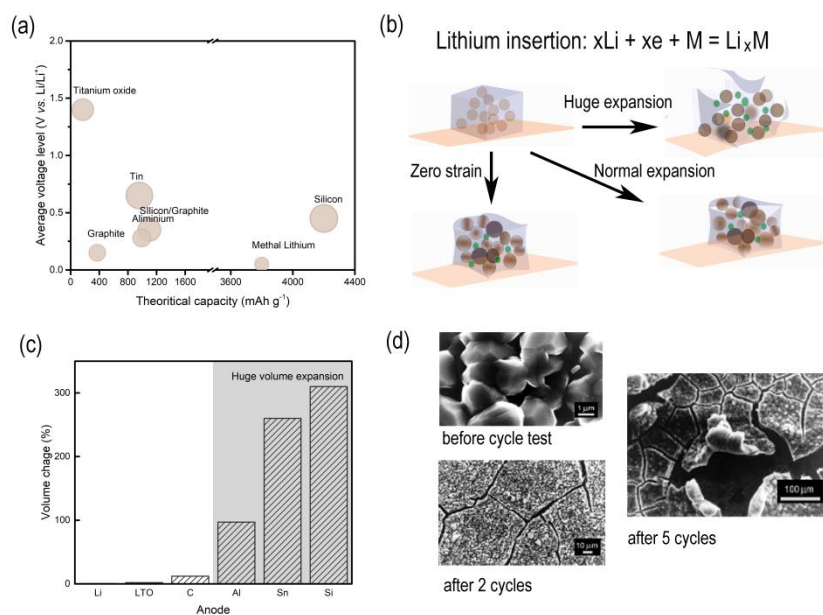


Figure 2-3 Volume exchange of insertion electrode materials in lithium cells

(a) Schematic illustration the Li ion capacity and electrochemical reduction potentials vs. Li/Li⁺ for active anode, (b) scheme of Li ion insertion and related various volume exchange, (c) comparison of volume change, and (d) SEM image of LiM before and after cycling test.^{5,13}

Thus, the reversible cycling of lithium insertion is associated with various volume expansions which occur during charge and discharge processes.^{2,3,6,14-19} Herein, various volume change of insertion anode may be practically ordered to zero strain, highly, and huge change, which is related to a molecular structure and morphology of insertion active material; due to highly ionic characterization and brittle of Li_xM that induce a rapid decay in mechanically properties and finally, pulverization of the electrode compared to lithium metal as clearly seen in Figure 2-3 (c-d). For example, the large number of lithium ion insertion/extraction results in huge volume change ($\sim 370\%$ assuming final alloy of $\text{Li}_{15}\text{Si}_4$).^{2,20-23}

A present mostly carbon typical materials are used as negative electrode of commercial researchable LIBs. Because of the higher specific charges and more negative redox potentials than most metal oxide and their directional stability, related to less volume change, are provided to better cycling capability. In general, both the theoretic specific capacity and charge density of lithium-alloy (such as $\text{Li}_{22}\text{Si}_5$ and $\text{Li}_{22}\text{Sn}_5$) are higher than those of the commonly used graphite (Li_xC_6) and titanium oxide ($\text{Li}_4\text{Ti}_5\text{O}_{12}$).²⁴ Unfortunately they cannot be still commercialized that reason is gotten huge volume expansion that of lithium graphite i.e. about 310 times for Li-Si and 260 times for Li-Sn versus 10 times of for Li-C (Figure 2-3 (c)). As the result, it is followed a disintegration of electrode with consequently failure in of the round cycles. The problem has been solved by optimizing the electrode morphology and dimensional stability with the small particle size materials, porous materials and carbon containing dispersion.^{16,24,25} While their solutions show more attractive results, the development of sustainable adhesive binder materials have turned out to be very critical in maintain the electrode structure and long-term stability cyclic performance.⁸ The importance role of binder in the electrodes of LIBs will be discussed thereafter in the next part.

2.1.3 Electrodes: Conductive agent and Binders

The both negative and positive electrode in LIBs is consisted of three main materials: an active material, conductive material, and binder with metal foil used as current collector (as shown in the Figure 2-1 and Figure 2-4).

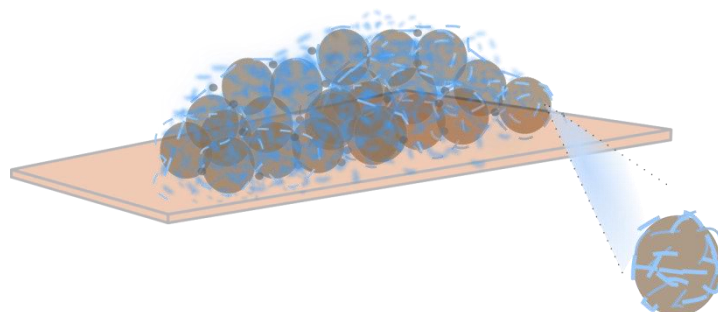


Figure 2-4 Schematic drawing of electrode components

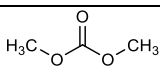
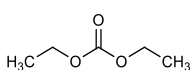
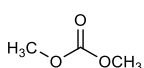
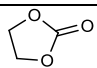
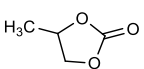
Herein, an active material is mainly employed the lithium ion source and acceptors in the electrode whereas the binder plays of holding the active materials and conductive materials together and contacting onto the current collector. The addition of conductive agents to electrode has been

demonstrated to decrease the electrical inside resistance and ensure the electric conductivity of the entire electrode while polymeric binder adhere the active materials and other additives together.⁷ In present time, most common used conductive materials are carbon black, SuperP and graphite with small particles and large specific surface area. The fluorinated polymer, most widely polyvinylidene fluoride (PVDF), is used as polymer binders in these systems due to its binding capability, good electrochemical stability, and the ability to transport ions to the active material surface. To ensure high performance of LIB cell in any application, i.e. portable devices, laptop, both binder and conductive materials can be influenced as well as the active materials. For intense, the optimized amount of conductive agent and binder can improve high retention of cell capacity at high rate by using less of all the inactive materials (i.e. conductive material and binder) without capacity fade.⁷ In this thesis we hope discussed about effective of water-based binder system for high capacity anode based cell, which the major rules and requirements of polymeric binder have widely detailed in next sub-topic soon.

2.1.4 Electrolyte Solutions

The key role of liquid electrolytes in battery system allows for ionic movement whereas lithium ion backward and forward between negative and positive electrodes while batteries charge/discharge. Most common lithium ion batteries electrolyte is based on solution of lithium salt in mixture of carbonate solvent. The organic solvents are selected together from cyclic carbonates to linear carbonates whose commonly used solvents are listed in Table 2-2. Because the combination of linear and cyclic carbonates makes available to high conductivity and solid electrolyte interface (SEI) forming ability.^{1,7,26} The SEI is act as the decomposition of liquid electrolytes on the negative electrode during first charge, thus formation of SEI impacts on the improvement cell performance such as a reversible capacity, storage life, cycle life and safety.

Table 2-2 The most common organic solvents in lithium ion electrolyte

Solvent	Structure	T _f , °C	D, g cm ⁻³	μ, D	E _{red} , V vs. Li/Li	E _{homo} , eV	E _{lumo} , eV
Linear							
Dimethyl Carbonate, DMC		18	1.063	0.59 (40 °C)	1.32	-12.85	1.88
Diethyl Carbonate, DEC		31	0.969	0.75	1.2	-12.59	1.93
Ethyl Methyl Carbonate, EMC		24	1.006	0.65	0.50-1.00	-12.71	1.91
Cyclic							
Ethylene Carbonate, EC		160	1.321	1.90 (40 °C)	1.36	-12.86	1.51
Propylene Carbonate, PC		132	1.200	2.53	1.00-1.60	-12.72	1.52

2.1.5 Porous Separator

The building block of battery cell has four major components consisting as anode, cathode electrode,

separator and electrolyte. These two electrodes isolated from each other by separator which is soaked in the liquid electrolyte. Without separator, two electrodes would come into electric conducted, thus it would occur short circuit and prevent battery from working suitably.²⁶ As increasing the demand of high capacity batteries in nowadays and unknown new technology, requirement of separator used in LIB cell must be weighed because the separator also effects on battery's safety, and cost. They should not be reacting in any electrochemical reactions. Therefore, they should be very good electronic insulator and have high capability of ionic conductive with rapidly electrolyte soaking.

2.2 The binder for lithium ion battery

Many advances have been made in traditional development of electrode composite since commercialized the lithium ion cell in 1991, binder expect. However, most attempts have been recently concerning on the creating of binder to further improvement battery performance.^{8,27} In general, the polymeric binder is utilized either to adhere electrode particles or between their particles and current collector. Even though, the binder is preferably insulator material, it can be impacted buffer volumetric changes occurring in negative insertion electrode during lithium charge/discharge, as the result increase cycle life and battery performance.^{7,26,28}

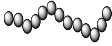
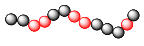
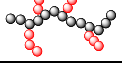
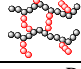

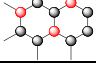
Two types of polymeric binder have been commercially used for LIB: organic based polyvinylidene fluoride (PVDF) and water-based carboxymethyl cellulose (CMC) combined with dispersed styrene butadiene rubber (SBR).²⁶ Initially PVDF is employed by glue material in preparation of anode electrodes but nowadays all size of combination binder as CMC/SBR become more popular one.²⁹⁻³¹ PVDF has more adventures using as binder but it is pre-dissolved into toxic organic solvent, most commonly n-methyl-2-pyrrolidone, and has poor binding ability through active materials (especially its negative electrode) and current collector.^{32,33} At this point, CMC/SBR binder is produced by Zeon corporation in global battery market and that technically name is BM-400B or ZEON binder.²⁵ Because of their stronger adhesion ability compared to PVDF, ZEON binders can be used in smaller quantities and enable a smaller battery or increased amount of active materials. ZEON binders have good flexibility, making it possible to produce thinner batteries. The major requirements for effective binder in lithium ion battery are summarized by following notes:

- Good cohesion and adhesion ability
- Electrochemical stability in the requirement electrochemical potential
- Undergo minimal electrolyte-swollen
- Good ionic and electronic conductivity

Herein, if the amount of binder decies in electrode slurry, it should still be a good retention of active materials and a good adhesion to current collector.^{1,26} It should not participate in any anode and cathode cell reactions. A swollen of polymeric binder within carbon electrolyte should show low rate. That led to

a balance of electrolyte-uptake and electrolyte-penetration on surface active material offers a good mechanical stability and formation possibly environment for the ion conductivity between electrolyte and all active materials. Furthermore, the binder could be functionalized by ionic or electric conductivity well; it would be influence into satisfying lithium ion transport inside electrode and minimizing the presence of inactive components (such as traditional binder/conductive material combination) within the electrode formulation. Finally, all of these requests should be able to optimize in the binder system as the result of there will favor the overall gravimetric capacity of an electrode in long-term cycles, which underlies the use of silicon within new generation LIB negative electrodes in the first place.²⁶ Recently, synthetic or bio-derived water-soluble polymers containing hydroxyl groups and carboxyl groups such as polyvinyl alcohol (PVA), polyacrylic acid (PAA),^{20,35–38} alginate³⁹ and other polysaccharides as polar functional groups, demonstrated providing binder characteristics to hold active material particles without severe disintegration of the electrode. In particular, the high-capacity anodes could not exhibited sufficiently stable cyclic performance for commercial application due to huge volume expansion during lithium insertion and extraction as shown in the Figure 2.3. Developing new polymer binders may be a critical factor to achieve Si-based electrode in the commercial application. Herein, lots of researches attractive have been proposed to different structured polymers used as efficient binders systems for Si-based electrode, which are summarized in the Table 2.3. Inside of linear structured commercial binders (etc. PVDF and SBR/CMC), the branched and cross-linked structured polymeric binder with enhanced adhesion ability have been suggested as effective ways to suppression huge volume change of Si while lithium insertion and extraction and thus maintain good electric conduction network in the electrode and without rabid capacity fade.^{40–44}

Table 2-3 Various structured polymer as binder system for Si-based anode electrodes

	Linear type		Branched type	Cross-linked		Self-healing
	Homopolymer	Copolymer	Graft	Physical	Chemical	
Polymer chemistry	Identical unite	More than two different monomers unite	Polymer with two or more chain each per molecules	polymer molecules are linked to each other at points than their ends		3D crosslinked structure based on hydrogen and dipole-dipole, pi-pi bond
						
Binders	PVDF, CMC, PVA, PAA, PAA-Na, chitosan (CS), PAN,PI	SBR, Alginate, P(AA-co-VA), PEM, PAI, PAmA, PAA-PMA, PAA-PAM, PVDF-HFP	b-cyclodextrin, Karaya gum, CMC-g-NaPAA, GC-g-LiPAA, PVDF-g-PtBu, PVDF-g-PAA	Alg-Ca, PAA-PBI (PAA), c-PAA-CMC/SBR	c-PAA-CMC, PVA-PAA, c-PAA, cPAA-BP, c-PANi, c-PAA-PCD, c-PAA:SS (soluble starch), c-CS-GA	K15S42.5M42.5
Functions	No/weak interaction between a binder and Si	Weak interaction between a binder and Si	Strong interaction between a binder and Si	Physical recover weak bond between a binder and Si	Covalent bond between a binder and Si	Recovering binder-Si or binder-binder interaction

Recently, many researchers in the battery technology field have been interested in studying polymer binders as simple and cost-effective materials. Herein, polysaccharide is most candidate material for

cost-effective and it can be easily modified through graft and cross-linking without special condition. For instance, the highly cross-linked alginate network showed superior mechanical properties and further showed strong in action.^{41,42}

On the other report, NaPAA grafted on the CMC backbone as binder showed much better cycling stability and higher columbic efficiency compared with pure CMC and Na PAA.⁴³ The author introduced that the grafting with acrylic groups led to an increase of binding bridge with Si anodic materials and the current collector foil while forming a stability SEI on the Si surface. To helpful further understanding, we need to be interested in basic of polymer chemistry around polysaccharide and its modified network.

A number of recent papers have demonstrated the importance of binder selection in high capacity anodes experiencing huge volume changes, such as silicon with superior capacity retention.

2.3 Polysaccharide based graft copolymer and its cross-linked network

Polysaccharide constitute a wide functionally important polymer and polysaccharide-based modified polymers are of great importance and widely to their advantages over the synthetic polymers such as non-toxic, biodegradable, adhesively and inexpensive. Polysaccharide has plentiful free hydroxyl and carboxyl groups distributed along the backbone, which can easily cross-linked with multivalent captions, grafted copolymerization with hydrophilic vinyl monomers, and polymer blender with other functional components.^{34,45-47} Modification of polysaccharide through graft copolymerization and crosslinking provides tool in the hands of researchers to incorporate targeted properties in backbones for specialized application. Graft copolymerization of various vinyl monomers onto different polysaccharide and formation its cross-linked network as cross-linked agents have been represented by various workers.

2.3.1 Polysaccharide

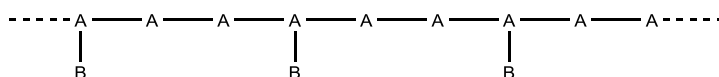
Polysaccharides are polymeric carbohydrate structures which are formed by repeating units bounded together by glycoside linkages and contained various degree of branching. Polysaccharides have a general formula $C_x(H_2O)_y$, where y is a large number that ranged of 200 and 2500. Polysaccharides are non-toxic, biodegradable, renewable, and ecofriendly materials. At global world market, there are lots commercially polysaccharide-based products that include starch, cellulose, and their derivatives, e.g. carboxymethyl cellulose, methyl cellulose, sodium alginate, pectin, xanthan gum, and hydrofluoric acid.⁴⁵ The physical and chemical properties of polysaccharide directly depended on the presence of polar functional groups, high molecular weight and relatively rigid backbone. For example, the stiff backbone makes them brittle and has high degree of crystallinity leading to insolubility in water and common organic solvent.^{45,48}

Hydroxyl groups in the natural polysaccharides are key features which provide the reactive sites for the modification and production materials with new industrial properties. Esterification, etherification, and crosslinking with various vinyl monomers and polyfunctional reagents are the common reactions

employed for the modification of polysaccharides such as carboxymethyl cellulose, chitosan, sodium alginate, and pectin etc.

2.3.2 Graft copolymers

When the repeating units are of two different monomers, a polymer is called copolymers. Herein, copolymer can be typed random, alternate block and graft copolymers that are depend on how monomers attached themselves in an ordered main chain.^{45,48} Graft copolymerization is a commonly used method for modification of surface polymer. This has a performed polymer acting as a backbone to which polymeric chains are covalently linked at several points that result formation of copolymer with branched structure. Both the backbone and side-chain polymers can be homopolymers or copolymers. The generalized structure of graft copolymer is shown below, where the monomer (B) is incorporated on the backbone of a polymer having building unit (A).



Depending on chemical structure of the side chain or monomer grafted onto polymer backbone, grafting copolymers gain new properties such as water absorption, mechanical ability, improvement elasticity, hydrophilic or hydrophobic character, heat resistance, pH sensitive, etc.

Basic principle that the synthesis of graft copolymerization is the generation of active sites, in the form of free radicals or a functional group, on the backbone.⁴⁵ Monomers is bonded onto activate sites of backbone to form graft copolymer. Creation of an active sine on the polymeric backbone is informant step for the synthesis of graft copolymer. According to the reacted monomer on the backbone, preparation of graft copolymerization can be classified to several methods that include mainly chemical, heat, radiation, enzymatic method etc. Herein, we carried out on chemical method for preparation of copolymer which involves the use of chemicals which act as initiators to generated active sites on backbone. Grafting of vinyl monomers onto polymeric backbones has been accomplished by using a range of free radical initiators and redox systems like dibenzoyl peroxide, Azobis(isobutyronitrile) (AIBN), ceric ammonium nitrate, potassium persulphate.⁴⁵ Resent, most reports have been introduced a redox initiator system of ammonium persulphate with reaction accelerator for polymerization of vinyl monomers such as acrylic-based derivative monomer onto polysaccharide in water-based medium at 50°C.^{46,49-55} Figure 2-5 shows general reaction mechanisms that various steps involves in the graft copolymerization of polysaccharide with vinyl monomers. Herein, hydroxyl groups present on the backbone and monomers are the active sites for graft polymerization to take place.

Initially, ammonium persulphate is activated by thermal condition to formation free radial as $\text{SO}_4^{\cdot-}$ which on following reacted with backbone and monomer resulting in generation of active sides. Activated monomers and backbone molecules propagate future and growths of grafting chains begin from its activation site on polysaccharide backbone.

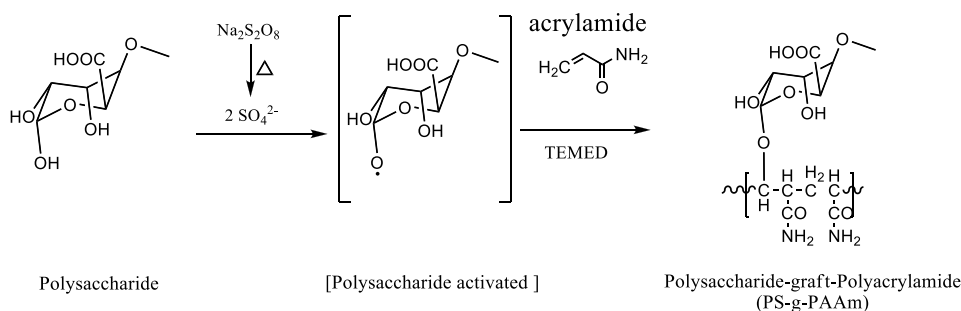


Figure 2-5 Synthesis step of graft copolymerization between vinyl monomers and polysaccharide

2.3.3 Polysaccharide-based copolymer hydrogel

Polysaccharide-based cross-linked network, as related commonly nothing as hydrogels, are eco-friendly, cost effective, biodegradable, and biocompatible in nature. In general, hydrogels are three-dimensional network systems which can adsorb large amount of solvent without showing solubility.⁴⁵ They form by various cross-linkage methods between homopolymer and copolymers which general includes chemical and physical cross-linking system. On basic of method of synthesis, hydrogel can be physical cross-linked and chemical cross-linked:

- Physical cross-linked hydrogel are reversible and unstable hydrogel in which polymer networks are joined together by secondary force like ionic, hydrogen bonding, or hydrophobic interactions. For intense, ionic interaction results by mixing of opposite charged two polymers and so this can be achieved di or trivalent counter ions. The stability of physical cross-linked polysaccharide hydrogels depends upon the external conditions. The interactions may get weak by change in environment or by application of stress.
- Chemical cross-linked hydrogel are irreversible and stable hydrogels involving chemical cross-linking between polymeric networks. Chemical cross-linking involves reaction of polymeric backbone with cross-linking agents. Polysaccharides have functional groups like hydroxyl or amine group which on reaction with cross-linking agents form gel structure. These hydrogels having strong covalent bonds can attain equilibrium swelling state which depends upon the polymer-solvent interactions and cross-link density.

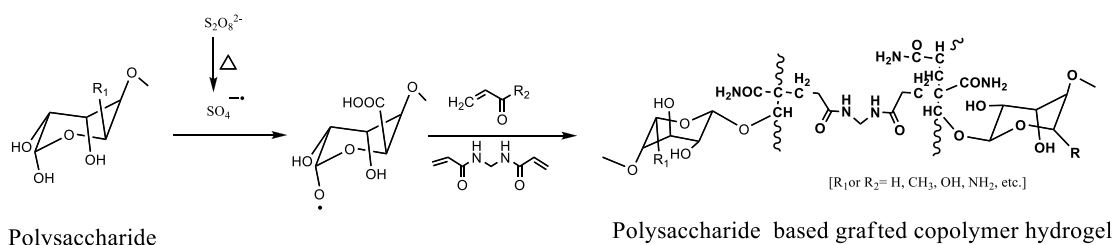


Figure 2-6 Preparation of grafted copolymer hydrogel based on polysaccharide

Furthermore, copolymerization/cross-linking free radical polymerizations are commonly utilized together to produce hydrogels by reacting hydrophilic vinyl monomers with multifunctional cross-linkers

(as shown in Figure 2-6). In particular preparation of superabsorbent, the graft copolymerization is one of the achievement methods for the synthesis of chemical cross-linked hydrogels. Grafting contains covalent linkages of a monomer onto polymeric backbone. The presence of initiators activates the –OH functional group onto polysaccharide backbone chain which leads to infinite branching and crosslinking.^{45,47,52,56–59}

2.4 Study object

As increasing power demands for various applications in the coming years, the optimization of lithium ion cell technology increases that should be characterized by high specific energy, high efficiency, long-life, and environmental sustainability and cost benefit.^{2,5} In particular, Si is demonstrated next generation anode materials for LIBs technology owing to its high theoretical specific capacity and low electrochemical potential between 0 and 0.4 V vs. Li⁺/Li. However, Si-based electrode is not still came to nearly commercial market because its high capacity could not remain stable in long-term cycles that result from suffering from repeated huge volume change of Si particles.^{5,6,17,20,24,31,60} To further enhance the durability of Si-based electrode, more researches have been attempted to inhibit huge volume expansion of electrode utilizing as various structure polymeric binder as shown in above part.

Polysaccharides (PS) are the most abundant natural functionally organic with many commercial applications, for instance, drug deliver, food packaging, high biodegradable materials, coating adhesive etc.²⁸ Recent, PS and its modified polymers are considered to be a good choice of binder for Si-based anode due to high mechanical stiff and rigid properties while compared with elastic PVDF. The oldest PS's derivatives used as commercial binder for electrode manufacture and process is carboxymethyl cellulose that consists $\beta(1\rightarrow4)$ linkages glucose, due to rapid rigid and thus high viscosity material compared to other PS (alginate, chitosan, guar gum, pectin etc.).^{20,29–31,61} However, the mechanical property of PS is still several limited their applications because its original form could not be remained stability undergo high pulverization of Si particle upon charge/discharge process. Although, highest brittle polysaccharides might be not sustainable condition during slurry preparation with high loading of active material and thus it does not provide structural stability of electrode film.²⁸ The modification of PS through graft copolymerization and crosslinking provides tool in the hands of researchers to incorporate targeted properties in backbones for specialized application. That knowledge has already practiced a development new binder system in various batteries, as the result as the branched and single cross-linked designed binder provides to better adhesion modest and structural stability of electrode film compared with pure linear polysaccharides.

In this study, demonstrating central role played to improve mechanical properties and preserve memory initial state in three common polysaccharides through graft copolymerization and dual-cross-linking method; we have studied a novel characteristic of the dual-crosslinking in the graft polymeric binder to alleviate huge volume exchange of Si-based electrode, which can be treated in water solvent. We are

selected the three most populated PS as source backbone materials for graft copolymerization component: alginate (Alg), pectin (Pec) and carboxymethyl cellulose (CMC) that consist carboxyl- and hydroxyl- functional groups and they differ solely in their monomer linkages shown as Table 2-4 and Figure 2-7.

Table 2-4 Structure of three polysaccharides

Polysaccharide	Composite		Linkage	Structure	Functional group	Viscosity
	First unit	Second unit				
Alg	D-mannuronat (M)	L-gulonate (G)	$\beta(1\rightarrow4)\alpha$	linear	-COOH	++
Pec	D-galacturonic acide		$\alpha(1\rightarrow4)$	linear	-OH	+
CMC	Glucose		$\beta(1\rightarrow4)$	linear	-CH ₂ COOH -OH	+++

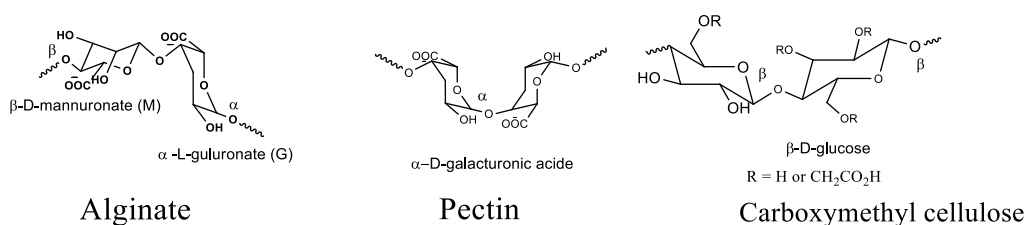


Figure 2-7 Chemical structure of selecting three polysaccharides

At first, we have grafted copolymerized between the PS backbone and acrylamide (AAm) monomers with a free radical initiator system to produced polysaccharide-*graft*-polyacrylamide (PS-*g*-PAAm) and then that graft copolymer is prepared the crosslinked network binder used as two different crosslinker agents to prepare dual-crosslinked PS-*g*-PAAm as noted by *c*-PS-*g*-PAAm. The novel characteristics of the dual-crosslinked *c*-PS-*g*-PAAm are investigated using a variety of characterization techniques and applied by high adhesion binder for silicon/graphite (Si/C) with 1/3 weight ratio electrode in LIB.

3 Experimental Method

The main experimental methods used for this work are introduced in this chapter. In particular, these include the synthesis methods for graft copolymer, preparation of dual-crosslinked network, manufacturing of electrode slurry by solvent casting method, fabrication methods for half-coin cell, as well as chemical, physical and electrochemical characterization methods, and the setup used for a galvanostatic, an electrochemical dilatometer, a voltammetry, and an impedance experiment.

3.1 Fabrication of new polymeric binder

Herein, the fundamental description of chemical reactions is introduced in first chapter and that our attention new binder system is based on combination methods of graft copolymerization/cross-linked with different two cross-linker agents through acrylamide monomer and types polysaccharides. Attention two methods such as graft copolymerization and cross-linking carried out step by step for preparation of dual cross-linked polymeric binder whereas copolymerization in water medium and then cross-linked in slurry medium as shown in Figure 3-1.

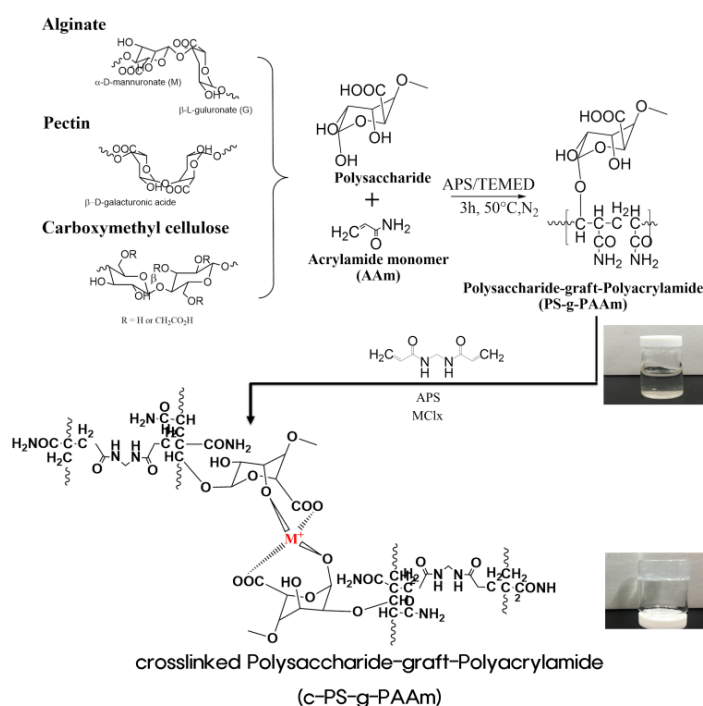


Figure 3-1 Schematic diagram of preparation of dual-crosslinked c-Pec-g-PAAm.

3.1.1 Synthesis of polyacrylamide grafted onto polysaccharide

The polysaccharide-*graft*-polyacrylamide (PS-g-PAAm) were synthesized by grafting copolymerization of acrylamide monomer onto polysaccharide backbone via a redox initiator system in an aqueous system^{58,59,62}. While constant the polysaccharide-to-acrylamide monomer ratios and calculate amount initiator system carried out in this study, how affection of three different types of polysaccharide backbone were purchased from Alfa Aesar Co. Ltd for alginate and Sigma-Aldrich for pectin, and Daicel FineChem

Ltd., Japan for CMC, respectively. Both 2.8 g of polysaccharide and 10 g of acrylamide monomer (AAM, Junsei chemical. Co, Ltd) were dissolved in 80 ml distilled water for overnight in a 250-ml three-necked flask equipped with a mechanical stirrer, a reflux condenser, a nitrogen line, and a thermometer. The solution was then heated to 50 °C in a water bath and maintained the temperature during the following polymerization. Before adding a free radical initiator, nitrogen bubbling was performed to eliminate the oxygen in the solution for one hour because oxygen easily inhibits the free radical polymerization. For the polymerization of AAM, 0.06 g of ammonium persulfate (APS) initiator was first added to the solution, followed by the addition of 0.055 g of tetramethyl-ethylenediamine (TEMED) after 30 min as a reaction accelerator. These chemicals were purchased from Sigma-Aldrich. Here the weight ratios of APS and TEMED to AAM were 0.006 and 0.0055, respectively, to produce an optimized graft copolymer. This grafted polymerization was continued for 3 h to completely produce polysaccharide grafted with polyacrylamide. The resulting viscous solution was precipitated using acetone and washed with the mixture of ethyl alcohol and water several times to remove unreacted monomers including small molecules. For instance, a synthesis schematic is driven our imagination in Figure 3-1 that is shown for the modification of pectin based polymeric binder. Here, they are noted as polysaccharide-*g*-PAAm (et. alginate-*graft*-polyacrylamide as Alg-*g*-PAAm; pectin-*graft*-polyacrylamide as Pec-*g*-PAAm; and carboxymethyl cellulose-*graft*-polyacrylamide as CMC-*g*-PAAm).

3.1.2 Preparation of crosslinked binder

Acidic polysaccharide, which relates to contain carboxylic and other groups, can be physically crosslinked by some metal ions such as calcium, aluminum, iron, and zinc ions.⁶³ Here CaCl₂ with 2 wt.% solution (Daejung Chem. Metals Co. Ltd) was used for physical crosslinking of alginate and pectin chains in Alg-*g*-PAAm and Pec-*g*-PAAm samples; and AlCl₃ was used as physical crosslinker for CMC-*g*-PAAm, respectively. For the chemical crosslinking of PAAm chains, N,N'-methylenebis(acrylamide) (MBAA, Sigma Aldrich Co. Ltd) chemical crosslinker with APS was used to three polysaccharide-*g*-PAAm samples.^{59,63} Either non-crosslinked polysaccharide and its graft copolymer with PAAm samples was dissolved in distilled water and stirred at room temperature to form 5 wt.% solution. Then some extent of metal chlorides (CaCl₂, AlCl₃) or metal chlorides and MBAA with APS was added to the non-crosslinked solutions and stirred for 30 min, leading to high viscosity hydrogels. These hydrogels were exposed to 80 °C in a convection oven for 4 h to form physical or physical-chemical crosslinking. For convenience, physically crosslinked-polysaccharide and dual (physically and chemically) crosslinked-polysaccharide-*g*-PAAm are noted such as *c*-Pec-*g*-PAAm in what follows, respectively, which are shown as Figure 3-1. The non-crosslinked and the crosslinked polymer films casted from their solution at 70 °C overnight were used for the purpose of polymer characterization.

In addition, these hydrogel dried samples were used only for determining their chemical structure and their swelling behavior over organic liquid electrodes. Due to the crosslinked, the dried polymer did not dissolve in water, but swell in water that is illustrated in Figure 3-2.

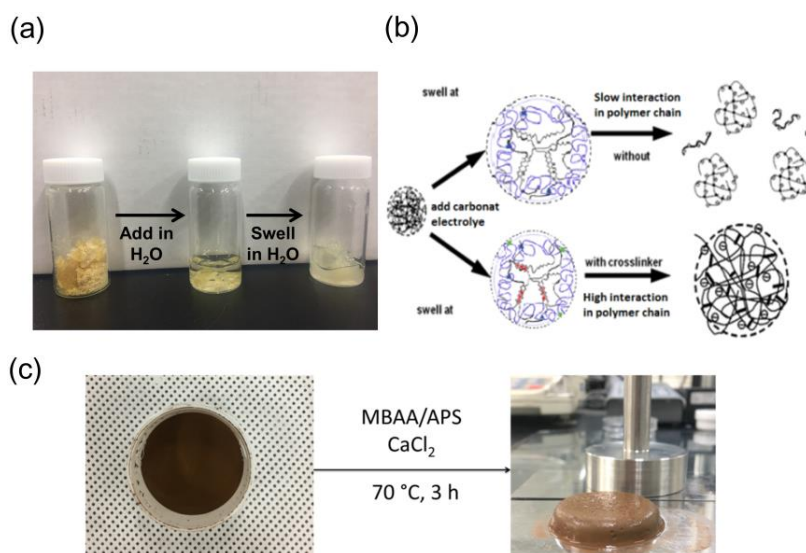


Figure 3-2 Schematic of dissolving of hydrogel in water; and a formation of hydrogel slurry sample
 (a) Photograph of dissolving progress of hydrogels, and (b) schematic of swelling process of non-crosslinked and crosslinked network; and (c) Preparation of Si slurry with the dual-crosslinked binder

Thus, the dried samples crosslinked by CaCl₂ and MBAA were not directly used as binders for slurry preparation. The crosslinking agents were added to the slurry so that the crosslinking network was achieved in the course of the drying process of electrodes. As shown in Figure 3-2(c), the slurry sample with the crosslinkers formed a gel-like phase, indicating a possibility of the formation of crosslinking that the sample is fully dried at 70 °C overnight and applied to confirm the formation of dual-crosslinked network of the binder in the presence of Si active materials.

3.1.3 Preparation of sulfonated alginate backbone

To prepare sulfonated alginate (denoted by SAlg), a certain amount of sodium alginate (Alfa Aesar Co.Ltd.) was dissolved in 100 ml of phosphate buffer solution (PBS, pH~6.0) with harsh stirring at room temperature. Some amounts of N-Ethyl-N'-(3-dimethylaminopropyl) carbodiimide hydrochloride (EDC) and N-hydroxysuccinimide (NHS) dissolved in PBS was added into the Alg-PBS solution under stirring to active the carboxylic groups in Alg. After 15 min, 3-amino-1-propanesulfonic acid (3APS) was added to the solution and trimethylamine was also added dropwise to adjust pH ~ 7.4. The reaction was kept for 9 h under continuous stirring at room temperature. The reaction products collected by suction filtration were washed with water and subsequently ethanol, and then dried in a vacuum oven at 50°C.

3.1.4 Synthesis of sulfonated alginate grafted with polyacrylamide

One-step free thermal polymerization was used to produce polyacrylamide grafted onto polysaccharide (pure Alg and sulfonated-Alg) backbones in water medium with ammonium persulfate (APS) as a radical initiator and tetramethyl-ethylenediamine (TEMED) as a reaction accelerator. All chemicals used here were purchased from Sigma-Aldrich Co. Ltd, and the total composition is listed in Table 8.1. More details on the grafting procedure were described in our previous study.⁶⁴

3.2 Preparation of the slurry film

Initially the 5 wt.% non-crosslinked binder solutions were mixed with silicon, graphite, and conducting agent (et. water-dispersed carbon nanotube for 19% and 57% in the solid of electrode slurry, respectively, whereas those of binder and alginate and pectin; and SuperP for CMC). The contents of silicon and graphite as active materials conductive materials were 15 and 9%. After added 0.5 g water into the slurry, it was stirred at 10000 rpm for 15 minutes. The resultants were coated onto copper foil, dried in a convection oven at 70 °C for 30 min, and followed by vacuum drying at 70 °C overnight. Since the crosslinked polymers did not dissolve in water, the cross-linkage proceeded in course of the slurry preparation such as mixing in water solvent and drying (as seen in Figure 3-3). For our target electrode, the same steps were conducted expect for using defined amount of two different crosslinking agents such metal chloride and MBAA with APS. Herein, the chemical cross-linker was firstly added in the slurry and slurry was stirred for nearly 10 minutes. Continuously, the physical cross-linker was added to viscosity slurry and future stirred at last 5 minutes. Subsequent drying processes made the polymer binder crosslinked while the electrodes were dried. The mass loading of electrodes was controlled to be around $1.3 \pm 0.2 \text{ mg cm}^{-2}$.

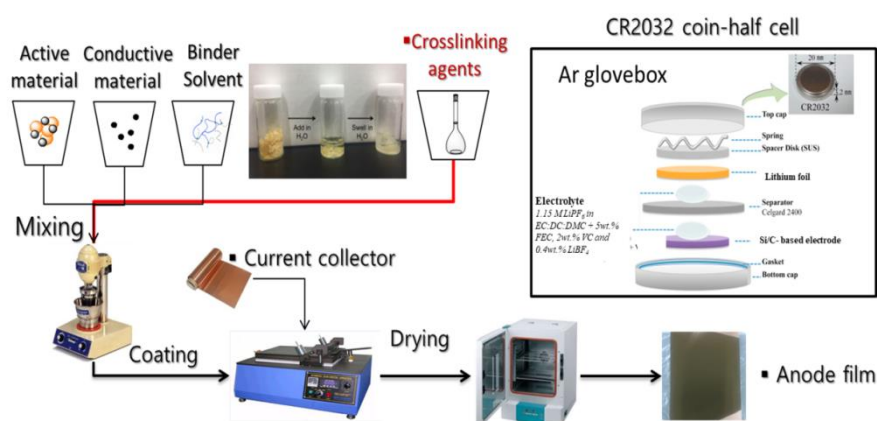


Figure 3-3 Electrode preparation

3.3 Fabrication of 2032 coin half cells

For electrochemical characterization, CR2032-type coin-half cells were assembled in an argon-filled glove-box using the Si/C working electrode, Li foils as a counter and reference electrode, in ethylene carbonate (EC): diethyl carbonate (DEC): dimethyl carbonate (DMC) 3:5:2 v/v% with additive (5wt.% FEC, 2wt.% VC and 0.4wt.% LiBF₄) as an electrolyte, and polypropylene film (Enchem Ltd.) as separator. Each coin-half cells were rested one day before getting electrochemical tests.

3.4 Physical characterization

3.4.1 Fourier transform infrared spectroscopy (FT-IR)

FT-IR spectra of dried non-crosslinked polymers and crosslinked polymers were obtained to confirm the existence of functional groups. FT-IR (Thermo Scientific Nicolet iS5 Infrared Spectrometer) was

conducted in the range of 4000–400 cm^{-1} using potassium bromide pellets.

3.4.2 Thermal analysis

The thermal analysis of pure polysaccharide and modification of polysaccharide through grafted copolymers and cross-linking polymers were carried out with thermal analyzer in nitrogen atmosphere using the Q50 in TA Instruments. The thermogravimetric analyze (TGA) was performed from initially room temperature to 600°C with a heating rate of 10 $^{\circ}\text{C min}^{-1}$. The sample was placed in platinum pan. For the differential scanning calorimeter (DSC), sample in aluminum cell is scanned from 30 to 350 $^{\circ}\text{C}$ at the heating rate of 10 $^{\circ}\text{C min}^{-1}$ compared with air reference samples.

3.4.3 Electrolyte uptake

The electrolyte uptake of the binder films were also studied through an electrolyte absorption test. The binder films were prepared by a cast solution method in the Teflon evaporation dish at 60 $^{\circ}\text{C}$ overnight and each sample was weighted. Dried binder film was initially weighted (W_{before}), immersed in the mixed solvents composed of ethylene carbonate (EC): diethylcarbonate (DEC): dimethyl carbonate (DMC): (1:1:1 by volume) at room temperature for 24 h, and weighed (W_{after}) again after the removal of excess electrolyte from their surface. The swelling ratio was calculated as:

$$s = \frac{W_{\text{after}} - W_{\text{before}}}{W_{\text{before}}} \times 100\% \quad (\text{Equation 3-1})$$

3.4.4 Contact angle measurement

The contact angles of the polymer films are measured by an optical tensiometer (Theta life, Biolin Scientific) after 60 sec exposing to an electrolyte droplet.

3.4.5 Tensile test

The elongation of binder films is carried out at room temperature by a texture analyzer (TA-PLUS, Lloyd Instruments Ltd.). For preparing test samples, grafted copolymer was first dissolved in distilled water at room temperature and 30 wt.% of glycerol to polymer as a plasticizer was added to the solution. After stirring for 15 min, the physical and the chemical agents were added to the mixture followed by 10 min stirring again. The solution was then poured into a polystyrene petri dish and dried in a convection oven at 50 $^{\circ}\text{C}$ for overnight. Subsequently the film was cut to strips (10×50 cm) and mounted between the abrasive papers. The tension speed of the film strips was 5 mm min^{-1} .

3.4.6 Adhesion strength

Using a texture analyzer (TA-PLUS, Lloyd Instruments Ltd.), the adhesion strength of Si/C anode film was obtained by measuring the 180° peel strength of electrode strips with the peel rate of 20 mm min^{-1} . The thickness of anode film is arranged about 45±5 μm and before the

peeling test; all samples were immersed in carbonate electrolyte medium for 24 hours and then released by DMC to remove surface solvent. At finally anode film is dried in room temperature for 20 minutes.

3.4.7 Ionic conductivity of polymeric membrane

The graft copolymer was dissolved into the distilled water containing with 30 wt% glycerol to polymer as a plasticizer of the copolymer solid and then the solution mixed with both crosslinker agents: with MBAA/APS and metal chloride salt. At final, the polymer membrane was prepared by solvent cast method on the Teflon Petri dish at 40°C overnight. All membranes had a thickness of about 70–110 μm. The polymeric membrane was sandwiching between two stainless steel electrodes in 2032 coin cell with or without electrolyte. A BioLogic Science Instrument (VSP 350) was used for impedance spectroscopy analysis of the membranes. Complex impedance measurements were carried out in AC mode, in the frequency range 100 kHz-10 Hz, and 10 mV amplitude of the applied AC signal. The ionic conductivity calculated by following Equation (2):

$$\sigma = \frac{L}{SR} \quad \text{(Equation 3-2)}$$

Where, σ is a proton conductivity ($S\text{ cm}^{-1}$); L is the thickness of the membrane; R is the resistance of the membrane (Ω) and S is surface area (cm^2).

3.4.8 Morphology analysis as scanning electron microscopy

After Galvanostatic charge-discharge test, the cells were disassembled in an argon-filled glove box. The electrodes were washed with anhydrous dimethyl carbonate (DMC) to remove the electrolyte residues. The morphology of surface of the silicon-graphite electrode was operated by field-emission scanning electron microscopy (FE-SEM, Jeol, JSM-6500F).

3.5 Electrochemical properties

3.5.1 Galvanostatic charge-discharge test

The electrochemical properties were conducted by the cycling performances in the voltage window of 0.005 to 1.5 V at 0.1 C for the first 2 cycles, and 0.5 C for the next 200 cycle using as the PEB0501 system (PNE solution. Co., Korea). The rate capacity test was carried out at various current rate range of 0.1C to 10C with final returning back to 0.1C current rate and each current rate is scanned 10 times at related constant current rate.

3.5.2 Voltammetry and Impedance analysis

Cyclic voltammograms (CV) of the coin-half cell can be recorded at the different scan rates within a voltage range of 0.005 to 1.5 V as a BioLogic Science Instrument. The CV performed at various scan rates (such as 0.1, 0.2, 0.5, 1.0, 1.5, 2.0, 5.0, and 10 mV s^{-1}) were preformed to determination of the Li-ion insertion into the Si/C anodes. Herein, the Randles-Sevcik equation^{65–68} describes the effect of scan

rate on peak currents to calculate the diffusion coefficient of lithium ion in an electrode:

$$I_p = 2.69 \times 10^5 A n^{3/2} C_0 D^{1/2} v^{1/2} \quad (\text{Equation 3-3})$$

Here I_p , A , n , C_0 , D , and v are the peak current, the electrode surface area, the number of electrons transferred, the concentration of reactants, the diffusion coefficient, and the scan rate, respectively.

Electrochemical impedance spectroscopy (EIS) was tested into potentiostatic mode that is fixed with AC amplitude of 10 mV and a frequency range can be scanned at the frequency range from 100 kHz to 0.01 Hz. The open circuit voltage (OCV) in EIS measurements was controlled 0.2 V vs. Li/Li⁺. In order to achieve an equilibrium state, all cells for EIS were relaxed for 2 h before measurement. Nyquist plot was fitted by the equivalent circuit as shown in Figure 3-4 where the R_s and R_{ch} is reported solution resistance and, charge transfer resistance, and W is the Warburg impedance of solid phase diffusion, respectively. In furthermore, the low frequency Warburg region of the EIS enables to calculate the diffusion coefficients of lithium ions.

$$D = 0.5 \left(\frac{RT}{AF^2 \sigma_\omega C} \right)^2 \quad (\text{Equation 3-4})$$

where A , F , C , R , and T are surface area, Faraday constant, concentration of lithium ions in solid, gas constant, and temperature, respectively^{69,70}. σ_ω is indicated the slope of real part of impedance versus $\omega^{-0.5}$ (angular frequency in the Warburg region).

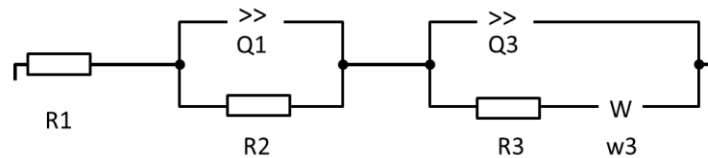


Figure 3-4 Equivalent circuit edition for impedance analysis.

3.5.3 Electrochemical dilatometer (ECD)

The change in electrode thickness during 0.05 C discharge/charge processes was traced with an in-situ electrochemical dilatometer ECD-3 (EI-Cell GmbH) in thermostat. The displacement (with an error range of about 50 nm) is recorded as a function of time with simultaneous electrochemical reactions. A stiff glass frit, which is fixed in position, is placed between the Si/C electrode as a target one and Li foil as a reference one inside. The target electrode is then sealed through a thin metal membrane, which transmits any charge-induced height change to the sensor unit on the top.

4 Dual crosslinked Alginate grafted Polyacrylamide for high capacity electrode

Here it will be focused on the electrochemical performance improvement of high capacity silicon/graphite (Si/C) composite electrode by employing new synthetic dual-crosslinked binder system. The performance of Si/C electrode is enhanced by modification of alginate through graft and crosslinking reaction as seen in Figure 4-1.

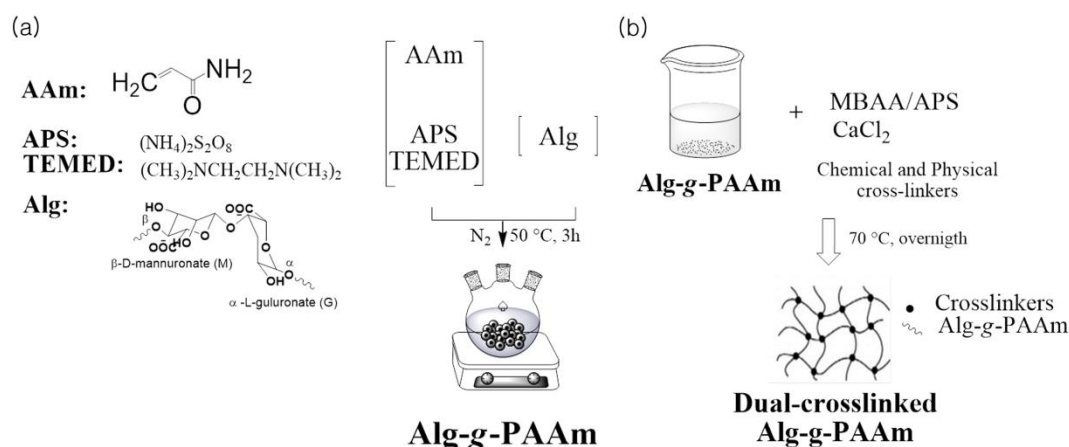


Figure 4-1 Synthesis of (a) Alg-g-PAAm and (b) c-Alg-g-PAAm
 (a) Graft copolymerization between alginate and PAAm with the terminal initiator system, (b) preparation of crosslinked network c-Alg-g-PAAm

4.1 Introduction

A synthetic or bio-derived water-soluble polymers containing carboxyl groups, such as polysaccharide (alginate, CMC, etc.) and polyacrylic acid (PAA), demonstrated promising binder characteristics for high-capacity silicon and silicon/graphite anodes, due to the high adhesion of carboxyl groups.^{8,35,40,71} Sodium alginate (SA) is recently candidate as binder application to both anode and cathode electrode in LIB. A biopolymer extracted from brown seaweeds, SA is a linear copolymer with homopolymeric blocks of (1-4)-linked β -D-mannuronate (M) and its C-5 epimer α -L-guluronate (G) residues, respectively, covalently linked together in different sequences or blocks. At firstly, Kovalenko et al.³⁹ reported that the Si anode with SA binder exhibited a stable capacity of 1700 mAh g^{-1} up to 100 cycles, which was significantly better than that with PVDF or Na-CMC binder. Liu et al.⁴¹ and Yoon et al.⁴² proposed an alginate hydrogel binder is prepared through the cross linking effect of SA with $Ca(2+)$ ion which leads to a remarkable improvement in the electrochemical performance of the Si/C anode of a Li-ion battery. In their results, the calcium-crosslinked alginate improved the mechanical properties of the binder when compared to SA and other commercial binders, and ultimately increased the capacity of the Si/C anode with a stable cycleability. Other water-soluble binders such as poly(acrylamide-co-diallyldimethylammonium chloride) (PAMAC) have been reported for graphite electrodes.⁷² PAMAC binder was shown to assist the formation of a more conductive solid electrolyte interface (SEI) and faster penetration of electrolyte in the graphite anode compared to a typical PVdF binder. Consequently, the

graphite anode with PAMAC was able to retain constant dimensions even at an elevated temperature. The polyacrylamide (PAAm) also helped to retain the original networks of the electrode in the course of charge/discharge. Tensile experiments have shown that PAAm fully recovers its original dimension after unloading.⁵⁹

In spite of these endeavors, further improvement of the electrochemical performance of electrodes is still required. In particular, high-capacity anodes have not exhibited sufficiently stable cyclic performance for commercial application. Developing new polymeric binders may be a critical factor for achieving their commercial application. Herein, we propose a significantly better method of improving the electrochemical performance of the Si-based electrode by introducing dual-crosslinked alginate with polyacrylamide. The polyacrylamide provides strong adhesion in the electrode with resistance to the penetration of the organic electrolyte. Both ionic and covalent crosslinkings in the binder maintain their intrinsic good binding properties and additionally enhance lithium ion diffusion. More interestingly, an in-situ electrochemical dilatometer study indicates that the dual-crosslinked binder is considerably helpful to prevent volume expansion beyond the inevitable value caused by active materials in electrodes during the cycle. Consequently, the Si/C (1/3) electrode retains nearly 900 mAh g⁻¹ high capacity even after one hundred cycles with excellent cyclic ability.

4.2 Result and Discussion

4.2.1 Confirmation of dual-crosslinking

Successful synthesis of Alg-g-PAAm polymers was confirmed by comparing their FT-IR spectra with pure Alg and by the physical mixing of Alg and PAAm, as shown in Figure 4-2(a). In the spectrum of the Alg network, the broad peak observed between 3500 and 3200 cm⁻¹ is assigned to O-H stretching, whereas the peaks at 1715 and 1614 cm⁻¹ are attributed to C=O in carboxylic acid and asymmetric COO-stretching, respectively.^{49,58,73} Additionally, two peaks at 1417 and 1365 cm⁻¹ for C-H in secondary alcohol are observed and another two peaks at 1092 and 1033 cm⁻¹ correspond to C-OH and C-O-C stretching, respectively. The FT-IR spectra of Alg-g-PAAm show these peaks and new peaks related to PAAm: peaks at 3420 and 3194 cm⁻¹ for N-H stretching in primary amide, peaks at 1653 and 1616 cm⁻¹ for C=O and NH₂ stretching, and a peak at 1420 cm⁻¹ for C-N stretching. Compared with pure Alg and the physically mixed samples, the Alg-g-PAAm shows a sharp FT-IR peak at 2930 cm⁻¹ attributed to the C-H stretching due to the grafting reaction.^{74,75} The peak intensity of C-O stretching in the C-OH of Alg-g-PAAm decreased compared to that of the physical mixture of Alg and PAAm, while the peak intensity of symmetric C-O in the C-O-C structure increased when the Alg is grafted with PAAm. This indicates that the hydroxyl groups of Alg react with the C-H groups of the AAm monomers, forming ester bonds between them, providing further polymerization of PAAm as a branch of the Alg backbone. This is consistent with previous studies.^{49,59}

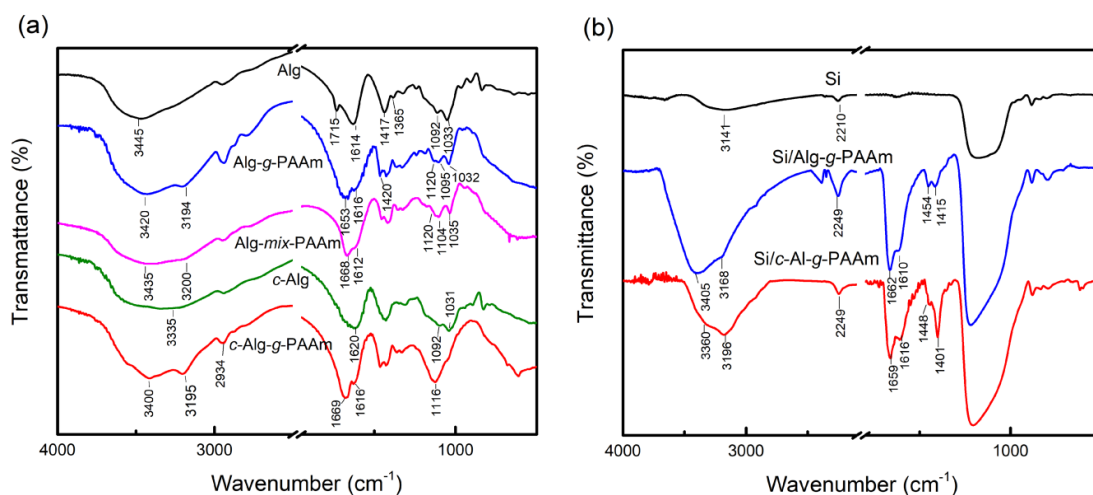


Figure 4-2 Spectrometry analysis of alginate based polymers and Si slurry
 (a) FITR spectrum of pure binder and (b) slurry of silicon and binders

Furthermore, the PAAm chains in the Alg-g-PAAm are chemically linked by MBAA and the Alg chains are then physically crosslinked through their ionic bonds with divalent cations (Ca^{2+}). The FT-IR spectra of this dual crosslinked *c*-Alg-g-PAAm are also shown in Figure 4-2(a) with a comparison of the physically crosslinked *c*-Alg. In the spectra of *c*-Alg, the width of the peaks corresponding to O-H, COO- (symmetric and asymmetric stretching), and C-O-C (asymmetric) increase and the relative intensity of O-H decreases compared to non-crosslinked Alg, indicating the existence of strong coordination bonds between the Ca^{2+} ions and functional groups of Alg.^{41,76} The doublet between 3500 and 3000 cm^{-1} in *c*-Alg-g-PAAm, which is attributed to N-H stretching, vaguely increases compared with the non-crosslinked Alg-g-PAAm sample, due to the involvement with the crosslinking reaction by MBAA.⁷⁷ In addition, the peaks assigned to the C-O stretching (at 1095 and 1032 cm^{-1}) and NH_2 stretching (at 1120 cm^{-1}) in Alg-g-PAAm were overlapped to a singlet at the 1116 cm^{-1} peak in *c*-Alg-g-PAAm due to an increase in the NH_2 stretching by the chemical crosslinker, MBAA.⁷⁴ These results imply the formation of ionically and covalently crosslinked networks within *c*-Alg-g-PAAm.

These crosslinks were also observed in the slurry samples prepared by mixing silicon active materials and binders, and subsequently drying the mixtures as illustrated in Figure 4-2(b). The FT-IR spectra of the mixed samples were compared similar to that of the pure Si particle. The pure silicon powder shows a strong Si-O-Si band at 1136 cm^{-1} and a broad Si-OH peak in the region 3400-3000 cm^{-1} . The characterization peaks of the Si-H group are observed at 2210 cm^{-1} and 883 cm^{-1} , respectively.⁷⁸ The FT-IR peaks at a range of 3000-3500 cm^{-1} were broad and increased in intensity for Si/Alg-g-PAAm and Si/*c*-Alg-g-PAAm, due to the hydroxyl and amino groups in the binder as well as the hydroxyl groups on the surface of the Si particles. In addition, while the peak intensity of OH stretching in Si/*c*-Alg-g-PAAm is less than that in Si/Alg-g-PAAm, the intensity of C-N stretching at 1401 cm^{-1} increased significantly in the Si/*c*-Alg-g-PAAm sample. These results confirm the physical and chemical crosslinkings of the grafted polymers with crosslinking agents, CaCl_2 and MBAA. Moreover, it was clearly seen that a gel-like phase was formed during the preparation of the Si/*c*-Alg-g-PAAm slurry at 70 °C (not shown here).

4.2.2 Physical characterization of binder and electrode

One of the most important properties of the binder is the adhesion ability between active materials and the current collector. Especially, Si or Sn anodes undergoing high volumetric change during the cycle require a strongly adhesive polymeric binder in order to endure the severe mechanical stress developed by lithiation/delithiation. The adhesion ability was measured by a 180° peeling test of the electrodes, after the electrodes with different binder were immersed in the electrolyte for 24 h and fully dried at room temperature.⁷⁹ As illustrated in Figure 4-3(a), the grafting of Alg with PAAm significantly increases the adhesion ability of Alg in the Si/C anodes, regardless of the existence of crosslinking. This might be due to the multipoint functional groups in the branched structure for Alg-g-PAAm, which form strong hydrogen bonds with active materials and current collector.^{37,79} In addition, both the physically-crosslinked *c*-Alg and dual-crosslinked *c*-Alg-g-PAAm binders enhance the adhesion strength slightly further when compared to non-crosslinked binders, even though the increase was not as high as expected. Sun et al.⁵⁹ and Yang et al.⁶³ reported that the hydrogel between Alg and PAAm created by crosslinking greatly increased the mechanical property. Thus, the crosslinking network may contribute to the mechanical stability of the composite in Si/C anodes, leading to an increase in adhesion.

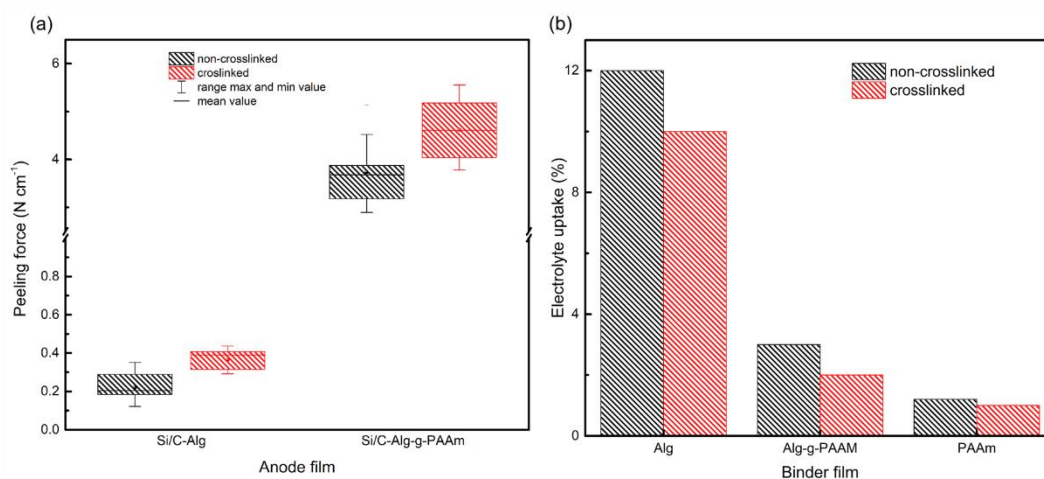


Figure 4-3 Adhesion and swelling ability of alginate based binders

(a) Adhesion strength of Si/C electrodes with different binders measured according to 180° peel strength and (b) Amount of electrolyte uptake of polymer film immersed in electrolyte solution at 25 °C for 48 h.

The adhesion capability of the binder may be affected by the amount of electrolyte uptake that can be determined using the swelling test of binder film in an excess electrolyte solution for 48 h.^{80,81} Electrolyte swelling decreases the mechanical properties of the polymer, caused by a softening binder and weakening interaction between active materials and the current collector.^{49,63} As seen in Figure 4-3(b), the electrolyte uptake of the Alg polymer film is approximately 12%, whereas the grafted Alg with PAAm (Alg-g-PAAm) shows a much lower value in the uptake with approximately 3%. This is because PAAm is very resistant to the swelling of organic electrolyte, although not resistant to water.^{75,77} In fact, the electrolyte swelling of PAAm was less than 2%, as shown in Fig. 4.2(b). When either an ionic- or dual-crosslink is formed in the Alg and Alg-g-PAAm films, the electrolyte uptake decreases further due to the decrease in free space of the polymer.³⁷ Actually, the electrolyte uptake of the *c*-Alg-g-

PAAm film is close to 2%, as shown in Figure 4-3(b). The lower electrolyte uptake of the Alg-g-PAAm and *c*-Alg-g-PAAm binders might somewhat contribute to the relatively high adhesion when compared to non-grafted and non-crosslinked Alg or ionic-crosslinked Alg, as indicated in Figure 4-3(a).

4.2.3 Electrochemical characterization

To better understand the impact of the binders on the charge-discharge processes of the Si/C electrodes, the CV of Si/C fresh electrodes with different binders was performed, with CV at 0.2 mV s⁻¹ for five cycles, and their results are shown in Figure 4-4. As expected, minimal difference was observed among the redox peak potentials of the electrodes containing different binders, because they are inactive to electrochemical reactions. Nevertheless, the potential difference between the redox peaks, $\Delta E_p = |E_{p,a} - E_{p,c}|$, was approximately 0.3 V for the Si/C with *c*-Alg-g-PAAm binder, which was the least when compared to the Si/C electrodes with Alg, Alg-g-PAAm, and *c*-Alg. Here $E_{p,a}$ and $E_{p,c}$ are the peak potentials of oxidation and reduction at the 5th cycle, respectively. In addition, the Si/C electrode with *c*-Alg-g-PAAm has a higher redox peak current than any other electrodes. This implies that the dual-crosslinked binder is favorable for reducing the polarization resistance and thus the lithium insertion/desertion processes are promoted when *c*-Alg-g-PAAm is used as a binder. Moreover, the magnitude of the peak currents of the Si/C electrode containing the dual-crosslinked binder was maintained during the five cycles, whereas the magnitude of the other electrodes, especially the electrodes containing Alg only, showed a decrease as the cycle increased. This indicates good reversibility of lithium ions insertion and desertion for Si/C when the dual-crosslinked binder is used.

The CV performed at various scan rates is preformed to determination of the Li-ion insertion into the Si/C anodes. Herein, the Randles-Sevcik equation⁶⁵⁻⁶⁸ describes the effect of scan rate on peak currents to calculate the diffusion coefficient of lithium ion in an electrode. From the slopes between I_p and $v^{1/2}$ shown in Figure 4-4(b), the diffusion coefficients of lithium ion are calculated for the four electrodes. The diffusion coefficients are 1.22×10^{-6} for *c*-Alg-g-PAAm, 4.47×10^{-7} for *c*-Alg, 3.87×10^{-7} for Alg, and 2.33×10^{-7} cm²/s for the Alg-g-PAAm-containing electrode. This also demonstrates that the dual crosslinked binder is most favorable for lithium ion insertion/desertion kinetics.

The electrochemical performance of the Si/C electrodes is shown in Figure 4-5. Compared to the Alg-containing electrodes, the Si/C electrodes containing Alg grafted with PAAm binders showed higher reversible capacities (Figure 4-5a). In particular, the dual-crosslinking of binder further improved both the reversible capacity and the Coulombic efficiency of the Si/C electrodes; 849 mAh g⁻¹ and 72.8% for the *c*-Alg-g-PAAm-containing electrode, but 807 mAh g⁻¹ and 68.9 % for the Alg-g-PAAm-containing electrode. As expected from Figure 4-3, the non-grafted and non-crosslinked Alg is not an efficient binder for the Si electrodes that undergo significant volume change, due to its severely poor adhesion ability compared with the other modified Algs. This is clearly seen from the cyclic tests of the Si/C electrodes shown in Figure 4-5(b).

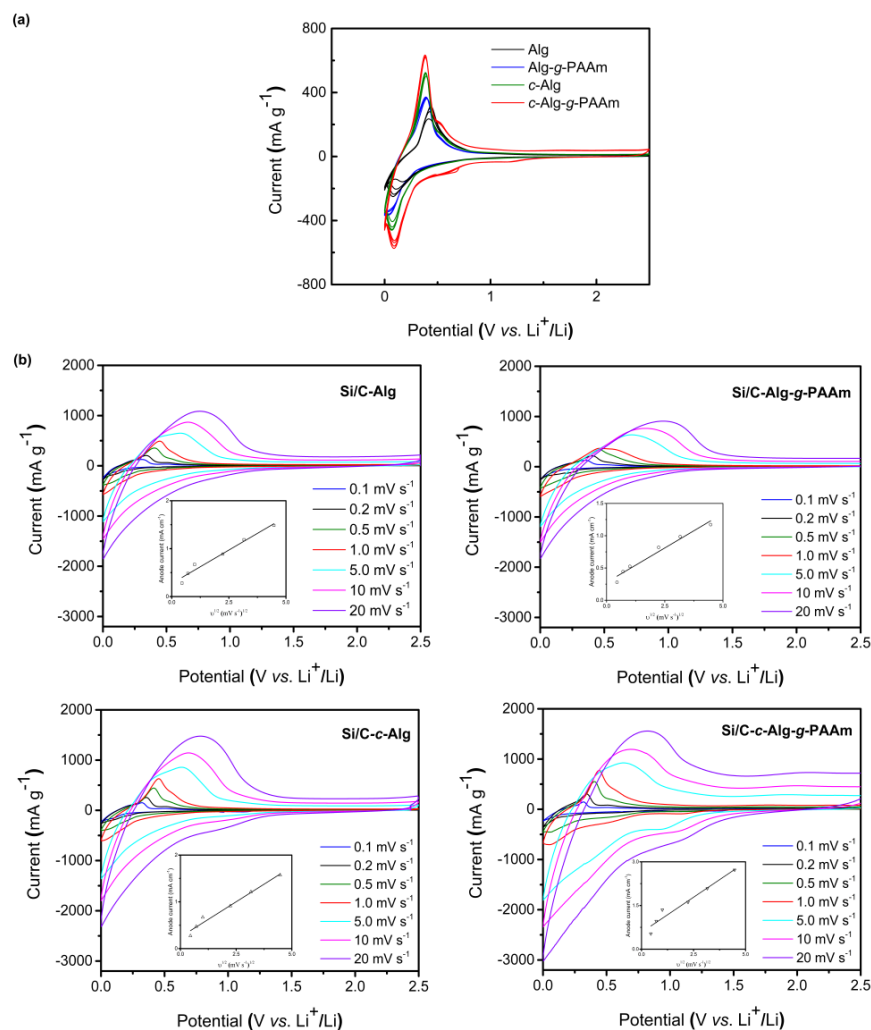


Figure 4-4 Cyclic voltammograms of Si/C electrodes with alginate based binders

(a) Cyclic voltammograms of Si/C electrodes with various binders measured at 0.2 mV s^{-1} , (b) Cyclic voltammograms with different scan rate

After over 100 cycles, the Si/C electrode containing the non-crosslinked Alg remains the specific capacity of 387 mAh g^{-1} , with approximate capacity retention of 39.4%. The cyclic performance could be improved by using *c*-Alg binder. Liu et al.⁴¹ and Yoon et al.⁴² reported that the recovering ability of physically crosslinked calcium-Alg repaired the mechanical damage occurring at the binder of Si electrodes during the charge-discharge process. However, the binder could alleviate only the initial rapid capacity of the Si/C electrode and it did not help to maintain the cyclic performance for a relatively long cycle up to one hundred cycles. Good long-term recyclability was achieved by the introduction of grafting with PAAm; i.e, by the use of Alg-g-PAAm binder. This may be attributed to a close connection between the active materials and Alg-g-PAAm because of the multipoint functional groups in the branched structure for Alg-g-PAAm. Furthermore, the dual-crosslinked *c*-Alg-g-PAAm was more effective in the cycling performance than the grafted Alg-g-PAAm as a binder for Si/C electrodes. The capacity remained at 836 mAh g^{-1} after one hundred cycles, approximately 71.6% from its initial capacity when *c*-Alg-g-PAAm was used as a binder for the Si/C electrode. This might be attributed to

the highest diffusion coefficient of lithium ions with its highest adhesion ability, as well as to the recovering ability of *c*-Alg. The chemical crosslinking in PAAm may also enhance the robustness of the network against extremely large volumetric change in the Si/C electrode. This will be discussed later through dilatometer experiments.

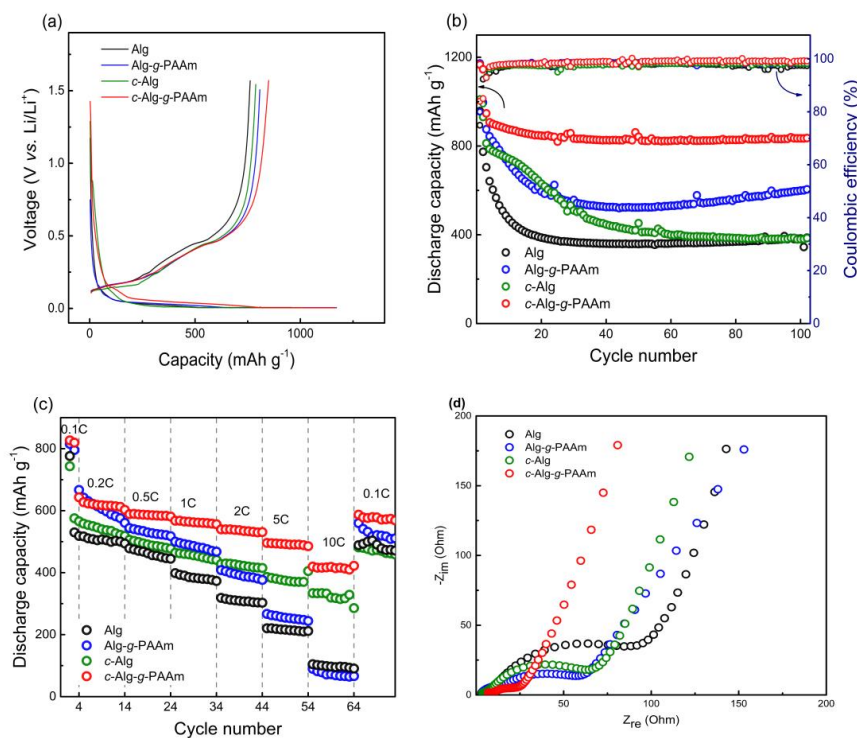


Figure 4-5 Galvanostatic charge/discharge performance of Si/C electrode with alginate based binders
 (a) Initial charge/discharge profiles, (b) cyclic performance and coulombic, and (c) rate capacity test of the Si/C electrode with four binders, (d) Nyquist plots generated for 100-cycled Si/C electrodes

Independently of the cyclic performance, the rate capability of Si/C electrodes containing different binders was tested in the range of from 0.1C to 10C with the final cycles returning to the current rate of 0.1C. The results are also shown in Figure 4-5(c). Compared to the other binders, the novel dual-crosslinked binder-based anode exhibits relatively good rate capacity. The ratios of 10 C to 0.2 C of the electrodes are 24% for Alg, 61% for *c*-Alg, 15% for Alg-g-PAAm, and 83% for *c*-Alg-g-PAAm, and their capacities at 10C are 120.9, 333.5, 90.1, and 422.4 mAh g⁻¹. Comparing these results with the restored values by means of the 0.1C current rate, the values correspond to 21.2% for Alg, 59.6% for *c*-Alg, 18.9% for Alg-g-PAAm, and 71.5% for *c*-Alg-g-PAAm, respectively. These results clearly demonstrate that the use of the dual-crosslinked binder significantly improves the cyclic performance of high-capacity electrodes that accompany very large volume change.

This directly implies the need to explain the Li-ion mobility through Si/C electrodes using the four binders. EIS analysis was performed using cycled Si/C electrodes and the result is shown in Figure 4-5d. The resulting Nyquist plot facilitates understanding of the capacity fading of the Si/C electrodes containing Alg or its modification binders. All four electrodes show two semicircles, one of which is associated with the resistance (RSEI) caused by the solid electrolyte layer at high frequencies and the

other is associated with the charge-transfer resistance (RCT) at middle frequencies.⁸² The RCT of the cycled Si/C electrodes, represented by the size of semicircles, was 84.5 $\Omega \text{ cm}^2$ for Alg, 56.1 $\Omega \text{ cm}^2$ for Alg-g-PAAm, 60.1 $\Omega \text{ cm}^2$ for *c*-Alg, and 22.3 $\Omega \text{ cm}^2$ for *c*-Alg-g-PAAm. The Si/C electrode containing Alg has the highest value, resulting in its relatively rapid capacity fade. On the contrary, the Si/C electrode with *c*-Alg-g-PAAm showed the lowest RCT among all of the anodes, demonstrating that the dual crosslinked binder forms a suitable electrode network for lithium ions and electron transfer, and interferes least with their movements. Consequently, this leads to more stable cyclic and rate performance than any other binders.

In designing the LIB cells, one of the most important factors is the amount of volume change that can be limited by users. Thus, the volumetric change should be minimized in the course of use. In this respect, the polymer binder should contribute to reducing the extrinsic volume expansion in the composite electrode with any method, although it is not possible to confine inevitable intrinsic expansion caused by active materials. Very recently, Choi et al.⁸³ showed through SEM analyses that a dual component polyrotaxane-polyacrylic acid (PR-PAA) binder greatly reduced the volumetric expansion of Si microparticle anodes when compared to a conventional linear PAA binder. In this study, the volume expansion in the Si/C electrodes during discharge and charge was traced with an in-situ electrochemical dilatometer measurement⁸⁴⁻⁸⁶ and the result is illustrated in Figure 4-6 as a relative change to initial thickness. When the potential is decreased from 3 V to 5 mV, the electrodes are lithiated, and subsequently delithiated in the range of 5 mV to 1.5 V. The constant voltage discharge at 5 mV followed by the constant current discharge with 0.05 C was maintained for a maximum of 24 h. On the contrary, the constant voltage charge at 1.5 V was maintained for 24 h at maximum after a constant current charge of 0.05 C. In the lithiation process, all electrodes exhibit a very slight increase in electrode thickness until approximately 0.2 V Figure 4-6a. However, significant increase occurs in the thickness of the Si/C electrodes when they are lithiated from 0.2 to 0.005 V and followed by a moderate increase during the remaining lithiation process. Compared to non-crosslinked binders, the crosslinked *c*-Alg and *c*-Alg-g-PAAm binders reduce the volume expansion of the Si/C electrodes. In particular, the Si/C electrode containing the dual-crosslinked *c*-Alg-g-PAAm binder expands to 97% from its original thickness, which is very close to its theoretical value of 100% calculated from theoretical values of 310% and 10% for Si and graphite, respectively. Therefore, it is very clear that the crosslinking of the binder is considerably helpful to prevent volume expansion beyond the inevitable value caused by active materials in electrodes.

Unlike lithiation, a steady decrease in electrode thickness occurs during the CC charge from 0.005 to 1.5 V with almost no decrease in CV charge. The residual volume expansion is approximately 287% for the Alg-containing Si/C electrode, 216% for the Alg-g-PAAm, 83% for the *c*-Alg, and 4% for the *c*-Alg-g-PAAm. Choi et al.⁸³ showed that the growth of SEI among pulverized Si particles led to the volume increase and were reduced by the efficient PR-PAA polymer binder.

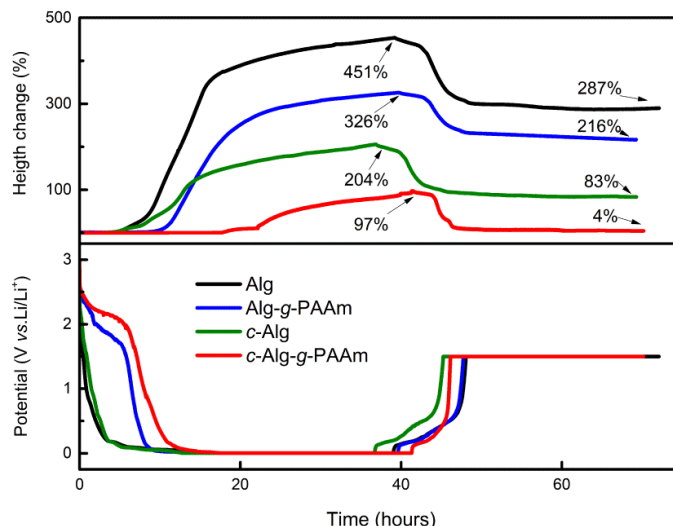


Figure 4-6 Change in the thickness of Si/C electrodes during discharge and charge process at 0.05C

From the top-viewed SEM images of 100-cycled Si/C electrodes (Figure 4-7a), it is clear that the dual-crosslinked *c*-Alg-g-PAAm binder makes the Si/C electrode less pulverized than any other binders, leading to smaller SEI growth. This is also confirmed by FT-IR analysis shown in Figure 4-7b. Compared to the fresh electrodes in Figure 4-7a, the electrodes cycled at 0.1 C in Figure 4-7b exhibited more absorption peaks appeared at 1416, 1305, and 870 cm^{-1} , corresponding to lithium ethylene dicarbonate.⁸⁷ These peaks in the Si/C-*c*-Alg-g-PAAm electrode were less grown than those in the other electrodes. This implies that the dual-crosslinked *c*-Alg-g-PAAm binder contributes to the formation of thinner SEI layer.

Connecting the in-situ electrochemical dilatometry method with the electrochemical performance in Figure 4-5, the smaller thickness change in the electrode containing dual-crosslinked *c*-Alg-g-PAAm polymer binder might be the main reason for the stable long-term cycleability and high rate-capacity retention owing to the increased adhesion sustainability in the course of use.

In Figure 4-8a, it shows optical photos taken after the dilatometer experiments. Compared the other electrodes, the dual-crosslinked *c*-Alg-g-PAAm-containing Si/C electrodes did not show obvious delamination between the electrode layer and current collector. In Figure 4-8b, the low magnification of SEM images of the Si/C electrodes before and after 100 cycles is shown. The fresh Si/C electrodes containing non-crosslinked Alg and Alg-g-PAAm binders exhibit smooth surfaces, whereas those containing the crosslinked *c*-Alg and *c*-Alg-g-PAAm binder have clumped and rough surfaces formed by the crosslinked network during the drying process.

After 100 cycles, cracks appear on all electrodes; especially, the non-crosslinked Alg- and Alg-g-PAAm-containing electrodes have severe cracks compared to the crosslinked *c*-Alg and *c*-Alg-g-PAAm-containing electrodes. On the contrary, the crosslinked electrodes lead to a decrease in the somewhat clumped surface and having shallow cracks through the recovery process. This may be attributed to the effect of self-healing of the crosslinked PAAm. Recently, considerable attention has been paid to the

addition of chemically or physically crosslinked PAAm into polysaccharide.^{51,52,59,88,89}

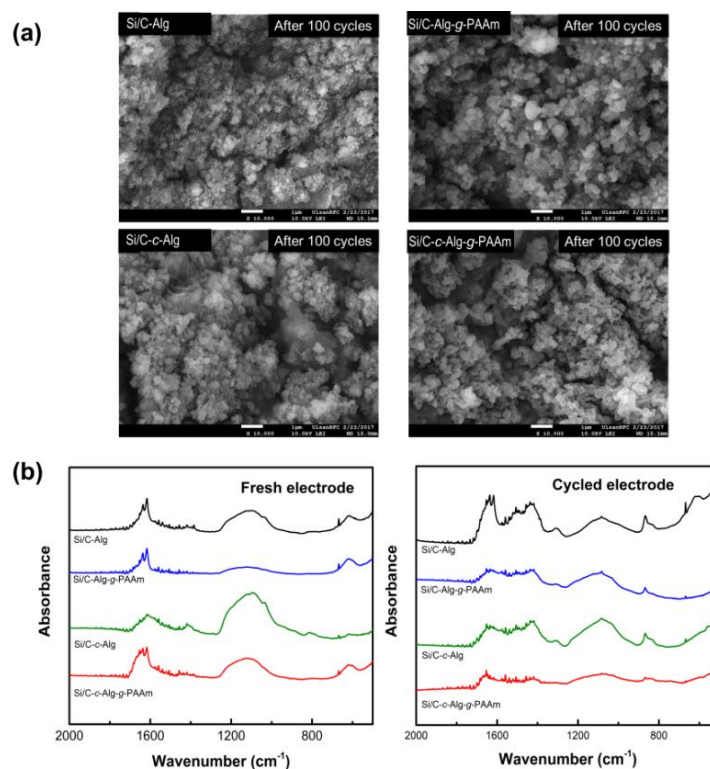


Figure 4-7 Morphology and FTIR study of cycled Si/C electrode

(a) Top-view SEM images of the cycled Si/C electrodes containing (A) Alg, (B) *c*-Alg, (C) Alg-*g*-PAAm, and (D) *c*-Alg-*g*-PAAm binder, and (b) FT-IR spectra of (a) the fresh Si/C electrodes and (b) the Si/C electrodes after the first cycle at 0.1 C.

A partial increase was observed in the mechanical properties and the self-healing efficiency of the double network hydrogels after deformation and fracture.

In the extension of their observation of our case, when lithium ions insert into and extract from Si/C, chemically crosslinked PAAm in *c*-Alg-*g*-PAAm may stabilize its original state of anode from an inevitable deformation of the electrodes, while physically crosslinked Alg contributes to its progressive recovery when any fractures occur from the deformation. Nevertheless, further study of the details of the self-healing effect of PAAm will be very valuable, though it is briefly discussed here.

In summary, the dual-crosslinked *c*-Alg-*g*-PAAm will be a very good choice for high-capacity anode materials and will greatly enhance their LIB properties.

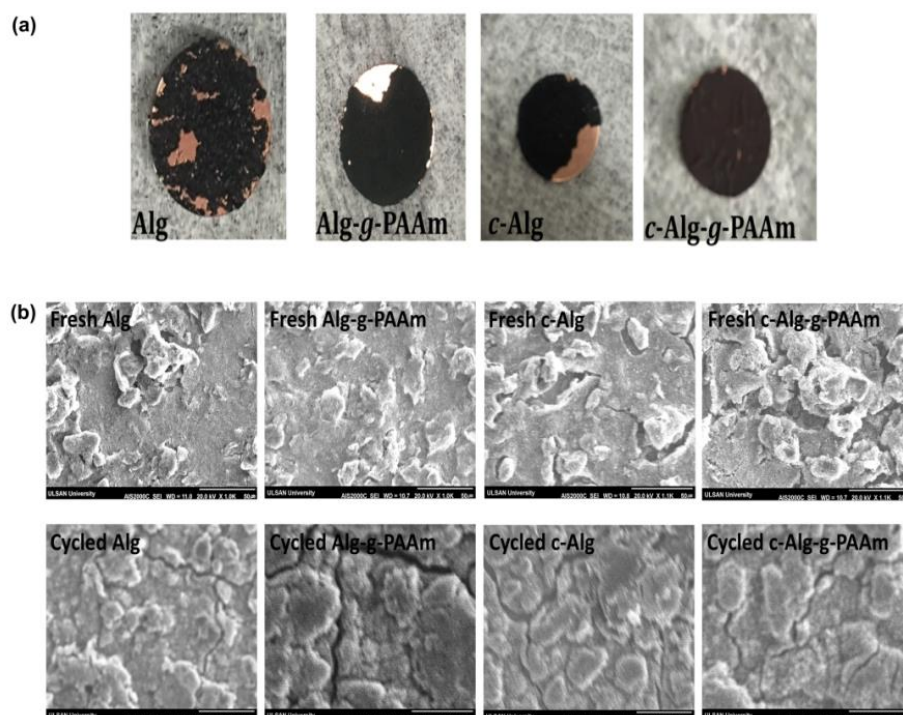


Figure 4-8 Morphology of the Si/C electrode after ECD and after 100 cycling

(a) Photos taken after the dilatometer experiments depicted in Figure 4-6, and (b) Low magnification SEM image of Si/C electrodes with Alg (a and e), Alg-g-PAAm (b and f), *c*-Alg (c and g), and *c*-Alg-g-PAAm (d and h) before and after 100 cycles, respectively.

4.3 Conclusion

We examine the modification of Alg via a graft polymerization with PAAm and subsequent chemical/physical crosslinking and investigate these effects on a highly adhesive water-based binder for Si-graphite composites. The grafting with PAAm actually contributes to the mechanical stability of the Si/C composite anodes. The dual-crosslinked polymer noted as *c*-Alg-g-PAAm is found to have lower electrolyte uptake and to improve lithium ion kinetics in the Si/C electrode, ultimately leading to good reversibility of lithium ions insertion/desertion. These properties of the newly developed binder are significantly effective for the electrochemical performance of a high-capacity anode when compared with Alg, *c*-Alg, and Alg-g-PAAm binders. Most interestingly, the in-situ electrochemical dilatometer measurement shows that the dual-crosslinked *c*-Alg-g-PAAm effectively controls the volume expansion developed during lithiation. This may be attributed to the effect of the self-healing of the crosslinked PAAm. This is very advantageous for the design of LIB cells from the commercial point of view.

5 Dual crosslinked CMC grafted Polyacrylamide for high capacity electrode

Sodium carboxymethyl cellulose (CMC) jointly used with styrene butadiene rubber (SBR) has become a standard binder formulation for graphite negative electrodes in Li-ion batteries. Including Si-alloys in the electrode formulation can increase capacity; however pure CMC and CMC/SBR based binders are not optimal for this task. Other advanced binders (e.g. PAA, Alg, polyimide, etc.) have been found to be far superior to CMC based binders Si composed electrodes are used, however such binders can be difficult to use commercially. CMC with chemically reactive groups (primary, secondary -OH and -COOH) can be easily modified by chemical reaction (Figure 5-1 a-b). In this chapter, I investigated four CMC based binders for the Si based electrode is explored.

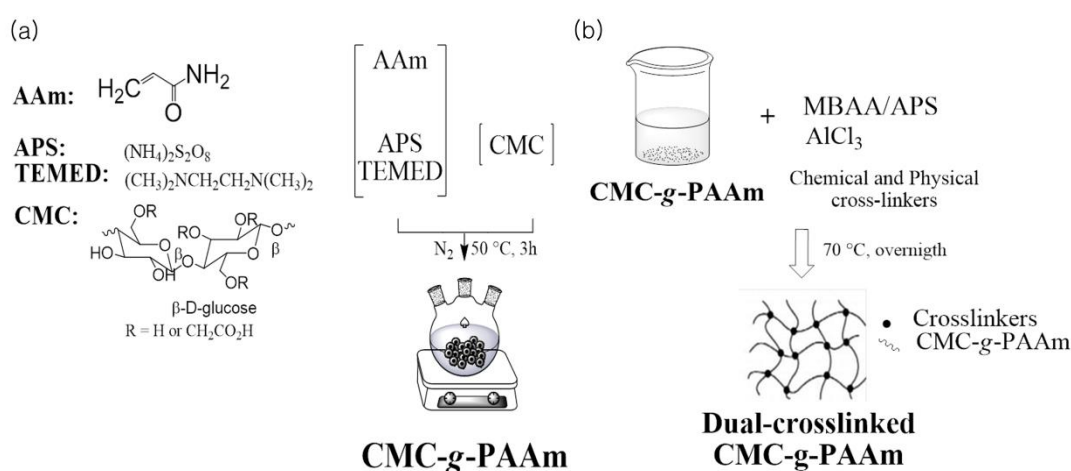


Figure 5-1 Preparation of synthetic CMC based polymer

(a) Graft copolymerization between CMC and PAAm with the terminal initiator system, (b) preparation of crosslinked network

5.1 Introduction

In an electrode manufacturing process, two types of polymeric binder have been commercially used for lithium ion battery which are organic-based polyvinylidene fluoride (PVDF) and water-based CMC combined with dispersed styrene butadiene rubber (SBR).²⁶ Initially PVDF is employed by more adventures glue material in preparation of both cathode and anode electrodes but it is pre-dissolved into toxic organic solvent, most commonly n-methyl-2-pyrrolidone, and has poor binding ability through high-capacity metal alloy negative electrodes (especially tin and silicon active materials) and current collector.^{32,33} Although, a smaller quantities of CMC based binders (such as pure CMC and composite CMC/SBR) can be stronger adhesion ability for the Si-based electrodes compared to non-functional PVDF²⁹⁻³¹ due to formation of chemical bond between carboxyl group of binder and silicon dioxide layer at silicon surface, the high-capacity metal alloy insert anode could not be completely a candidate for the commercial main components with strangely enough cyclic performance due to huge volume expansion during lithium insertion and extraction. At historically development of binder, Li et al.³¹

reported that the brittle CMC binder exhibited better suppressing function in Si based electrode which it has around 100% of volume change for the 1200 mAh g⁻¹ capacity after over one hundred cycles compared with both the SBR/CMC and PVDF. However, CMC contained electrode performance still depended on the structural parameters of CMC (molecular weight, degree of substitution, cationic), pH value of the slurry and the electrode porosity. In practice, by choosing a right drying condition for removal of water is one of most important parts of the electrode slurry preparation to enhance cycling performance of high capacity electrode. For instance, Na-CMC is dissolved in distilled water with a concentration of 5 wt.% (pH 6.7) whereas the electrode slurry contained with CMC (pH 7) is easy peeled during drying process compared with acidic slurry condition which the best pH value is between 3.1 and 4. As the result, the electrode with Na-CMC (pH 3.5) shows the best capacity retention during long-term cycles.⁹⁰

Inside of linear structured commercial CMC binders, the branched and cross-linked structured of CMC-based binder with enhanced adhesion ability have been suggested as effective ways to good condition for slurry film preparation without acidic additives, suppression huge volume change of Si while lithium insertion and extraction and thus maintain good electric conduction network in the electrode and without rapid capacity fade.⁴⁰⁻⁴⁴ Herein, the modified CMC investigates as candidate binder system for the huge volume change Si based electrode compared with pure CMC. The modification process is followed the graft copolymerization of acrylamide monomer saccharide backbone as CMC and then a graft product as CMC-g-PAAm is linked by two different crosslinked agents. Besides, the modified CMC through the graft copolymer and dual-crosslinking are much effective in better preparation of electrode slurry without peel-out during drying process than the Si/C electrode with CMC that indicated to an increase binding contact with active materials and good adhering to the current collector by the PAAm side chain on the polysaccharide backbone and cross-linker agents. As the result, Si/C electrode contained with s-CMC-g-PAAm are yielded 800 mAh g⁻¹ after 200 cycles while maintained high discharge capacity and high columbic efficiency compared to that electrode based on nature CMC binder.

5.2 Result and Discussion

5.2.1 Confirmation of dual-crosslinking

The general mechanism of grafted reaction on polysaccharide is a covalently binding between hydroxyl group on polysaccharide and vinyl group in acrylate monomers under redox initiator. Herein, ammonium peroxide is used as thermal initiator for the graft copolymerization of PAAm onto CMC chain (Figure 5-1 detailed). FTIR spectrum of pure saccharide and modified saccharide through as graft and crosslinked is shown in Figure 5-2a. The spectrum of the pure CMC observed an adsorption peaks at 3480 cm⁻¹ (OH stretching vibration), 2917 cm⁻¹ (CH₂ stretching), 1605 cm⁻¹ (C=O stretching), 1267 cm⁻¹ (OH stretching in ring alcohol), and at range of 1000 to 1170 cm⁻¹ (C-O-C in ethers and CH-OH in cyclic alcohols), respectively, there are associated to saccharide structure. After grafting reaction, the

adsorption peak of OH stretching at 1267 cm^{-1} is disappeared and other characteristic peaks at $1000\text{--}1170\text{ cm}^{-1}$ are steadily weakened and shifted to left hand that corresponds to the chemical bond of hydroxyl of CMC with vinyl group in acrylate monomers. In addition, a new two bands at 3334 and 3190 cm^{-1} (NH_2 stretching in primary amide), other new two bands at 1675 and 1610 cm^{-1} (from $\text{C}=\text{O}$ stretch and NH_2 deformation bending in amide) and new peak at 1420 cm^{-1} (C-N stretching of amide group) were appeared in Figure 5-2a which is suggested to acrylamide monomer have been successfully grafted onto CMC backbone to formation CMC-*g*-PAAm.

Continuously crosslinking reaction of graft copolymer, the intensity of COO^- antisym stretching in carboxylic acid salt at 1725 cm^{-1} and the intensity of C-N stretch in amide at 1410 cm^{-1} is significantly increased for physical crosslinked CMC-*g*-PAAm and chemical crosslinked CMC-*g*-PAAm, respectively. That is indicated to Al^{3+} ions and carboxylic group in CMC connected by coordination bond each other's to formation physical crosslinked network. Therefore, PAAm chain of grafted polymer is reacted with MBAA under radical initiator at $70\text{ }^\circ\text{C}$ and finally they covalently bonded. Furthermore, the spectrum of dual crosslinked CMC-*g*-PAAm (*d*-CMC-*g*-PAAm) is included the same intensity behavior with the single crosslinked CMC-*g*-PAAm (*s*-CMC-*g*-PAAm) as seen Figure 5-2a. As the result, we could completely prepare the dual-crosslinked grafted copolymer at related condition.

The TGA curves of CMC, pure PAAm, CMC-*g*-PAAm, and dual crosslinked binder (*d*-CMC-*g*-PAAm) samples in nitrogen medium are shown in the Figure 5-2b. In the pure CMC, the initially mass loss is observed at $68\text{ }^\circ\text{C}$ due to evaporation of water in the surface. From above $200\text{ }^\circ\text{C}$ the thermal stability is decreased and the main decomposition of polysaccharide occurs at $280\text{ }^\circ\text{C}$ with 47.1% of the weight loss. That is corresponded to the loss of functional groups from saccharide chain and then the weight loss is gradually decreased with increase in temperature. After acrylamide monomer was graft polymerization onto CMC, graft product shows three-step decomposition process at different temperature for occurring maximum degradation. The initially weight loss about 11.5% at $64\text{ }^\circ\text{C}$ is occurred by the water evaporation. At temperature range of 245 to $300\text{ }^\circ\text{C}$, there shows second weight loss about 11.2% that may be indicated to the degradation of saccharide ring and breaking of C-O-C bond of acrylic chain on the saccharide backbone. The maximum decomposition of polymer backbone has appeared at $365\text{ }^\circ\text{C}$ and the weight loss is about 51.0% . Compared non-grafted CMC, different degradation behavior of CMC-*g*-PAAm can be explained by presences of acrylic polymer on the surface of CMC. In addition, the thermal degradation of pure PAAm has three-step at different temperature range compared with the graft copolymer. In addition, thermal-degrade steps of dual-crosslinked samples are immediately characterized with graft copolymer but the degradation temperature of its side and branched chain in *d*-CMC-*g*-PAAm was found to decrease compared to grafted copolymer because it may be depended from low weight of crosslinker agents but dual crosslinked polymer has a high yield with 28% at $800\text{ }^\circ\text{C}$ compared with graft copolymer. From TGA result we can also show that PAAm is successfully grafted on surface of CMC and then graft copolymer is completely linked as two different agents.

DSC of all CMC based modified samples displayed in Figure 5-2c, herein, at around 100 °C for all samples shown the deposition of moisture. DSC of pure CMC show one endothermic peak at 158 °C which is related to the functional group of CMC is lost and one exothermic peak at 290 °C due to the crystallization in the structural chain and then it began to the decomposition of saccharide chain at high temperature then 290 °C. The synthetic PAAm illustrated three endothermic peaks on the DSC profile. First two degradations at 156 and 231 °C are attributed to be changed of amino group in PAAm by imide. Finally it is melted at around 296 °C and then it is degraded of the imine group and the main chains together. The graft copolymer of CMC-g-PAAm was similarly decomposed at 175 °C with pure CMC but the another endothermic peaks returned the two stages of PAAm degradation were displayed to high temperature of 261 and 345 °C.

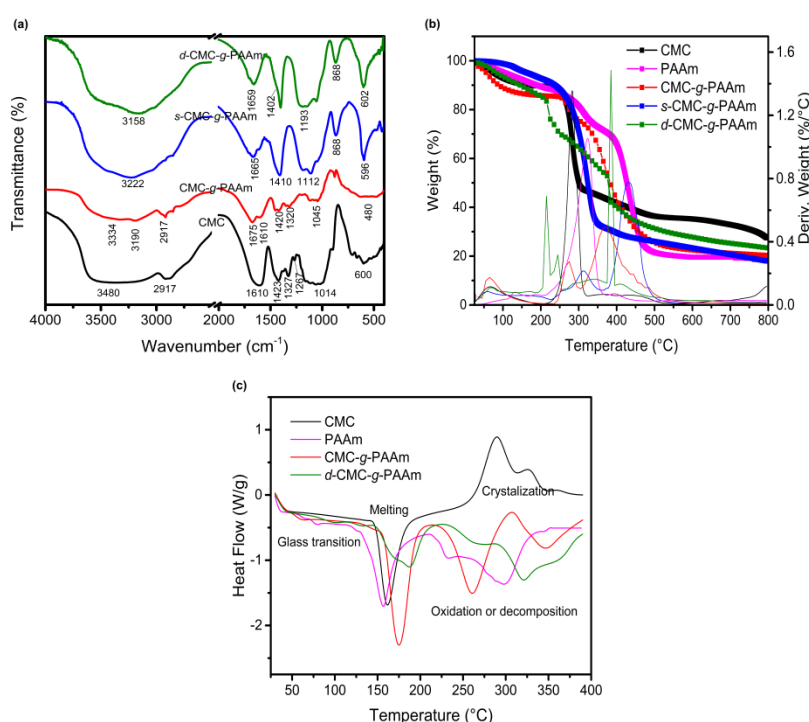


Figure 5-2 Chemical structure analysis of dual crosslinked CMC-g-PAAm sample

(a) FT-IR spectra; (b) Thermal gravimetric analysis and (c) Differential scanning calorimetry analysis of pure CMC, CMC grafted with PAAm (CMC-g-PAAm), and dual-crosslinked *c*-CMC-g-PAAm polymers

After dual-crosslinking converting of graft sample, there are also three endothermic peaks at little high temperature range, due to high energy is expended for breaking crosslinking structure. At finally, TGA and DSC results have suggested to synthesis of graft copolymer and formation of dual crosslinked polymer.

5.2.2 Physical characterization of binder and electrode

Electrolyte uptake test of the synthetic polymer films was based on swelling process of the polymer film in medium of carbonate electrolytes. After modified grafting reaction of CMC, the graft copolymer sample shows about 4.3 % of electrolyte uptake that is almost lower swelling ability compared to 13.7 % for non-modified CMC as seen Figure 5-3a. This reason described to PAAm is non-sensitive in most of

organic solvents, expect water but it shows high wettability of electrolyte as explaining in chapter 4. Assuming decrease free volume of polymeric binder as crosslinking, the electrolyte uptake value is still decreased to 1.98 for *s*-CMC-*g*-PAAm and 0.75 % for *d*-CMC-*g*-PAAm, respectively. As the result, the much lower swelling ability of the carbonate electrolyte into binder might be slightly decreased the ionic exchange of lithium ion through Si/C electrodes but it remains stable of highly adhesion ability during electrochemical reactions in long-term.

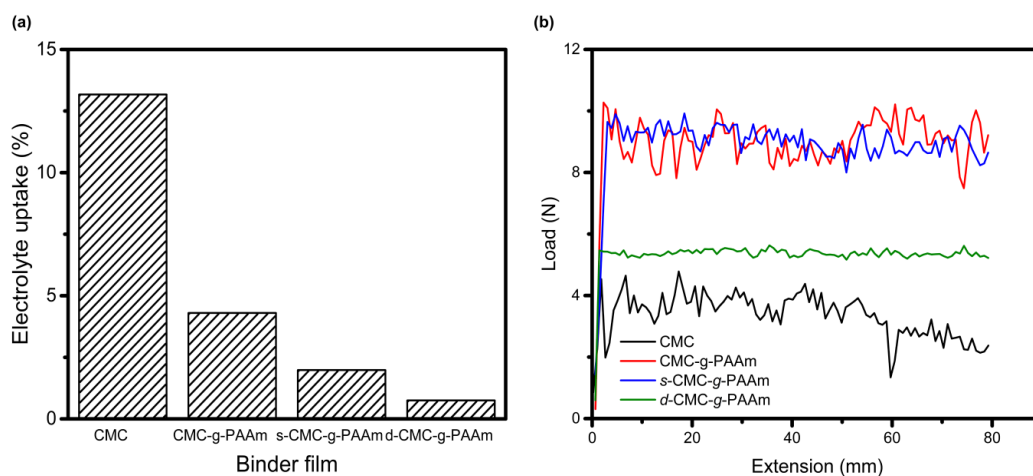


Figure 5-3 Physical characterization of CMC based polymer binders
 (a) Electrolyte uptake of pure polymeric binder and (b) Adhere ability of Si/C anode with four investigation polymers

Figure 5-3b shows the adhesion force correlated to different binder in Si/C slurry films that was carried out the 180° peel strength of electrode strips with the peel rate of 20 mm min⁻¹. After grafting reaction onto CMC backbone, the adhesion force of the Si/C electrode with CMC-*g*-PAAm can be significantly improved from around 4 N to 10 N. Because Si/C-CMC electrode have low adhere compared to same anode with modified CMC such as CMC-*g*-PAAm and its crosslinked binders. To effect of crosslinking on adhere for Si/C, *s*-CMC-*g*-PAAm show similar fluctuation line with non-crosslinked graft copolymer of CMC-*g*-PAAm on the load *vs.* extension, but the adhesion value is slightly higher than around 10.5 N. We are prepared dual-crosslinked binder using by chemical crosslinker as MBAA/APS and physical crosslinker as AlCl₃, however the adhesion force between active materials and current collector is steadily decreased to 6 N. It might be connected to formation of 3 D network anode film and softness by physical crosslinker. In addition, it might be connected to Cu foil surface may be oxidized during dual crosslinking reaction. That is indicated that the surface color become slightly drack compared with other anode film after peeling.

5.2.3 Electrochemical characterization

The impedance was conducted to explain lithium ion storage properties through Si/C electrode with four different binders as seen in Figure 5-4. The half-coin cells were recorded for two precycling at 0.1 C, and then continued at 0.5 C for 2 cycles in the voltage of 0.2 V. All investigation Si/C electrodes with four binders are illustrated two semicircles on Nyquist plots, which are related to the resistance for solid

electrochemical interface layer (R_s) at high frequency and the resistance for charge-transfer reaction (R_{ct}) whereas R_{ct} displayed by the size of semicircle at medium frequency range. The low frequency range of the straight line is mentioned the Warburg impedance of Li diffusions into bulk of the electrode materials. Compared to the charge-transfer conductance ($1/R_{ct}$) of Si-based composite electrode with pure CMC, the modified all CMC-based binders show an increase value of $1/R_{ct}$ in Table 5-1 which is indicated to enhance transferred Li-ion movement through electrode. This may be caused by enhanced wettability and critical adhesion compared to CMC.

In furthermore, diffusion coefficient calculated from the plot of the real impedance (Z_{re}) and the square roots of the lower angular frequency (σ_w) that is mainly accorded to the equation 3-2 in chapter 3 and that slopes illustrated the inside of Figure 5-4(a-b) and Table 5-1 after precycling and 2th cycles, respectively. Figure 5-4b, the diffusion coefficients were $0.38 \times 10^{-11} \text{ cm}^2 \text{ s}^{-1}$ for CMC, $2.65 \times 10^{-11} \text{ cm}^2 \text{ s}^{-1}$ for CMC-g-PAAm, $2.36 \times 10^{-11} \text{ cm}^2 \text{ s}^{-1}$ for *s*-CMC-g-PAAm, and $3.95 \times 10^{-11} \text{ cm}^2 \text{ s}^{-1}$ for *d*-CMC-g-PAAm electrodes, respectively. In summary, modification CMC through graft and crosslinking is effectively influence on easy lithium charge transfer kinetics into the electrode while it is compared to pure CMC binders.

The half-coin cells were scanned for two precycling at 0.1 C, and then continued at 0.5 C for 200 cycles in the voltage range of 0.01 to 1.5 V. The loading of electrode is maintained 1.0 g cm^{-1} for all Si/C composite anodes. The Si/C composite anode with CMC showed the initial charge capacity of 1271 mA g^{-1} at 0.5 C and the strange capacity degradation above 50 cycles compared to same electrode containing with graft copolymer.

At finally, capacity retention of first discharge capacity at 0.5 C obtained 46.8 % for the Si/C anode with pure CMC binder after 200th cycle. Herein, 62.0 % of the capacity retention in first discharge capacity at 0.5 C can retain for the CMC-g-PAAm binder which is better stability (low fading) than unmodified CMC binder with 48.2 % of the capacity retention. That is indicated to adhere between Si/C composite particles and current collector is improved as using the graft copolymer binders and followed to maintain a good stability during long cycle life.

Table 5-1 Impedance parameters of Si/C anodes with CMC based binders

Investigation samples	Cycle number	R_s	R_{ch}	$1/R_{ch}$	$D (\times 10^{-11}) \text{ cm}^2 \text{ s}^{-1}$
CMC	2nd at 0.1 C	4.99	175.22	0.006	0.21
	4th at 0.5 C	5.83	73.85	0.014	0.38
CMC-g-PAAm	2nd at 0.1 C	3.86	50.7	0.020	1.52
	4th at 0.5 C	2.33	19.47	0.051	2.65
<i>s</i> -CMC-g-PAAm	2nd at 0.1 C	4.13	38.1	0.026	0.93
	4th at 0.5 C	2.10	13.79	0.072	2.36
<i>d</i> -CMC-g-PAAm	2nd at 0.1 C	3.66	16.0	0.063	2.26
	4th at 0.5 C	2.62	14.39	0.069	3.95

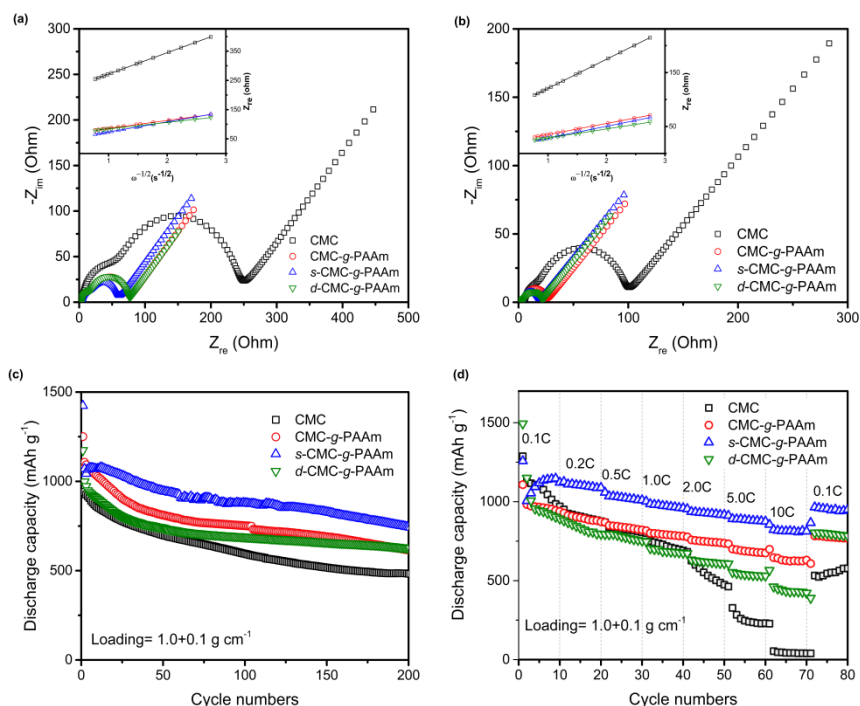


Figure 5-4 Electrochemical performance of Si/C electrode with CMC based binders

The Nyquist curve of four Si/C electrodes at 0.2 V (a) after two percycles at 0.1C and (b) after 2th cycles at 0.5C rate, (c) cyclic performance and (d) rate performance of Si/C electrodes with CMC, CMC-g-PAAm, s-CMC-g-PAAm, and d-CMC-g-PAAm binders, respectively.

In addition, modification of CMC through graft copolymerization with acrylic monomer is significantly influenced on solving the slurry preparation compared to Si/C electrode with pure CMC binder due to peeling progress for pure CMC binder in drying slurry at 70°C as seen the Figure 5-5.

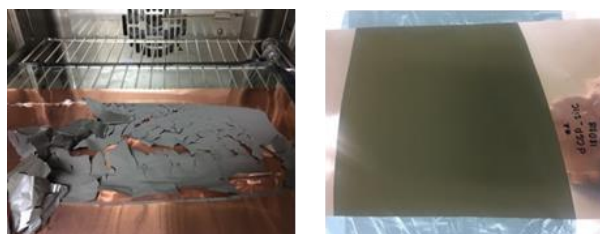


Figure 5-5 Si/C slurry films with pure CMC (left hand) and CMC-g-PAAm binders (right hand)

Furthermore, effect of crosslinked graft copolymer binders on the electrochemical performance of Si/C were investigated in our experiment, whereas there are added two different crosslinker agents into slurry mixture. One of them is only contained chemical crosslinker that is marked by single crosslinked binder, s-CMC-g-PAAm; and another of them is contained two different crosslinker agents that is named dual crosslinked binder, d-CMC-g-PAAm. Strong achievement was illustrated as using single crosslinked binder on cycling performance of high capacity Si anode in long-term cycles. The reversible capacity after 200 cycles was obtained 800 mAh g⁻¹ for single-crosslinked binder and 697 mAh g⁻¹ for dual-crosslinked binder. In the result, the dual crosslinked binder shows lower capacity retention for Si/C electrode compared to CMC-g-PAAm binder with or without single crosslinking progress. That is indicated to the progress of ionic crosslinking between Al³⁺ and CMC shows decrease adhesion ability

and an increase solvent resistance compared to single crosslinking. Both physical properties of dual crosslinked binder are negatively influenced on the electrochemical performance of Si/C electrode. In addition, very lower electrolyte uptake of binder through electrode has shown a weakly lithium ion kinetic during lithium ion charge and discharge process and followed to appearance lower capacity retention. But the lower capacity fade and enhanced reversible capacity of 701.1 mAh g⁻¹ at 200th cycles can maintained by using *d*-CMC-*g*-PAAm binder for high capacity Si-based composite electrode with high active material loading of 1.4±0.1 g cm⁻¹ that compared to pure CMC binder with 551.5 mAh g⁻¹. While only chemical crosslinking progress, Si/C electrode with *s*-CMC-*g*-PAAm has higher electrochemical stability after 200 cycles (it is not showed here).

The Si/C electrodes with both CMC and *d*-CMC-*g*-PAAm binders showed instability rate capability performance, because rate capacity decreased as increasing current rate. In the other side, two Si/C electrodes contained both of CMC-*g*-PAAm with or without crosslinked with MBAA has better rate stability while rate current increase from 0.1 to 10 C. The target system of Si/C electrode with *s*-CMC-*g*-PAAm displays the higher rate capability performance of 1000 mAh g⁻¹ at 10 C compared to 20 for CMC, 500 for *d*-CMC-*g*-PAAm, and 780 mAh g⁻¹ for CMC-*g*-PAAm. As the result, the formation of single crosslinking network is accepted to suffer of Si polarization during at high rate state. Meanwhile, the capacity retention of the electrodes can completely remain to their initial capacity when the rate returns to 0.1 C from high current rate, expect pure Si/C electrode with pure CMC due to the low adhesion ability of CMC.

5.3 Conclusion

In the present chapter, we successfully applied the commercial CMC polymer with grafted and cross-linked 3D network as an effective binder for Si anodes in LIBs. Through grafting and cross-linking process for pure CMC forms a uniform interconnected network to buffer volume change of Si. Within grafting and crsooslinked network, the electrode slurry has not showed easy peeling acts during drying process compared with Si/C electrode with pure CMC, and mechanical stress can be distributed to pure CMC, which can substantially reduce the stress applied to each anchoring point. Consequently, single cross-linked network improved the cycle and rate performances of Si/C anode compared to pure CMC and grafted copolymer based electrode. Compared to single crosslinked binder as *s*-CMC-*g*-PAA, using dual-crosslinker agents for CMC-*g*-PAAm has not exhibited efficient improvement in high capacity Si/C anode in next-generation LIBs due to highly decreasing of both the adhesion ability to 6 from 10 and the electrolyte uptake to 0.75% from 2% after dual-crosslinking progress.

6 Dual crosslinked Pectin grafted Polyacrylamide for high capacity electrode

In the previous two chapters, we reported that dual-crosslinked *c*-Alg-*g*-PAAm and *c*-CMC-*g*-PAAm binder system regarded to enhancement stability cycling performance in the Si/C electrode of LIBs. Here it is focused on pectin based polymeric binder system through graft and crosslinked to improve performance of macro particle Si/C electrode. Modification of alginate through graft and crosslinking methods shows in Figure 6-1.

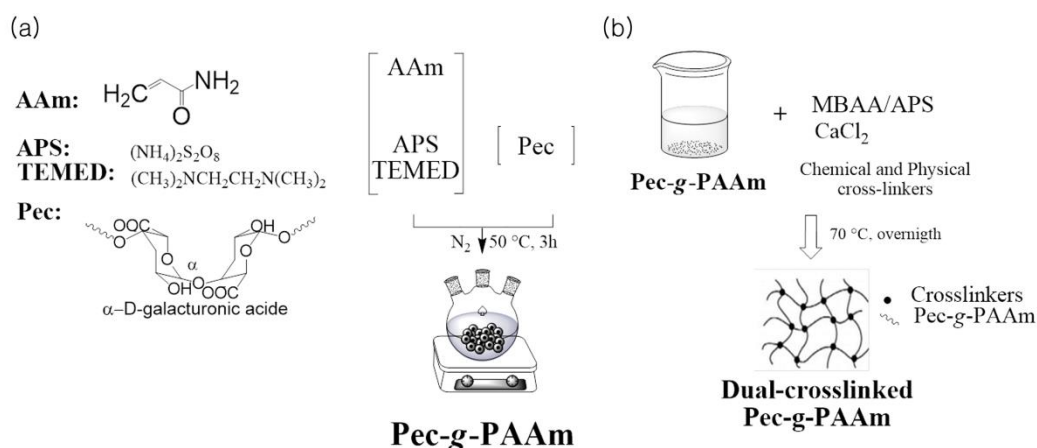


Figure 6-1 Synthesis of (a) Pectin-*g*-PAAm and (b) *c*-Pectin-*g*-PAAm

(a) Graft copolymerization between pectin and PAAm with the terminal initiator system, (b) preparation of crosslinked network *c*-Pec-*g*-PAAm

6.1 Introduction

A binder material, on the other hand, which provides an integrity in composite electrodes consisting of active materials and conducting agents, seems to have an attention recently because it greatly influences the long-term cyclic stability, rate capability, and irreversible capacity loss of the electrodes^{91,8,37,38}. It is aware that breakthrough for the high capacity anodes experiencing large volume change such as silicon strongly depends on proper choice of polymeric binder.^{39,64,83,92} Besides, a polysaccharides and their modification such as CMC, SA, chitosan and starch were applied to binder for high capacity anodes.⁹³⁻⁹⁶ Such linear polysaccharides have been extensively studied, whereas a certain number of research on the application of branched polysaccharides to LIB binder were recently reported.^{44,81,97-99}

The linear polysaccharide applied most recently to LIB is a pectin (Pec) material. Yoon et al.¹⁰⁰ reported that Pec composed of α -glycosidic bonds with -COOH functional groups, were superior to CMC, β -glycosidic bonds with -COOH, and amylose, α -glycosidic bonds without -COOH, in cyclability and rate capability of silicon anodes. Due to low chemical resistance and poor compact ability of Pec, however, the modification of Pec by grafting and crosslinking was generally suggested to copy with these limitation¹⁰¹. Similar to alginate, Pec contains numerous carboxyl and hydroxyl groups on chain-chain association and easily forms a physical crosslinking with divalent cations such as Ca^{2+} .¹⁰² On the other

hand, the crosslinked Pec network was more elastic than the crosslinked alginate network when they were linked with presences of the divalent calcium cations.^{102,103} The elastic property may be more beneficial to high capacity anodes experiencing large volume change during cycles^{83,92}. Zhu et al.⁹² showed that a highly stretchable crosslinked polyacrylamide (PAAm) had high strain resistance for the expansion of silicon electrodes and strong affinity to bonding with nano-Si surface, leading to remarkable cycling performance of the silicon electrode. In first chapter, we also proved that the dual-crosslinked binder of alginate with PAAm were greatly effective for the electrochemical performance of Si/C electrodes due to intrinsic good binding property, enhancing lithium ion transport, extremely low volume expansion.⁶⁴

In this chapter, modification of pectin polysaccharide through grafting with polyacrylamide and crosslinking is newly proposed as a powerful candidate for water-soluble binder of high-capacity Si anodes in lithium ion batteries. The pectin-*grafted*-polyacrylamide (Pec-*g*-PAAm) significantly enhances adhesion in electrode, a basic characteristic of binder, due to its multipoint functional groups. A strong carbonyl dipole in polyacrylamide also contributes to good electrolyte wettability of carbonate electrolyte. In present study, dual-crosslinking of the Pec-*g*-PAAm is achieved by ionic crosslinking of pectin with divalent calcium ions and chemical crosslinking of polyacrylamide with a bisacrylamide. The dual-crosslinking in binder provides good contribution on integrity of electrode and ease movement of lithium ions through electrodes. Therefore, the dual-crosslinked binder shows further improvement cycling performance of the Si/C composite anode with the loading of 1.2 mg cm⁻², which remains the specific capacity of 729 mAh g⁻¹ at 300th cycles.

6.2 Result and Discussion

6.2.1 Confirmation of dual-crosslinked binder

The dual-crosslink between Pec and PAAm was preceded in an aqueous medium by two step methods. First, the Pec-*g*-PAAm binder was synthesized by grafting PAAm onto Pec using a redox initiator system as APS/TEMED and then the graft copolymer was linked with physical crosslinker as CaCl₂ and chemical crosslinker as MBAA. Coordinate bonds of hydroxyl and carboxyl groups with Ca²⁺ ions are formed in the main chain of Pec and the PAAm side chains in the graft copolymer are covalently bonded with MBAA. The chemical structure of the dual-crosslinked *c*-Pec-*g*-PAAm is shown in Figure 6-2a.

Successful formation of Pec-*g*-PAAm polymer was first confirmed by the FT-IR spectra displayed in Figure 6-2b. The FT-IR spectrum of Pec showed several peaks as follows: a broad peak at 3410 cm⁻¹ for -OH group, a peak at 2940 cm⁻¹ for -CH₂ group of alkane, two sharp peaks at 1748 and 1632 cm⁻¹ for -COOH groups, a peak at 1444 cm⁻¹ for -CH₂ of secondary alcohol. The stretching vibration of C-O as complex bands, which are resulted from an ether (C-O-C) and a cyclic alcohol (CH-OH) in saccharide chain, were also observed at the range of 1000 to 1300 cm⁻¹: two peaks at 1266 and 1102 cm⁻¹ for C-O stretching in the cyclic alcohol, and two peaks at 1147 and 1014 cm⁻¹ for C-O stretching in the ether,

respectively^{101,104,105}. Owing to the formation of ether bonds between the hydroxyl group placed in anhydroglucose C2 and the p band of PAAm, the adsorption peaks at 1266 cm⁻¹ (C-O stretching) and 632 cm⁻¹ (C-OH bending) nearly disappeared in the spectrum of Pec-g-PAAm. In contrast, the overlapped peaks attributed to ether and cyclic alcohol still remained in the range of 1150 to 1000 cm⁻¹, though shrunk in their intensities. On the other hand, the adsorption peaks related to PAAm⁵⁹, the anti-symmetric and symmetric stretch of NH₂ at 3480 and 3180 cm⁻¹, an overlapped band from C=O stretching and NH₂ deformation around 1651 cm⁻¹, and the C-N stretching at 1413 cm⁻¹ newly appeared in the FT-IR spectrum of Pec-g-PAAm, even though all peaks were shifted when compared to original ones in PAAm spectrum. These evidences imply that the graft reaction between Pec and AAm monomers was successfully taken place.

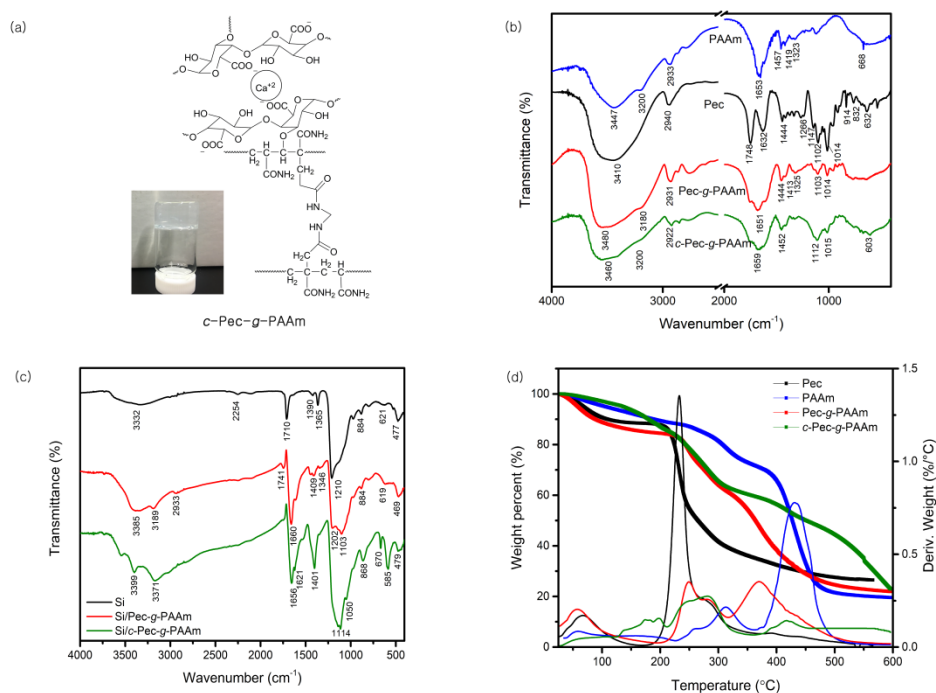


Figure 6-2 Spectrometry and thermogravimetric analysis of Pectin based polymeric binders

(a) Chemical structure of dual-crosslinked *c*-Pec-g-PAAm, (b) FT-IR spectra of as-synthesized PAAm, natural Pec, Pec grafted with PAAm (Pec-g-PAAm), and dual-crosslinked *c*-Pec-g-PAAm; and (c) FT-IR spectra of pure Si, slurry of Si and Pec-g-PAAm, and slurry of Si and *c*-Pec-g-PAAm; and (d) Thermal gravimetric analysis of the binders.

In Figure 6-2(b), the FT-IR spectrum of *c*-Pec-g-PAAm peaks is also displayed. The adsorption bands of the graft Pec-g-PAAm copolymer at 3480 cm⁻¹ (–OH) and 1651 cm⁻¹ (asymmetric COO⁻) were shifted in the dual-crosslinked *c*-Pec-g-PAAm. This must be attributed to strong coordination bonds between Ca²⁺ ions and Pec in the graft copolymer.^{106,107} Furthermore, the spectrum of *c*-Pec-g-PAAm shows sharp peaks at 1452, 1112, and 603 cm⁻¹, which are associated with N-H bending, C-N stretching, and N-C=O bending in amide groups of the chemical crosslinker MBAA, respectively.⁵⁹ This must be due to the presence of additional amide groups in MBAA as well as the amides in the graft polymer.

To confirm the formation of dual-crosslinked network of the binder in the presence of Si active

materials, silicon active materials were added to an appropriate amount of Pec-g-PAAm solution and mixed with or without the crosslinking agents. As shown in Figure 3-2, the slurry sample with the crosslinkers formed a gel-like phase, indicating a possibility of the formation of crosslinking. Moreover, this was also clarified from the comparison of FT-IR spectra of the slurry samples in Figure 6-2c. As mentioned above, the peak at 1656 cm^{-1} in the spectrum of the Si/*c*-Pec-g-PAAm sample implies the formation of the ionic crosslinking between carboxyl groups and Ca^{2+} ions. Additionally, the peak at 1741 cm^{-1} attributed to C=O stretching in the carboxylic acid becomes weakened by limiting the stretching due to the ionic crosslinking. Sharp peaks at 1401 and 585 cm^{-1} can be assigned to C-N stretching and N-C=O bending of the secondary amide in the chemical crosslinker, MBAA.⁷⁸ On the other hand, the strong peak at 1114 and 868 cm^{-1} are assigned to an ester-like bond between binder and Si particles, which is a strong covalent bond produced from the reaction between carboxyl groups in the binder and silanol groups (Si-OH) at the surface of Si particles.^{30,90,108} Based on these results, the grafted Pec-g-PAAm and its dual-crosslinked *c*-Pec-g-PAAm were successfully synthesized.

Thermal gravimetric analysis of the polymers was also performed and the result is presented in Figure 6-2d. Main thermal degradation of pure Pec, corresponding to the weight loss of 48.8%, occurs in the temperature range of $200\text{--}320\text{ }^{\circ}\text{C}$. As-synthesized PAAm has two thermal degradation steps with the exception of the low temperature weight loss below $150\text{ }^{\circ}\text{C}$ caused by water evaporation. At temperature range of 230 to $340\text{ }^{\circ}\text{C}$, there was the weight loss of 14.1% which is assisted to degradation of amino group loss.⁵⁴ Continually, a major weight loss of 50.2 % occurs in the range of $380\text{--}520\text{ }^{\circ}\text{C}$, which is attributed to the decomposition of the backbone chain to carbon dioxide and hydrocarbons. In the case of Pec-g-PAAm, the thermal stability is characterized as improved than pure Pec but no better than pure PAAm. It shows two thermal decomposition peaks related to Pec chains and acrylamide chains between $220\text{--}310\text{ }^{\circ}\text{C}$ with the weight loss of 21.4 %. The third decomposition occurs relatively broad temperature range between $320\text{ }^{\circ}\text{C}$ and $520\text{ }^{\circ}\text{C}$ with a large weight loss of 37.0 % due to the decomposition of the polymer backbone.⁶² On the contrary, the dual-crosslinked *c*-Pec-g-PAAm sample is very resistive to the high temperature decomposition of the polymer backbone above $320\text{ }^{\circ}\text{C}$. This indicates that the chemical crosslinking caused by MBAA also contributes to improving thermal resistance of PAAm backbone chain.

6.2.2 Physical characterization of polymer

It is generally known that an increase in the interaction between polymeric binders and hydroxyl groups on Si surface through hydrogen or covalent bonds leads to improving the adhesion of the Si-based anode.^{29,40} The adhesion capability of the binder was estimated by the 180° peel test of the Si/C electrodes and illustrated in Figure 6-3a. All modified Pec samples with grafting and/or crosslinking showed significantly higher adhesion than natural Pec. In particular, the grafted copolymers showed much higher adhesion than the physical blend between Pec and PAAm. This must be attributed to the multipoint functional groups in the grafted structure for Pec-g-PAAm, which form more flocculated

structure with strong hydrogen bonds in electrode.⁴³ On the other hand, the dual-crosslinking by Ca^{2+} and MBAA increases the interconnection among polymer chains in the Pec-g-PAAm and thus results in a decrease in the functional groups of binder, which are normally connected to active materials. This may be the reason for the slight decrease in the 180° peel strength of the dual-crosslinked c-Pec-g-PAAm (8.29 N of load force), compared to the grafted Pec-g-PAAm binder (10.48 N of load force).

The adhesion ability of polymeric binder in electrode is depended from the amount of solvent uptake causing the swelling of binder, ultimately leading to weakening the interaction between active materials and current collector.^{81,109} The data on the electrolyte uptake of all binder samples are collected in Figure 6-3(b). Pec has approximately 13% electrolyte uptake, which is relatively larger than other modified Pec samples. The poor adhesion of the Pec binder in Figure 6-3(a) may be partially attributed to the large electrolyte uptake. In our previous chapter⁶⁴, it was proven that PAAm was very resistant to the carbonate electrolyte swelling with the uptake less than 2%, even though it will be shown later that PAAm has an affinity to the carbonate due to the presence of carbonyl dipoles in amide groups. Therefore, the modified Pec samples containing PAAm have much lower electrolyte uptake, contributing to keeping integrity of Si/C electrodes during long-term cycles. Furthermore, the PAAm graft into saccharide significantly increase more rapid permeation of electrolyte on the electrode is suggested from decreasing electrolyte contact angle value on the surface of both Pec-g-PAAm and c-Pec-g-PAAm binder film.

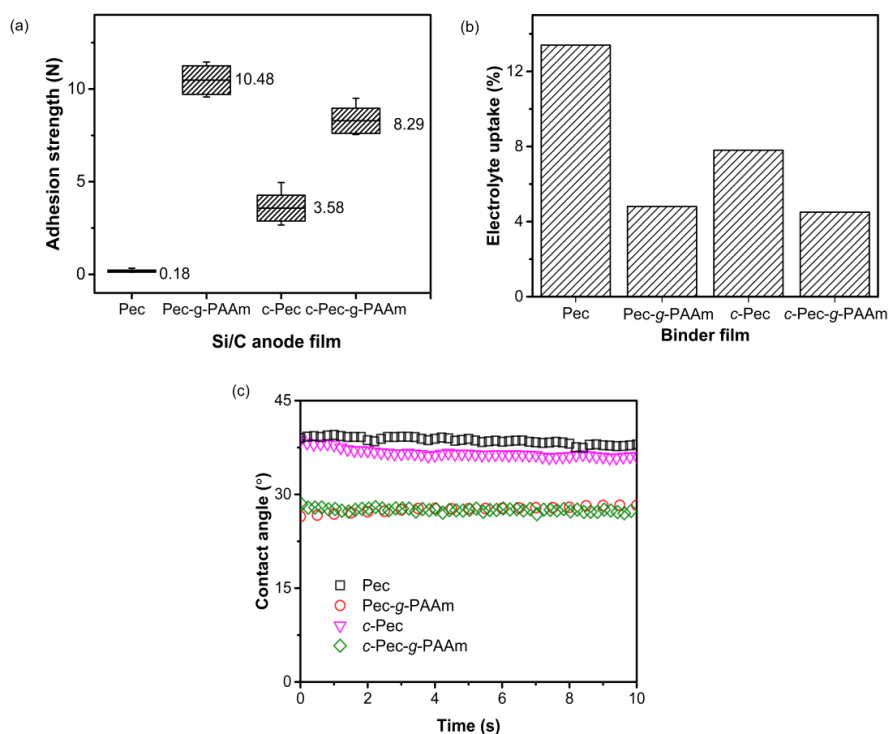


Figure 6-3 The effect of modifying Pec based binders for adhesion ability and swelling performance (a) Adhesion strength of the Si/C electrodes containing different binders measured by 180° peel test, and (b) the amount of electrolyte uptake of polymer films immersed in the electrolyte solvent (EC:DMC:EMC) at 25 °C for 48 h; and (c) Contact angle of the pure binder film with electrolyte

6.2.3 Electrochemical characterization

The effect of modifying Pec binder on electrochemical properties of Si/C anodes was investigated using CV, EIS, and galvanostatic cycle tests. Figure 6-4(a) shows the CV profiles of the Si/C fresh electrodes obtained in voltage range of 0 to 1.5 V (vs. Li^+/Li) with the scan rate of 0.2 mV s^{-1} . All fresh electrodes display two pairs of redox peaks; two cathodic peaks at approximately 0.0 and 0.2 V for Li insertion and two anodic peaks at approximately 0.4 and 0.5 V for Li extraction. The Si/C electrodes containing the PAAm modified-Pec binders exhibit higher redox currents than that containing natural Pec binder. This might be contributed to superior electrolyte wettability of the PAAm modified-Pec to the Pec binder. The strong carbonyl dipole ($\text{C}=\text{O}$) in an amide must have an affinity for the carbonyl groups in the carbonate structure so that the Si/C electrodes containing PAAm form considerably low contact angles with electrolyte, as shown in Figure 6-3(c). This indicates fast penetration of electrolyte into the electrode and leads to broader available active area for the CV experiment. In other words, the PAAm-containing binder helps to provide good contact of electrode particles to the carbonate electrolyte, resulting in more lithium ion movement through the electrode. In particular, the significant rise in redox CV peaks of the Si/C electrode with *c*-Pec-*g*-PAAm binder could be attributed to effective integration of electrode and a decrease in polarization resistance caused by the dual-crosslinking.^{64,110}

This is confirmed by EIS in Figure 6-4(b). The EIS of the Si/C electrodes was measured at 0.2 V after two precycling at 0.1 C followed by two more cycles at 0.5 C. The semicircles at the middle frequency range indicate the charge transfer resistance of the electrochemical reaction occurring at the interface, which is closely related to ion and electron transport characteristics. The PAAm-containing binders, in particular, dual crosslinked *c*-Pec-*g*-PAAm binder leads to the lowest charge transfer resistance. In addition, the low frequency Warburg region of the EIS enables to calculate the diffusion coefficients of lithium ions (as see experiment part). The σ_ω indicates the slope of real part of impedance versus $\omega^{-0.5}$ (angular frequency in the Warburg region). Based on the slope shown in inside of Figure 6-4b, the diffusion coefficients were $5.0 \times 10^{-12} \text{ cm}^2 \text{ s}^{-1}$ for Pec, $3.5 \times 10^{-12} \text{ cm}^2 \text{ s}^{-1}$ for *c*-Pec, $17.7 \times 10^{-12} \text{ cm}^2 \text{ s}^{-1}$ for Pec-*g*-PAAm, and $14.0 \times 10^{-12} \text{ cm}^2 \text{ s}^{-1}$ for *c*-Pec-*g*-PAAm electrodes, respectively. In summary, the dual-crosslinked binder helps to easy charge transfer kinetics and mass transport in the electrode, compared to the other binders.

From the cyclic performance test depicted in Figure 6-4c, the Si/C electrodes with Pec and *c*-Pec experience a severe drop in the discharge capacity to below 483 mAh g^{-1} during the first 20 cycles, then the capacity is stabilized to approximately 415 mAh g^{-1} . This initial severe drop must be responsible for weak binding strength, which is shown in Figure 6-3a, to endure huge volume change of Si component. On the contrary, the reversible capacity of the Si/C electrode remains around 540 mAh g^{-1} at 100 cycles when Pec binder is grafted with PAAm with much slow decay in the capacity for the first tens of cycles. Our target Si/C electrode construct with dual crosslinking in binder, *c*-Pec-*g*-PAAm, provides further improvement on the cyclic capacity; it has 625 mAh g^{-1} at the 100th cycle. If the average discharge

capacities within 100 cycles are readily compared, the *c*-Pec-*g*-PAAm-containing electrode has the highest value of 861 mAh g⁻¹; 732 mAh g⁻¹ for Pec-*g*-PAAm, 451 mAh g⁻¹ for *c*-Pec, and 463 mAh g⁻¹ for Pec, respectively. The grafting with PAAm contributes to the mechanical stability of the electrode due to numerous multipoint functional groups⁶⁴, as seen from the strong adhesion of Pec-*g*-PAAm (Figure 6-3a). The chemical crosslinking in PAAm and physical crosslinking in Pec improve the robustness of the network against significant strain in the Si/C electrode.^{64,92}

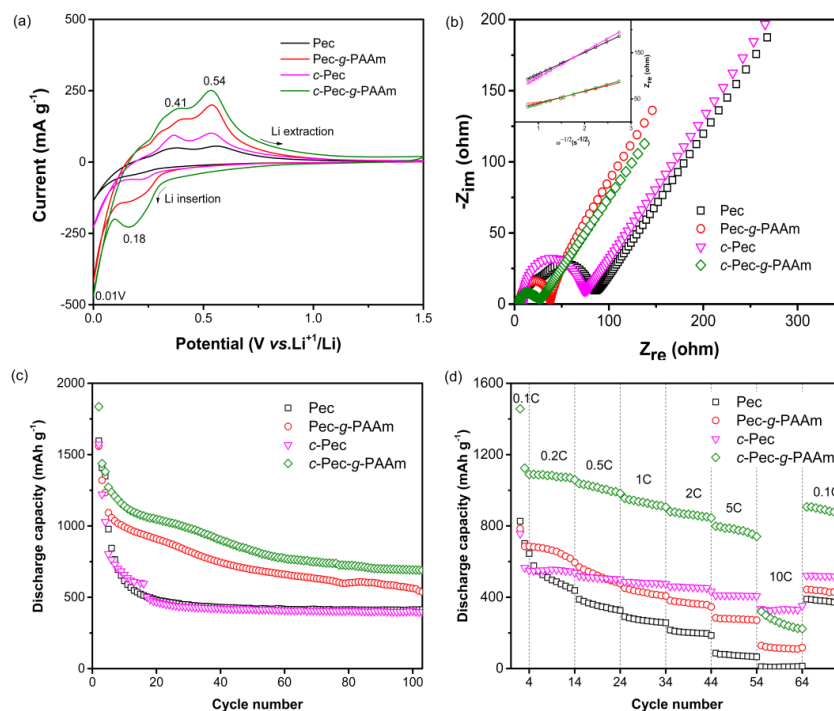


Figure 6-4 Electrochemical performance of Si/C electrode with binders

(a) Cyclic voltammogram of the fresh Si/C electrodes containing different binders, (b) EIS of the Si/C electrodes measured at 0.2 V, (c) cyclic performance, and (d) rate capacity test of the Si/C electrodes.

Separately, the effect of binder on the rate capability of Si/C electrodes was also investigated through various current densities in the range of 0.1 C to 10 C and its result is shown in Figure 6-4d. The Si/C electrode containing dual crosslinked *c*-Pec-*g*-PAAm binder presented overwhelmingly better rate performance than the other electrodes except the highest 10 C current density. The Si/C with *c*-Pec-*g*-PAAm retained 79.9% capability of 0.2 C current at 5 C rate and maintained more than 786 mAh g⁻¹, whereas the capacities of the other electrodes were lower than 425 mAh g⁻¹ at 5 C and their capacity retention at 5 C over 0.2 C were 16.7% for Pec, 43.2% for Pec-*g*-PAAm, and 74.8% for *c*-Pec, respectively. Even though the dual-crosslinked Si/C has an unexpectedly low capacity of 311.3 mAh g⁻¹ at the highest current density of 10 C, it quickly restores the capacity up to 822.4 mAh g⁻¹ when the current was returned back to 0.1 C.

The surface morphology of 100-cycled Si/C electrodes was characterized using top-viewed field-emission scanning electron microscopy (FE-SEM Jeol, JSM-6500F) to see the mechanical stability of electrode film. As shown in Figure 6-5, all electrodes except for the dual-crosslinked electrode exhibit

distinct cracks caused by severe volume change. The Si/C electrode containing *c*-Pec-*g*-PAAm binder appears no obvious cracks and thus the dual-crosslinking network formed by binder plays an important role for long-term cycling stability. This can be supported by the change in electrode thickness between fresh and 10-cycled electrodes, which are shown in Figure 6-5b. The thickness changes of the Si/C electrode after 10 cycles are 55.8 μm (131 %) from 42.6 μm for the Pec-containing electrode, 53.8 μm (124 %) from 43.3 μm for the *c*-Pec-containing electrode, 35.8 μm (84%) from 42.6 μm for the Pec-*g*-PAAm-containing electrode, and 32.8 μm (74%) from 44.4 μm for the *c*-Pec-*g*-PAAm electrode. Thus, the strong dual-crosslinking network is effective to reduce the extra volume expansion during the cycle and may contributes to better cycleability and rate-capacity retention of the Si/C electrode containing *c*-Pec-*g*-PAAm.

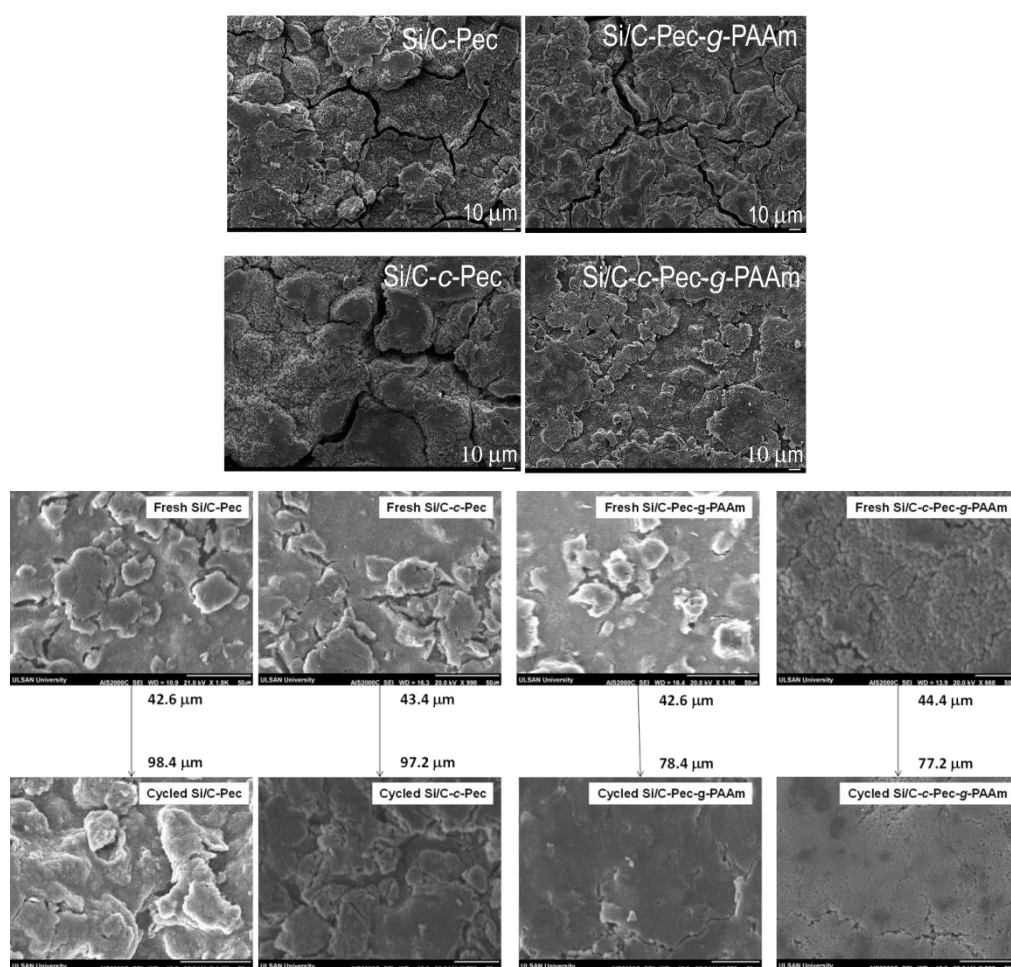


Figure 6-5 Top-viewed SEM-image of Si/C electrodes

(above) TOP-viewed SEM-image of Si/C electrode after 100 cycles and, (below) Top-SEM images of Si/C electrode with four binders before and after 10 cycles. After the 10-cycled electrodes were carefully disassembled, cleaned, and dried, their thicknesses were measured using a height gauge (TESA μ -HITE, Hexagon Manufacturing Intelli)

6.3 Conclusion

This chapter reports that the modification of a polysaccharide polymer, pectin, through grafting and crosslinking with polyacrylamide is quite effective as an adhesive water-soluble binder in high capacity

silicon anodes to endure the huge volume changes of Si/graphite composite electrodes. The pectin grafted with polyacrylamide, Pec-g-PAAm, polymeric binder is synthesized by an in-situ polymerization method using a redox initiator in an aqueous medium. The dual-crosslinked polymer, *c*-Pec-g-PAAm, is prepared from the graft copolymer in the presence of two crosslinking agents, CaCl₂, as an ionic crosslinker, and MBAA, as a chemical crosslinker, during the preparation process of the electrode slurry. The PAAm in the graft copolymer improves the mechanical strength of the electrodes through strong adhesion and facilitates electrolyte-penetration with low electrolyte swelling, leading to good mechanical stability and lithium ion movement through the Si/C electrode. Moreover, the dual-crosslinking in the target binder contributes to the efficient integration of the electrode and a further decrease in polarization resistance. As a result, the dual-crosslinking network prevents severe volume expansion of the high capacity Si/C electrode during the cycling and maintains good cycling ability and rate-capacity retention.

7 Comparison study of Dual crosslinked binders

In previous three chapters, we are explained for preparation of dual-crosslinked binder systems from three different most populated saccharides sources through grafting and crosslinking: alginate based (as seen in Chapter 4), carboxymethyl cellulose (CMC) based (as shown in chapter 5) and pectin (Pec) based (as seen in chapter 6), and. These dual-crosslinked binder systems have investigated as the target binder system for Si/C electrode compared to their parents such as pure polysaccharide (PS) and graft copolymer as polysaccharide-*graft*-polyacrylamide (PS-*g*-PAAm) without crosslinking network. Herein, CaCl_2 with 2 wt.% solution was used for physical crosslinking of alginate and pectin chains in Alg-*g*-PAAm and Pec-*g*-PAAm samples; and AlCl_3 was used as physical crosslinker for CMC-*g*-PAAm, respectively. MBAA/APS as chemical crosslinker was used to PAAm in PS-*g*-PAAm samples. As the result, the dual-crosslinked *c*-PS-*g*-PAAm binder show an improvement electrochemical performance of Si/C anode to greatly buffering huge-volume expansion of Si/C composite electrode at high current rate, expect CMC based dual crosslinked binder. At this current chapter, we have examined a comparison study of the dual-crosslinked *c*-PS-*g*-PAAm binders: *c*-Alg-*g*-PAAm, *c*-Pec-*g*-PAAm and *c*-CMC-*g*-PAAm.

7.1 Introduction

Over the last 20 years, much attention has been devoted to developing new electrode materials with high energy and power densities for LIBs. Silicon (Si) and tin (Sn) is an abundant, stable, and non-toxic material with a high specific capacity for lithium storage, and it is therefore an attractive target for use in lithium ion batteries. However, developing silicon anodes that outperform commercial graphite anodes is a significant challenge. Because the lithiation of Si produces a lithium-rich LiSi alloy and is associated with large volumetric changes, roughly 300 % of unlithiated silicon particles at full charge. These large volumetric changes produce mechanical stresses that can fracture Si nanoparticles, produce cracks in the electrode, cause delamination from the charge collector, and ultimately lead to irreversible capacity loss.¹¹¹⁻¹¹⁷ In addition, the polymeric binder maintains the structure of the electrode, serving as a glue to hold the various components of the electrode together and maintain contact with the current collector. Effective polymeric binders for Si and other alloy anodes perform multiple functions. Properly designed polymer binders can potentially address this capacity loss by suppressing cracking, maintaining cohesion between the various materials in the anode, ensuring strong adhesion to the current collector, and sustaining large changes in volume during lithiation and de-lithiation without rupture.

The need for a polymeric binder system designed specifically for Si and other lithium alloy materials was recognized as early as 2003.¹¹⁸⁻¹²³ These studies demonstrated that poly(vinylidene fluoride) (PVDF) was inadequate as a binder and suggested an extensible composite matrix as a potential alternative. For example, a copolymer of vinylidene fluoride, tetrafluoroethylene, and propylene poly(vinylidene fluoride-tetrafluoroethylene-propylene) (PVDF-TFE-P) and its crosslinked PVDF-TFE-

P binder were shown to be capable of accommodating much larger strains than PVDF and produced nanocomposite electrodes with better capacity retention under cycling when compared against PVDF.^{118,122}

Since these initial studies, an impressive variety of polymer compositions, architectures, and design principles have been implemented towards the goal of producing stable, high-capacity silicon anodes. For example Liu et al.⁴¹ and Yoon et al.⁴² proposed an supramolecular alginate binder is prepared through the cross linking effect of SA with Ca(2+) ion which leads to a remarkable improvement in the electrochemical performance of the Si/C anode of a Li-ion battery. By varying the composition of the supramolecular binder, the literature explored the role of modulus, rheological properties, adhesion, crosslink density, and ion mobility on performance. They identified an optimal network relaxation time and crosslink density that produced electrodes that could achieve stable cycling.¹²⁴⁻¹²⁶

In previous three chapters, we prepared the polysaccharide-graft-polyacrylamide (PS-g-PAAm) form different polysaccharide sources (such as alginate, carboxymethyl cellulose, and pectin) by graft copolymerization and then that copolymer is crosslinked with ionic and chemical crosslinkings to formed dual-crosslinked polymer system. We demonstrated that a water-treated dual-crosslinked graft copolymer between three saccharides and PAAm (*c*-PS-g-PAAm) was an effective binder for the high-capacity Si/C electrode compared with pure polysaccharides. Inspired by these resulting, we examine and compare herein three different *c*-PS-g-PAAm binders for Si-based electrode (there are included the Si/C-*c*-Alg-g-PAAm, Si/C-*c*-Pec-g-PAAm, and Si/C-*c*-CMC-g-PAAm electrodes, respectively). Herein, a variety of characterization tools are used to examine a physical characterization and an electrochemical performance of the Si based electrodes containing the dual-crosslinked binder systems.

7.2 Result and Discussion

7.2.1 Physical characterization of binder and electrode

The all crosslinked polymer samples were immersed in the carbonate solvent without salt for 24h, and then the change weight, which caused by the uptake of the solvent, was recorded. Figure 7-1a was shown the electrolyte uptake of dual-crosslinked polymeric films which are difference of difference polysaccharide backbone: *c*-Alg-g-PAAm, *c*-Pec-g-PAAm, and *c*-CMC-g-PAAm. All crosslinked films absorb more higher than 1% solvent by weight of *c*-PAAm and this over swelling causes the volumetric expansion of the saccharide backbone source in *c*-polysaccharide-g-PAAm polymer. In comparison of dual crosslinked samples, the *c*-CMC-g-PAAm polymer can uptake 3.5% carbonate solvent that is slightly lower than other two crosslinked system. That reason may be attributed to following the molecular difference on saccharide such as: CMC has much stiffness saccharide compared to alginate and pectin saccharide (Figure 7-1b). We examined the elongation characterization of the dual-crosslinked polymeric film containing glycerol plasticizer of 30 wt.%, in resulted, *c*-CMC-g-PAAm is

more brittle with higher stress and lower strain at break than both *c-Alg-g-PAAm* and *c-Pec-g-PAAm*. Silva et al.¹⁰² also reported that tensile strength of CMC-based samples were randomly higher with low elongation than Pec. Other investigation, the crosslinked Pec network, *c-Pec*, is more elastic than crosslinked alginate, *c-Alg*, in biochemistry application when they are physically crosslinked with $Ca(2+)$.¹⁰³ And so it may be followed to the increase electrolyte uptake from CMC to Pec typed saccharide. In particular, the high electrolyte uptake facilitates facial Li-ion kinetic to the active material through polymer binder and then increases the capacity of the electrode, especially the capacity at high rate current. In adding, the pectin based dual crosslinked sample with lowest stiffness accounts for 4.5% of electrolyte uptake. It is already known that crosslinked Pec network, *c-Pec*, is more elastic than crosslinked alginate, *c-Alg*, in biochemistry application when they are physically crosslinked with $Ca(2+)$.¹⁰³

Electrolyte uptake impacts mechanical properties that is correlated with the decrease adhesion ability and, correspondingly, poor electrode stability, because it can result in softening of the polymer binder. After immersed into electrolyte solvent for 24 hours, the Si/C anode with *c-Pec-g-PAAm* shows higher average adhesion ability with 5.22 N of average value in 180° peel strength of anode film compared to 4.97 N for *c-Alg-g-PAAm* and 4.81 N for *c-CMC-g-PAAm*, as shown in Figure 7-3c.

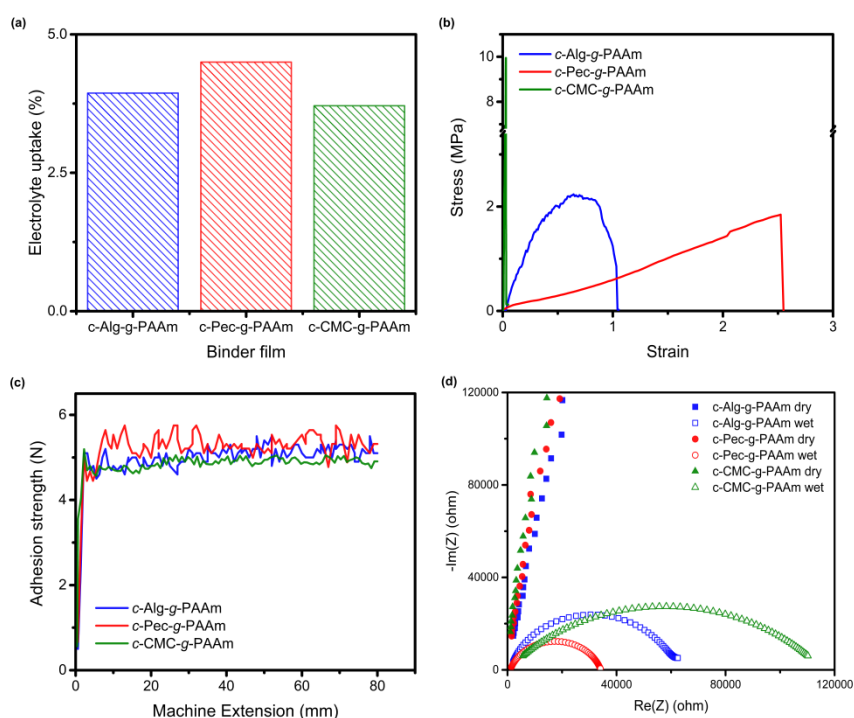


Figure 7-1 Physical characterization of various dual crosslinked copolymers

(a) Electrolyte uptake properties, (b) the stress-strain curve of three dual crosslinked polymer films; (c) adhesion strength of Si/C electrodes with different binders, and (d) Nyquist diagrams of polymer films at dry and wet with electrolyte state from 100 kHz to 10 Hz at OCV

In other to study the effect of polymer binders on the ionic conductivity through electrodes, the dual crosslinked membrane film was replaced between two stainless steel electrodes in 2032 coin cell. Nyquist plot of pure binder membrane film was recorded the impedance analysis at the frequency range

100 kHz-10 Hz, and 10 mV amplitude voltage as shown in Figure 7-1d. Herein, all impedance measurements were measured before and after electrolyte uptake of the membranes. All crosslinked membranes in dry form displayed a strength line as like the conductor at high frequency and continuously we calculated the ionic conductivities by Equation 3-2. As the resulted, the all dried samples are founded the similar values that are ranged between 2.08 and 2.18 $\mu\text{S cm}^{-1}$. After swelling into electrolyte, Nyquist plot illustrated one semicircle. The dual crosslinked polysaccharide-g-PAAm exhibited the ionic conductive in 2.72, 4.55, and 2.68 $\mu\text{S cm}^{-1}$ for *c*-Alg-g-PAAm, *c*-Pec-g-PAAm, and *c*-CMC-g-PAAm, respectively. To comparison of ionic conductivity of Alg and CMC based polymer binder system, *c*-Pec-g-PAAm membrane could be enabled the high ionic conductivity through electrode due to enhanced swelling ability.

7.2.2 Electrochemical characterization

The electrochemical performance of Si/C anodes was examined using galvanostatic cycling at room temperature using the coin-half cell which was contracted Si/C as the anode, Li foil as the counter and reference electrode, and polymer as the separator. Cyclic voltammetry measurement shows two anodic peaks at 0.37 and 0.1 V and two cathodic peaks at 0.19 and 0.02 V. Si/C electrode with *c*-Pec-g-PAAm has higher anodic current peaks compared to other two *c*-PS-g-PAAm binders.

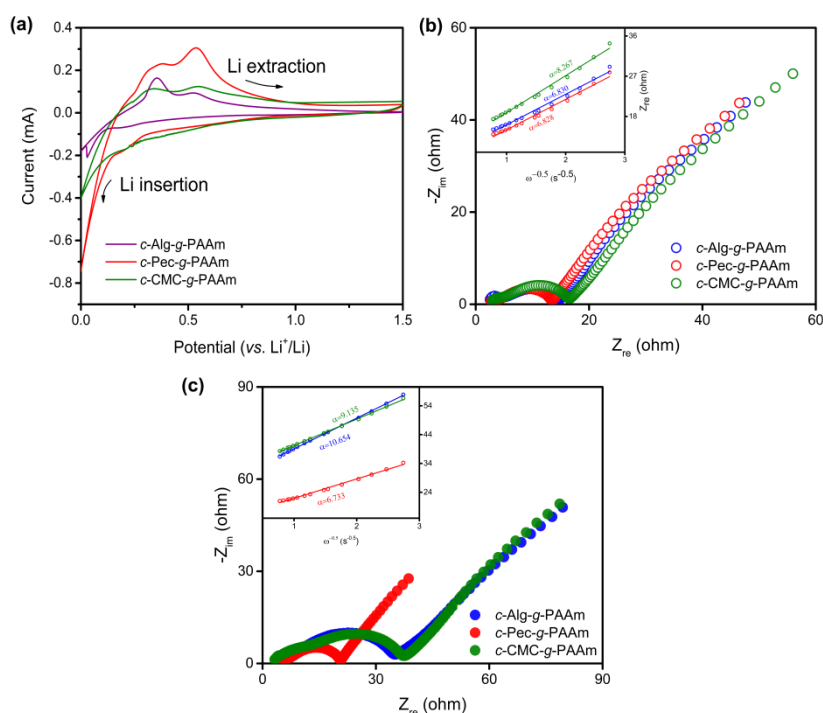


Figure 7-2 CV and Nyquist plots of Si/C electrode with various *c*-Ps-g-PAAm binders

(a) CV curve of fresh Si/C electrode, Nyquist plots (b) after 2th and (c) after 20th full charge/discharge cycled Si/C electrode with *c*-Alg-g-PAAm, *c*-Pec-g-PAAm and *c*-CMC-g-PAAm at 0.5 C

For furthermore, Li storage was carried out by impedance analysis to compare the Nyquist plot of Si/C electrode with *c*-Alg-g-PAAm, *c*-Pec-g-PAAm and *c*-CMC-g-PAAm after the second and the 20th full charge/discharge cycles at 0.5 C as seen in Figure 7.2 a and b, respectively. The Nyquist plot has two

depressed semicircles containing the high frequency semicircles and low frequency semicircle and the Warburg impedance of Li^+ diffusion in solid material, respectively. The equivalent circuit was drawn in Figure 3-4. The increase cycle numbers increase values of solution resistance (R_s) and charge transfer resistance (R_{ch}) for three electrodes in Figure 7-2b-c and the all value are reported in Table 7-1. Unfortunately, Si/C anode with *c*-Pec-*g*-PAAm is not much increased R_{ch} value from 10.51 to 17.2 Ω compared to same electrodes with *c*-Alg-*g*-PAAm (13.42 to 34.35 Ω) and *c*-CMC-*g*-PAAm (from 13.77 to 35.28), which means the lower loss electric conductivity inside electrode integrate after 20th charge/discharge cycles at 0.5 C. For future calculating the Li-ion diffusion coefficient, the relationship between the real impedance (Z_{re}) and the reciprocal square root of the angular frequency ($\omega^{-1/2}$) is plotted inside of Figure 7-2.

Table 7-1 Impedance parameters of Si/C anodes with various *c*-PS-*g*-PAAm binders

Investigation samples	Cycle number	R_s	R_{ch}	$1/R_{ch}$	$D (\times 10^{-10}) \text{ cm}^2 \text{ s}^{-1}$
<i>c</i> -Alg- <i>g</i> -PAAm	2nd	2.31	13.42	0.075	2.39
	20th	3.24	34.35	0.029	0.99
<i>c</i> -Pec- <i>g</i> -PAAm	2nd	1.54	10.51	0.095	2.39
	20th	4.12	17.27	0.058	2.46
<i>c</i> -CMC- <i>g</i> -PAAm	2nd	2.65	13.77	0.073	1.63
	20th	2.60	35.28	0.028	1.33

After the 20th, the lithium ion diffusion coefficients of Si/C-*c*-Alg-*g*-PAAm and Si/C-*c*-Alg-*g*-PAAm was decreased from 2.39 to 0.99 $\text{cm}^2 \text{ s}^{-1}$ and from 1.63 to 1.33 $\text{cm}^2 \text{ s}^{-1}$, respectively. In contrary, Si/C-*c*-Pec-*g*-PAAm electrode has not changed much compared 2th diffusion coefficient among all the anodes, demonstrating that dual-crosslinked *c*-Pec-*g*-PAAm was more stable in the charge/discharge process.

Charge-discharge cycling performance of Si/C electrode contained with tree dual-crosslinked binders showed stable anode performance for more than 200 cycles when measurement two percycles at 0.1 C and then continuously scanned 200 cycles at 0.5 C as seen in Figure 7-3a. The specific capacity of Si/C electrode contained with *c*-CMC-*g*-PAAm started at 947 mA g^{-1} in the first cycles at 0.5C and after 200 cycles its specific capacity was decreased to 567 mA g^{-1} which corresponding to 60% capacity retention. In compared to Si/C electrode with *c*-CMC-*g*-PAAm, another two saccharide based binders show several drops but the specific capacity of the Si/C-*c*-Alg-*g*-PAAm and Si/C-*c*-Pec-*g*-PAAm anodes remained 746 and 842 mA g^{-1} , respectively, after the 200 cycle. The poor performance of Si/C-*c*-CMC-*g*-PAAm anode can be explained higher stiffness and slight lower adhesion ability between binder and active material that cannot accommodate huge volume change of Si during lithium insertion and extraction. Even between Alg and Pec that function more elastic and high adhere, *c*-Pec-*g*-PAAm binder led to superior cyclic capacity to *c*-Alg-*g*-PAAm binder.

Furthermore, rate performance of Si/C electrode with *c*-Alg-*g*-PAAm, *c*-Pec-*g*-PAAm and *c*-CMC-*g*-PAAm were investigated at different scan rate from 0.1 C to 10 C and then current rate return back to 0.1 C from 10 C as displayed in Figure 7-3b. The Si/C electrode with *c*-Pec-*g*-PAAm shows a favorable high performance at all scan rate because of the high adhesion and better electrolyte uptake of pectin based

dual-crosslinked polymer. The specific capacity of Si/C-*c*-Pec-*g*-PAAm can reach from 1390.2 to 594.8 mA g⁻¹ at current rate from 0.1 to 10 C. After scanning at high rate, the capacity retention to its initial value at 0.1C was 73.8%, 71.74%, 69.54% for *c*-Alg-*g*-PAAm, *c*-CMC-*g*-PAAm, and for *c*-Pec-*g*-PAAm, respectively.

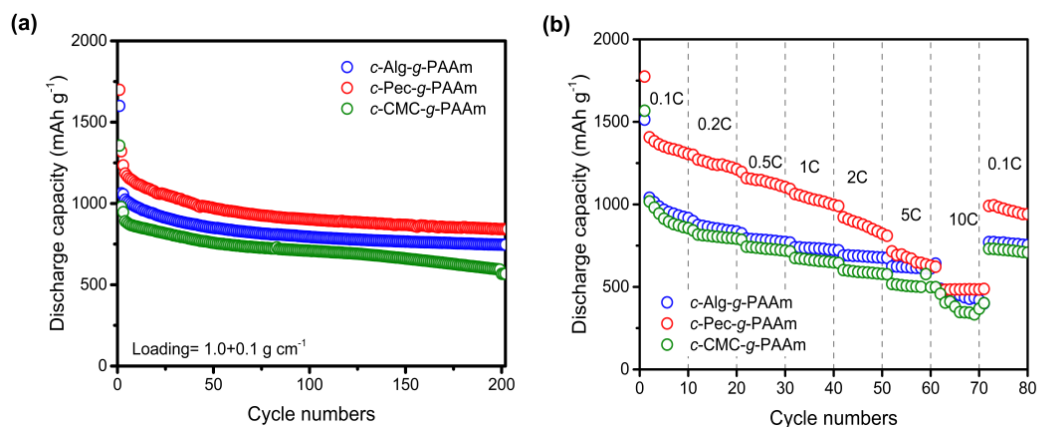


Figure 7-3 Electrochemical performance of Si/C with various *c*-Ps-*g*-PAAm binders anodes (a) cyclic performance, and (b) rate capability of Si/C electrodes with *c*-Alg-*g*-PAAm, *c*-Pec-*g*-PAAm and *c*-CMC-*g*-PAAm.

7.3 Conclusion

Herein, a comparative study of improving cyclic performance of high capacity Si/C electrodes was conducted with three *c*-PS-*g*-PAAm binders such as: *c*-Alg-*g*-PAAm, *c*-Pec-*g*-PAAm, and *c*-CMC-*g*-PAAm. At firstly, we examined the various characterizations of all three dual-crosslinked copolymer binders on physical and electrochemical performance of Si/C anode. Continuously, compared to highly stiffness CMC based dual-crosslinked binder, both *c*-Pec-*g*-PAAm and *c*-Alg-*g*-PAAm obtain a suitable electrolyte uptake, high ionic conductive and better mechanical ability after swollen in the electrolyte solvents for application as the binder for Si-based anode, resulting in the improvement of the cycling performance. In conclusion, *c*-Pec-*g*-PAAm can be potentially be utilized as a sustainable binder material to realize high-capacity and huge volume exchange Si-based materials.

8 Sulfonated alginate-graft-polyacrylamide

In this chapter, I focus on preparation of high ionic conductivity and adhesion binder based on polysaccharide through substitution reaction with various small sulfonated conjunction group and graft copolymerization with acrylamide monomer. Water-treated binders of sulfonated alginate-graft-polyacrylamide copolymer (SAlg-g-PAAm) with various sulfonate content have been synthesized and applied as a new candidate binder system for the stabilization of Si/C anodes. The structure and properties of Si/C-SAlg-g-PAAm-75 and Si/C-SAlg-g-PAAm-100 anodes were comparatively characterized by using pure alginate and Alg-g-PAAm without as reference binders.

8.1 Introduction

A number of recent papers have demonstrated the importance in the selection of the polymer binder to high capacity anodes experiencing huge volume changes such as silicon and their composites.^{20,21,127,128} Polysaccharide binders such as carboxymethyl cellulose (CMC),^{29,31} sodium alginate (Alg),³⁹ and other modified polysaccharides including their copolymerization and blend,^{71,129–131} showed excellent binder performance for silicon-based anodes, when compared to commercial polyvinylidene fluoride (PVDF) binder. But, their insulating nature on electronic and ionic conduction still suffers the high-power performance of Si electrodes, even though some progress was achieved by modifying the polysaccharide matrices through blending and grafting with electroactive oligomers or small molecular groups.^{132–135}

The blending of polysaccharide-based binders with a polymer containing ionically conductive groups provides a leap of lithium ion transport in electrode and ultimately improves cycling behavior of Si-based anodes. Recent works demonstrated that the lithium-ion conduction in polymeric binder significantly improved by the addition of polyethylene glycol (PEG) to polysaccharide and other polymeric binders, leading to the enhancement in the electrochemical performance of Si-based anodes^{19,20} Lee et al.¹³⁶ reported that blending and crosslinking between CMC and PEG showed stable cycling performance with a capacity of almost 2000 mAh g⁻¹ up to 350 cycles due to strong adhesion ability from CMC blocks and facile lithium ion movement originated from PEG block. PEG based block or graft copolymers have been also examined as a high performance binder for Si anodes.^{133,134,137} Triblock liner copolymer polydopamine-polyacrylic-polyoxyethylene (PDA-PAA-PEO) binder improved the cycle performance and reversible capacity for silicon anodes compared to Si/PVDF electrode due to its strong adhesion and high ion conductivity.¹³³

As a matter of fact, many works on grafting high adhesive polymer to polysaccharide binder contributed to improving the electrochemical performance of Si anodes. The polysaccharides grafted with PAA showed excellent binder properties for Si anodes compared to traditional linear polysaccharides due to the high binding ability of branched PAA to Si active materials.^{128,130,138} Recently, we investigated the alginate-graft-polyacrylamide (Alg-g-PAAm) as seen chapter 4 as a binder for Si-based anodes and showed better cycle life than the Si-based electrode containing Alg binder. It was originated from the

high adhesion of PAAm block.⁶⁴ Although the graft copolymer binder gives better adhesion to active material and current collector, it is still required to enhance the ionic conductivity for high powered electrodes.

The molecular designs of sulfonated polymers have been simulated as an ionic liquid membrane and an ionic conductivity binder for LIBs studies due to providing the high conductive with lithium ion from over sulfonated chain in polymer.^{139–142} For example, The sulfonated poly(ether-ether-ketone) (SPEEK) copolymers with sulfonic aromatic chains as applied the conductive binder in the cathode has great influence on the electrochemical performance, especially ionic conductivity through electrode compared with conventional PVDF binder.^{142,143} Qin et al.¹⁴⁴ developed the SPEEK with lithiated fluorinated sulfonamide groupsside (PSI) chains copolymer (SPEEK-PSI-Li) binder for Si electrode. The Si/SPEEK-PSI-Li electrode maintained over 500 mA g⁻¹ of specific capacity at high current rate compared with PVDF, CMC and Alg due to the lithium ionic transporting sulfonate groups, however high ionic conductivity SPEEK based copolymeric binders are still requested a non-ecofriendly 1-methyl-2-pyrrolidone (NMP) organic solvent for dissolving process and increase adhere.

Very recently, our group developed one-step process to prepare a sulfonated polysaccharide backbone to provide high ionic conductivity, increase adhere, and the thermal stability compared to its parent polysaccharide. Herein, the sulfonated alginate with graft polyacrylamide (SAIg-g-PAAm) which ionically conductive polymeric binder is constructed to silicon and graphite (Si/C) anode of LIB, leading to highly stable electrochemical performance compared to natural Alg and non-sulfonated graft copolymer.

8.2 Result and Discussion

8.2.1 Confirmation of sulfonated functionalized copolymer binder

Two-step synthetic procedure of sulfonated alginate-graft-polyacrylamide (SAIg-g-PAAm or SAGA) is illustrated Figure 8-1.

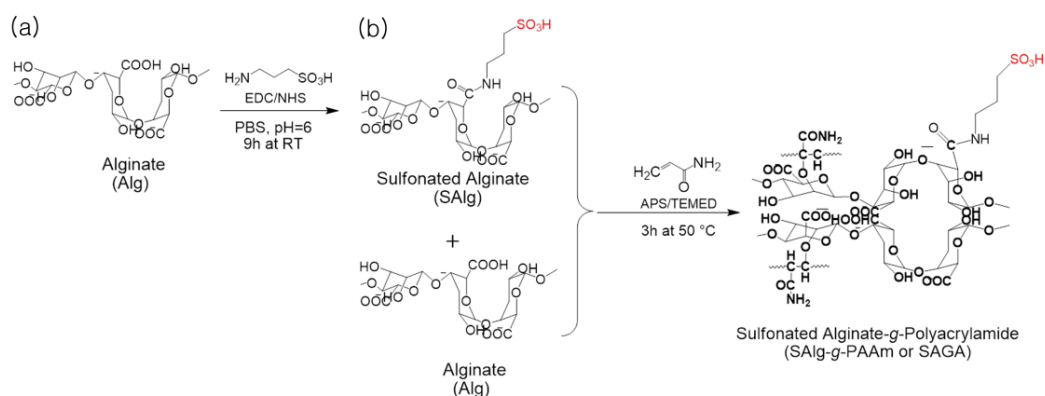


Figure 8-1 Synthesis schema of sulfonated graft copolymer

(a) Synthesis of Sulfonated Alg (SAIg backbone and (b) In-situ copolymerization of SAIg-g-PAAm

At first, we recently prepared the sulfonated polysaccharide backbone which 3APS conjugated onto the carboxylate functional groups in saccharide such as Alg using EDC (see Figure 8-1a) and characterized by FT-IR and TGA. In FTIR of sulfonated alginate (SAlg), the peak at 1082 cm^{-1} is attributed to a symmetric-stretching vibration of the sulfonic group, while the peaks at 1092 and 1033 cm^{-1} are designed to ester and hydroxyl group in alginate. After sulfonic group conjugated onto alginate backbone, thermal degradation yield is much over 50 wt% that than pure Alg that is indicated higher thermal stability is coming from percentage of sulfonated group onto alginate backbone. FTIR and TGA results show carboxyl group onto alginate backbone has replaced by sulfonated conjunction groups to produce SAlg (Figure 8-2a, b).

After preparation of sulfonated alginate source, we synthesized polyacrylamide grafted into the sulfonated alginate with different weight ratio of pure Alg and SAlg using as in-situ graft copolymerization method with radical initiator system for 3 h at 50 °C as seen in Figure 8-1b and Table 8-1. Finally, the synthesis product was washed by solvent mixture of ethanol and distillation water and was dried convection oven and vacuum oven to form SAlg-g-PAAm-75 as denoting as SAGA-75 and SAlg-g-PAAm-100 as denoting as SAGA-100.

Table 8-1 Ingredient of graft copolymerization (g)

Sample	Note	Alg, g	SAlg, g	Acrylamide monomer, g	APS, g	TEMED, g
Alg-g-PAAm	AGA	2.8	0.0	10	0.06	0.055
SAlg-g-PAAm-75	SAGA-75	0.7	2.1	10	0.06	0.055
SAlg-g-PAAm-100	SAGA-100	0.0	2.8	10	0.06	0.055

FTIR spectrum of pure saccharide and modified saccharide through as PAAm grafting on pure alginate and sulfonated alginate backbone is shown in Figure 8-2c. Compared to the FTIR spectra of pure Alg with highly observation peaks in the range of 1150 to 1100 cm^{-1} , a characteristic peak intensity at 1092 and 1033 cm^{-1} is reality weakened in Alg-g-PAAm (AGA) samples that corresponds to the chemical bond between hydroxyl group in Alg and p band in PAAm.^{54,64} In addition, the adsorption four new peaks indicated to PAAm (Figure 8-2a), were displayed in the spectrum of all PAAm graft copolymer samples as seen Figure 8-2c. In comparison the non-sulfonated conjugate group AGA sample, a distinguishing characteristic of sulfonated graft copolymer samples (SAGA-75 and SAGA-100) were a presence of new observation peaks at 1075 and 1160 cm^{-1} in spectra that assigned as sulfonic acid group.^{145,146} In addition, S-O and C-S stretching bands were observed at the range of 700-500 cm^{-1} on FTIR spectrum of all sulfonated copolymer (Figure 8-2c). As increase the ratio of SAlg backbone in PAAm grafted copolymer increased the sulfonate group peaks intensity in FTIR spectrum of SAGA-100 as seen Figure 8-2c.

Thermal characterization analysis as TGA was used characterization of degree of sulfonated group in graft copolymer. Figure 8-2d shows the TGA curve of SAGA typed samples compared to pure Alg and non-sulfonated group AGA. The pure Alg exhibit higher thermal stability than the all modified Alg

based samples until 750°C due to loss of the conjugating sulfonate groups and graft PAAm onto backbone.^{54,147} In moreover, the thermal stability was slightly increased with the high amount of sulfonic acid group on graft copolymer shown in Figure 8-2 b and d.¹⁴⁸ Those both of two results indicated that sulfonated alginate-graft-polyacrylamide was successfully prepared by radical imitator. It might be achieved that the sulfonated polymeric binder shows small effect in the improvement of thermal stability whereas it makes a big improvement for mechanical stability and ionic conductivity as the increase content of sulfonic acid group in the graft copolymer.

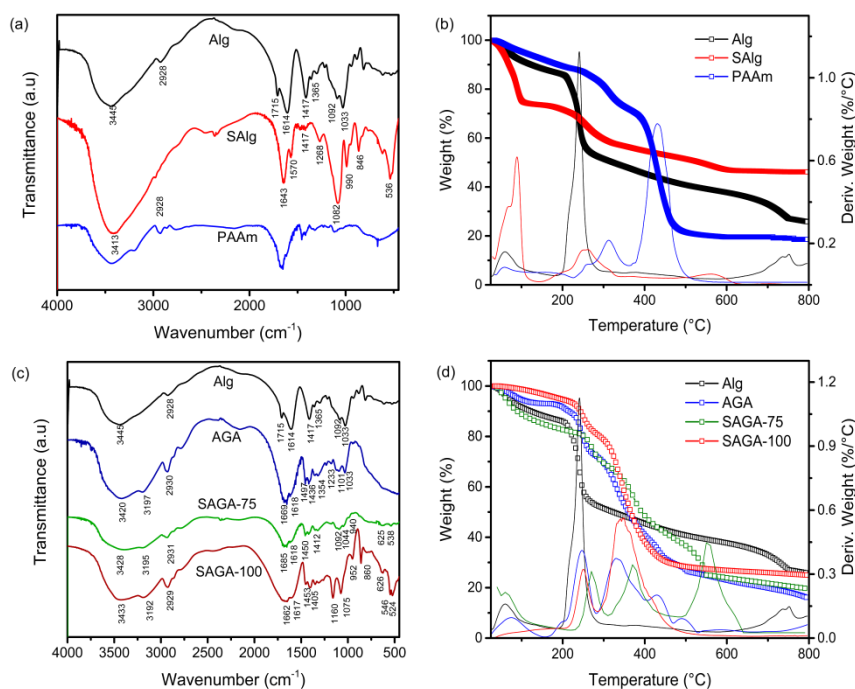


Figure 8-2 Spectrometer and thermal analysis of sulfonated graft copolymer

(a) FT-IR spectrometry and (b) TGA curve of pure Alg, conjugated sulfonated Alg, and a synthetic PAAm ; and (c) FT-IR spectra, (b) TGA curve of pure Alg and modified Alg through conjugating sulfonic acid group and grafting PAAm polymers

8.2.2 Physical characterization of polymer

The mechanical properties of the modified alginate-based film which cast from water with 30 wt.% of glycerol as plasticizer, was performed the tensile strength testing. The brittle Alg sample with low elongation, when modification through sulfonated and grafted PAAm onto backbone, was found to be enhanced mechanical ability with elongation at break of over 2 strains as shown in Figure 8-3a. Our target samples with increasing content of sulfonic acid group in the graft copolymer films exhibited relatively 4.5 mPA of mechanical strength with an elongation up to 3.2 strains due to formation of highly cohesion between polymers by ionic groups.^{145,147,149}

The ionic conductivity of the polymer membranes, where placed between two parallel stainless-steel (SS) electrodes with and without electrolyte was determined by EIS at room temperature (as seen Figure 8-3b) and that measurement was detailed well by Chauque et al.¹⁵⁰ At the first, the resistance value of the

membrane can be estimated from an extrapolation of real impedance at high frequency range in Nyquist plot as seen the left side-top inside of Figure 8-3b and the ionic conductivity are calculated using equation 3.2. As the result, the ionic conductivity value of dry membrane determined to be 1.16×10^{-6} for Alg, 2.06×10^{-6} for AGA, 2.31×10^{-6} for SAGA-75, and 6.09×10^{-6} S cm^{-1} for SAGA-100, respectively. Continuously, the ionic conductive values of wet state polymer membranes are improved with presence of carbonate electrolyte and there founded that 2.08×10^{-6} for Alg, 2.033×10^{-6} for AGA, 2.47×10^{-6} for SAGA-75, and 1.13×10^{-5} S cm^{-1} for SAGA-100, respectively. The high ionic conductivity of sulfonated membranes is mainly contributed by high content of sulfonic acid group in graft copolymer.^{145,151}

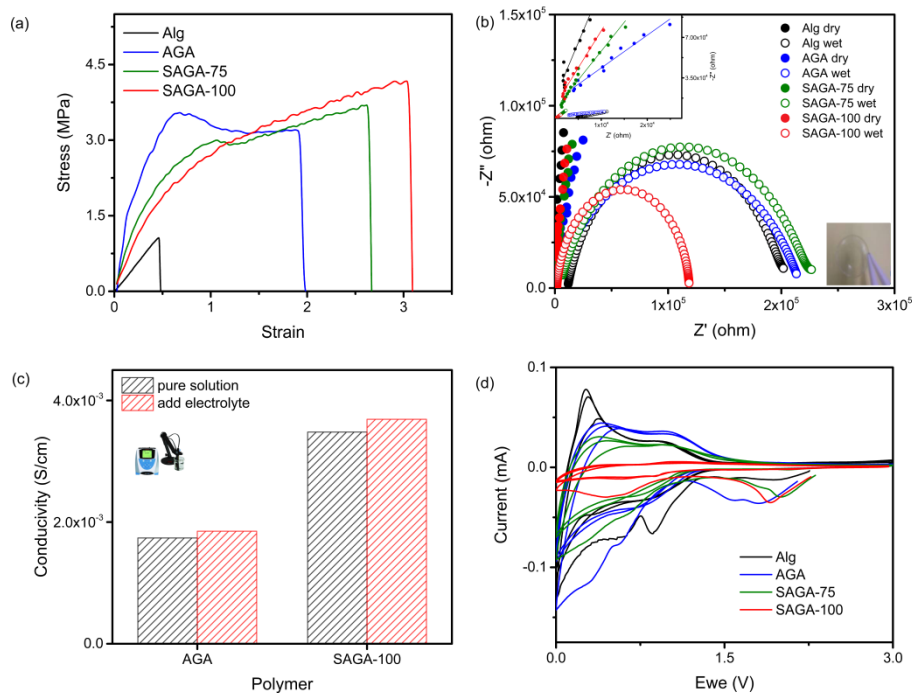


Figure 8-3 Mechanical and ionic conductivity properties of binder films.

(a) Stress-Straining curve of pure Alg and modified Alg through conjugating sulfonic acid group and grafting PAAm polymers (b) Nyquist plot SS/various polymer half-cell without and with electrolyte, (c) ionic conductivity of the polymeric binder in solvent by conductivity-meter and (d) cyclic voltammetry of four binder/Supper-P films

That result are also confirmed by the ionic conductivity of binder solution after adding electrolyte as seen in Figure 8-3d. In addition, to determine the electrochemical stability of binder, we prepared a composite electrode of binder/SupP with 50/50 wt.% and tested CV measurement at range of 0.0-3.0V vs. Li/Li^+ . As the result, all binder/SupP composite electrodes showed electrochemical inactivity at this current area due to its only appearance of electrolyte decomposing layer and the lithium insertion/extraction (Figure 8-3d). As all the result, modified alginate trough conjugating sulfonic group and PAAm graft, which is mechanically and electrochemical stable, is provided as the ionic conductive binder for high-volume exchange Si-based composed anodes.

The adhesion strength between active materials and current collector, however, a critical characterization

on huge volume exchange Si electrode during charge/discharge process, can be clearly depended upon mechanical properties and the electrolyte-uptake of polymeric binder.¹⁰⁹ In Figure 8-4, the peeling strength of Si/C with pure Alg was extremely improved from ~2 N up to over 10 N, whereas the electrolyte-uptake into binder films was decreased from 12 wt.% into lower than 5 wt.% due to building enable cohesion/adhesion in composite electrode by through conjugating sulfonated group and grafting PAAm on alginate. The enhanced elastomer and ionic conductivity SAGA-100 sample shows ~15 N of adhesion strength and 3.5 wt.% swelling ratio, which ensured good mechanical property for Si/C electrode as shown Figure 8-4. Consistent with the result in slurry, we examined the electronic conductivity of Si/C slurry films using the sheet resistance measurement by performed four-point probe instrument (Figure 8-4c).

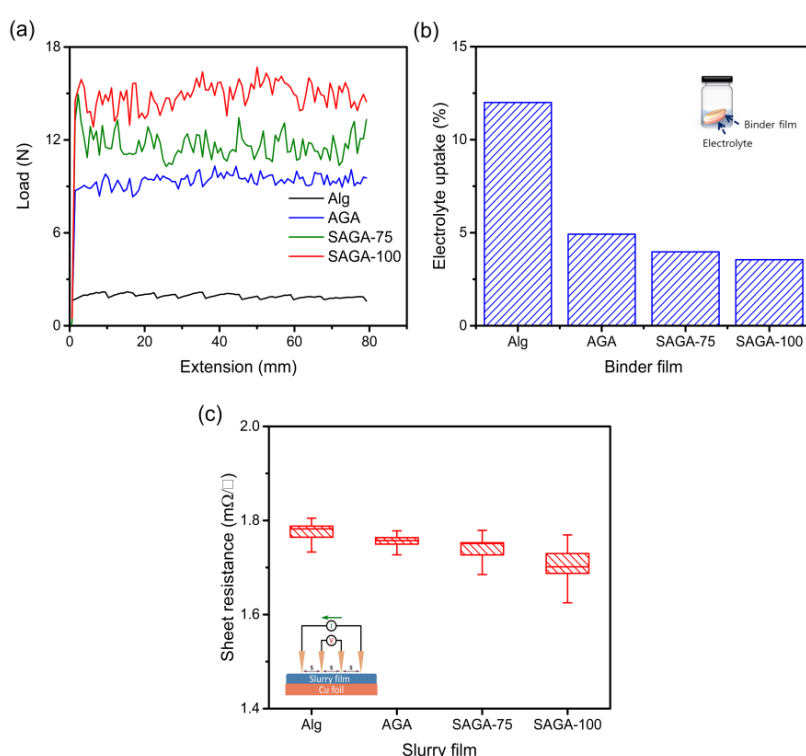


Figure 8-4 Adhesion and sheet resistance of Si/C slurry film.

(a) Adhesion strength of the Si/C electrodes containing different binders measured by 180° peel test, (b) the amount of electrolyte uptake of polymer films immersed in the electrolyte solvent (EC:DMC:EMC) at 25 °C for 48 h, and (c) Sheet resistance of 25 μm thick Si/C slurry films.

Herein, SAlg based copolymer binders were the lower sheet resistance than non-functionalized Alg and AGA, respectively. In the result, the conjugating sulfonic acid group in copolymer binder could help to improve the interconnection between electrode composite materials and current collector due to a decrease the sheet resistance of Si/C electrode, which was good issues on electrochemical performance for Si based electrode in LIB.

8.2.3 Electrochemical characterization

The electrochemical performance of Si/C electrode with different binders was obtained by CV, EIS, galvanostatic cycling, and in-situ ECD instruments. CV profiles of Si/C electrode with different binders

were displayed two anodic peaks around at 0.005 and 0.23 V for lithiation and two cathodic peaks at nearly to 0.28 and 0.47 V for delithiation (Figure 8-5a). It is clearly seen that the increase ionic conductivity of polymeric binders was directly affected on electrochemical activity area of Si/C electrode for lithium insertion and extraction due to showing higher current for SAGA-100 binder than pure Alg binder.

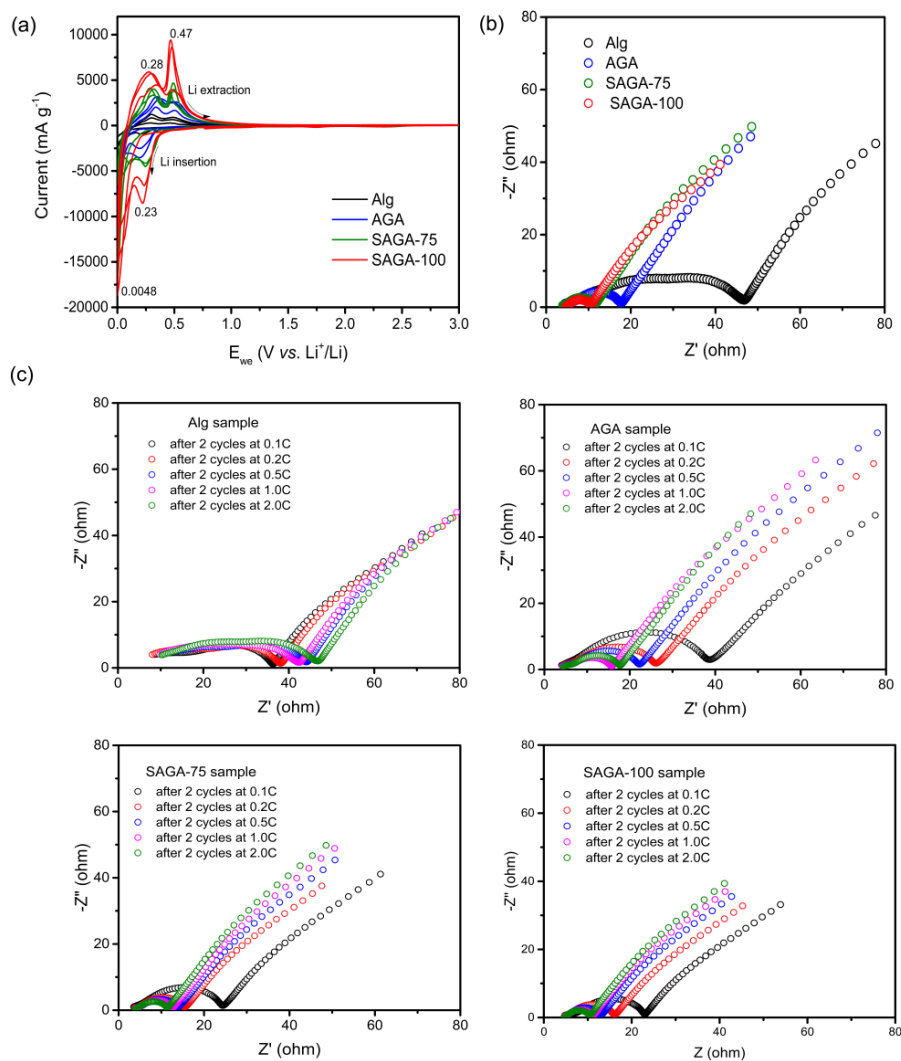


Figure 8-5 Voltammeter and impedance curve of Si/C electrode with various binders

(a) Cyclic voltammogram of the fresh Si/C electrodes containing different binders, (b) comparison study of EIS of the Si/C electrodes with four binders measured at 0.2 V, and (c) Nyquist plot of Si/C electrode containing four binders with the frequency range from 100 kHz to 0.01 Hz after charge-discharge at various current rates.

Continuously, the lithium ion storage property of Si/C electrode was evaluated using EIS after two galvanic cycles at various current densities from 0.1 C to 2.0 C (Figure 8-5 b and c). Herein, the semicircle behavior on Nyquist plot was decreased for all Si/C electrode with modified Alg binders as increase C-rate, expect same electrode with pure Alg that implicated to huge Si pulverization might occurred on pure adhere Alg binder. Figure 8-5b comparatively shows Nyquist plots for all binder with the applied voltage of 0.2 V vs. Li/Li⁺ at high current rate of 2.0 C, and summarized result of fitting

analysis and calculation of lithium diffusion coefficient at Table. 8.2. The modification through sulfonated and grafted PAAm onto alginate decrease a charge transfer resistance and increase a diffusion coefficient of Li^+ into bulk of electrode materials which is assigned to enhanced ionic conductive and adhere ability.

Table 8-2 Impedance parameters of Si/C anodes with various binder

Capacity rate, C	R_s , ohm	R_{ch} , ohm	$1/R_{ch}$, ohm^{-1}	$D (\times 10^{-10}) \text{ cm}^2 \text{ s}^{-1}$
Si/C-Alg				
0.1	5.35	32.88	0.030	1.75
0.2	5.25	34.04	0.029	1.26
0.5	8.05	35.19	0.028	0.98
1.0	6.79	34.39	0.029	0.88
2.0	7.04	41.81	0.024	0.77
Si/C-AGA				
0.1	4.13	34.0	0.029	1.57
0.2	4.41	21.6	0.046	1.79
0.5	4.32	17.9	0.056	1.82
1.0	4.27	10.8	0.092	1.02
2.0	4.52	12.5	0.080	0.95
Si/C-SAGA-75				
0.1	3.34	21.17	0.047	1.88
0.2	3.78	11.75	0.085	2.33
0.5	3.57	10.66	0.094	2.31
1.0	4.02	8.66	0.115	2.03
2.0	3.42	8.42	0.119	2.18
Si/C-SAGA-100				
0.1	6.59	16.3	0.061	2.03
0.2	4.83	11.6	0.086	2.71
0.5	4.67	8.5	0.118	2.88
1.0	4.84	5.9	0.171	2.84
2.0	4.83	5.4	0.185	2.87

The cycling stability of Si/C electrode with various binders at 0.5 C after 200 cycles illustrates in Figure 8-6a. As result, the high content sulfonated in graft copolymer samples, Si/C-SAGA-100 electrode remains the higher specific capacity of 750 mAh g^{-1} compared to Alg (381 mAh g^{-1}), AGA (576 mAh g^{-1}), and SAGA-75 (651 mAh g^{-1}), respectively. To compare both sulfonated copolymer based electrode with high mass loading samples, Si/C-SAGA-75 electrode shows the slower decay in the capacity since over 150 cycles and the capacity retention records 66% for SAGA-100 and 49% for SAGA-75 electrode as shown in Figure 8-6b. This is indicated the increase contents of sulfonic acid group in graft copolymer binder have achieved high stability and reversibility for Si/C electrode during lithium charge/discharge cycles. When the high-rate capability of Si/C electrodes test were completely recorded from 0.1 C to 10 C and finally returned to 0.1 C, the specific capacity and capacity retention of all four electrodes restored to its initial values that leading to be better rate capability of all electrodes as illustrated in Figure 8-6c. The highest reversible rate capability of 763.0 mAh g^{-1} at 10 C was recorded for Si/C containing SAGA-100 binder whereas it was determined 86.9 mAh g^{-1} for pure Alg, 432.7 mAh g^{-1} for AGA, and 718.7 mAh g^{-1} for SAGA-75 under same condition, respectively. This result is also supported by the charge transfer resistance values for SAGA-100 binder at high current rate of 2.0 C were lower than that of pure Alg as seen Figure 8-5c.

The technique of in-situ ECD is applied to study the volume exchange behavior of Si/C electrode with different binders during charge and discharge at 0.1 C, as detailed in our pervious study.⁶⁴ Herein, all electrodes illustrated the expansion by lithium insertion into electrode and a compression upon lithium extraction as seen Figure 8-6d. Herein, high electrode thickness in the first charging was showed for pure Alg and AGA with 225.0 and 120.0 μm , respectively, but that swelling behavior of Si/C electrodes was became smaller with the sulfonate group on Alg backbone due to the aggregate amount of ionic group to form high buffer action on huge volume exchange of Si based electrode.^{149,152}

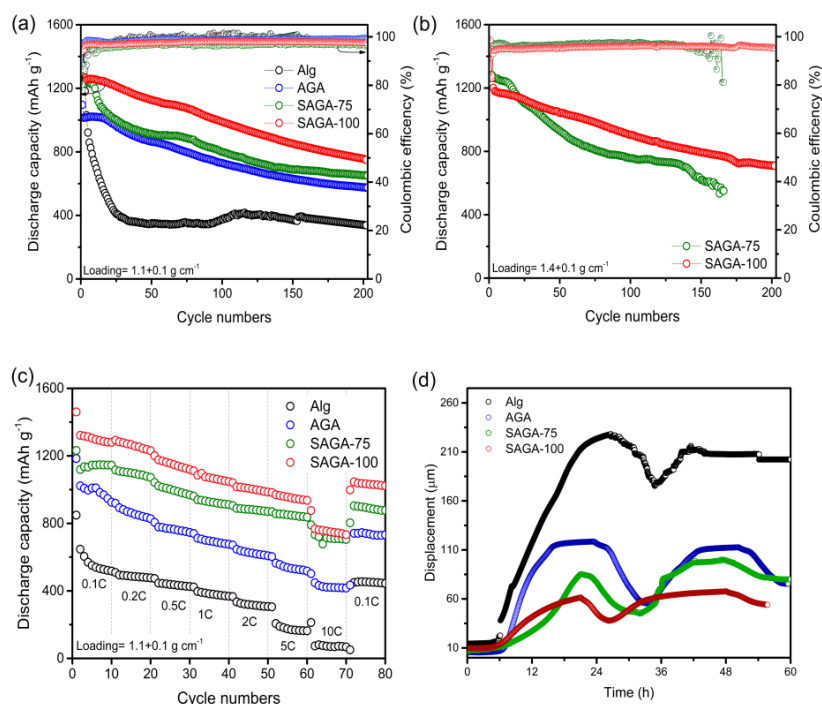


Figure 8-6 Galvanostatic performance of Si/C electrode

Cyclic performance of Si/C electrodes with difference electrode loadings: (a) 1.1 g cm⁻¹ and (b) 1.5 g cm⁻¹, (c) rate capability performance of the Si/C electrodes, and (d) the change in the thickness of Si/C electrode during charge/discharge cycling at 0.1C.

In order to connect the effect of binder on the electrode performance with surface morphology, Si/C electrode with four binders were visualized using SEM by disassembling the coin cell in Ar-filled glove box after 200 cycles at 0.5 C as shown in Figure 8-7. After cycling test, the surface of the pristine Si/C containing Alg electrode was fully covered a tickly smoother passivation film which is implied by uncontrolled grown of a solid electrolyte interphase (SEI) layer on the Si/C electrode due to its low adhesion between electrode integrity and the current collector. While modification of alginate through sulfonated and graft copolymer, its ionic ability and high adhesion, the surface of Si/C electrodes shows a preserved porous structure and a relatively stability SEI layer appearance. The increase of sulfonated content in graft copolymer decreases multiple-cracking on the surface (in Figure 8-7 right-hand column) thus leading to a significant improvement in the cycle stability and rate performance caused by SAGA binder.

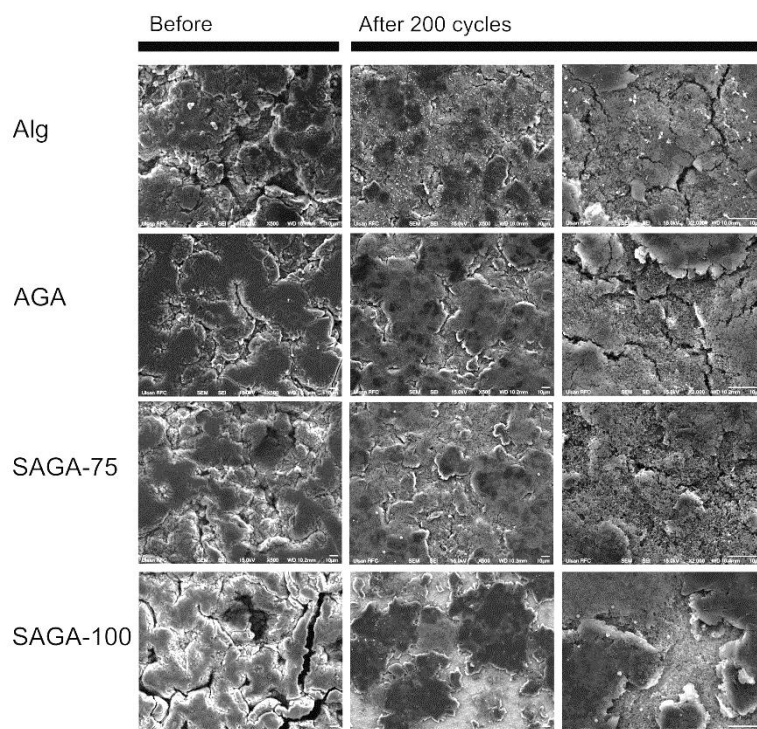


Figure 8-7 Top-view SEM analysis of Si/C electrode with four binders

8.3 Conclusion

In this study, we synthesis sulfonated alginate-graft-polyacrylamide (SAlg-g-PAAm) from pure alginate (Alg) by two in-situ step methods. Herein, sulfonated group propose to increase ionic conductivity and PAAm unite in graft copolymer improves an adhesion ability on poor mechanic ability of Alg. At first, pure Alg was substituted modification that carboxyl groups on alginate backbone replaced by sulfonated conjugation groups by condensation reactions to produce a sulfonated alginate (SAlg). Then both of Alg and SAlg with different ratio are in-situ copolymerized with acrylamide monomers with a free radical initiator at nitrogen atmosphere. Finally, we prepared three graft copolymers from the alginate backbone including Alg-g-PAAm (AGA), SAlg-g-PAAm-75 (SAGA-75), and SAlg-g-PAAm-100 (SAGA-100). Herein, all synthetic graft copolymers investigate by efficiency binder systems for high capacity Si/C anode. Compared to the pure alginate binder, sulfonated graft copolymer binders show benefitting from the structural advantages to high elongation and ionic conductivity properties for binder film. Thus, increasing of sulfonated content in graft copolymer increase adhesion ability between Si/C active materials and current collector, leading to has stable cycling performance after 200 cycles and capacity retention at high current rate. In addition, the Si/C electrode with SAGA-100 binder exhibits higher lithium diffusion and lower charge resistance at high current rate while the impedance study made at various current rates. That is correlated to increase of electronic conductivity and high adhesion ability provides by high content amount of sulfonic group in graft copolymer.

Summary

In this thesis, the experimental results on employing modification of polysaccharide through graft and crosslink progress as a new designed water-treat binder to improve performances of high capacity silicon based electrode as well as to provide an adhere ability between an active material particles and current collector and enable electrolyte-uptake, which will be briefly summarized here.

The work started with the design and synthesis for polysaccharide backbone grafted with acrylamide monomer by in-situ graft copolymerization with thermal initiator systems to product polysaccharide-*graft*-polyacrylamide (PS-*g*-PAAm). Then that graft copolymer was used for preparation of a dual-crosslinked PS-*g*-PAAm (*c*-PS-*g*-PAAm) as our target binder system for silicon/graphite (Si/C) with 1/3 weight ratio anode compared to pure PS and PS-*g*-PAAm. We have selected three most popular three polysaccharides as source backbone materials for graft copolymer such as alginate (seen in Chapter 4), carboxymethyl cellulose (as seen in Chapter 5), and pectin (as seen in Chapter 6). There are similarly consist carboxyl- and hydroxyl- functional groups in the molecular structure expect differ solely in their monomer linkages.

At firstly, all different backbone saccharides are modified through grafting and crosslinking and then these synthetic polymer products are employed by new candidate binder system for Si-based anode to compare their pure saccharide, respectively. All comparative examination results separately discussed into three chapter: alginate-based binder system as seen in Chapter 4, carboxymethyl cellulose-based binder system as shown in Chapter 5, and pectin-based binder system as seen in Chapter 6. For instance, I briefly conclude the chapter 4 inside of description above three chapters (from chapter 4 to chapter 6) in this current situation, because their examinations are systematically tested same procedure for improvement electrochemical performance of Si/C anode expect compared with various saccharide source. In chapter 4, the effect of pure alginate and modified alginate-based binders in Si/C anode investigated in 2032 half-coin cell with lithium foil as a counter and reference electrode. The physical and electrochemical properties of the dual crosslinked *c*-Alg-*g*-PAAm anode are characterized to compared with pure Alg, crosslinked Alg, and Alg-*g*-PAAm anode, It is found that the adhesion strength and electrolyte uptake of Si/C-*c*-Alg-*g*-PAAm anode is greatest than that other anodes. These properties of dual crosslinked binder contribute to smaller impedance, high lithium diffusion, and effectively buffering the volume expansion during lithiation. In summarize, all various dual-crosslinked *c*-PS-*g*-PAAm binders systems exhibit better specific discharge capacity and cycle performance compared to pure PS and graft copolymer PS-*g*-PAAm.

Future more, we demonstrated that a water-treated dual-crosslinked graft copolymer between three saccharides and PAAm (*c*-PS-*g*-PAAm) was an effective binder for the high-capacity Si/C electrode compared with pure polysaccharides in chapter 7. Inspired by these resulting, we examine and compare herein three different *c*-PS-*g*-PAAm binders for Si-based electrode (there are included the Si/C-*c*-Alg-*g*-

PAAm, Si/C-*c*-Pec-*g*-PAAm, and Si/C-*c*-CMC-*g*-PAAm electrodes, respectively). We examined the various characterizations of all three dual-crosslinked graft copolymer binders on physical and electrochemical performance of Si/C anode. Through compression study of various physical characterizations of three dual-crosslinked *c*-PS-*g*-PAAm, both *c*-Pec-*g*-PAAm and *c*-Alg-*g*-PAAm obtain a suitable electrolyte uptake, high ionic conductive and better mechanical ability after swollen in the electrolyte solvents that than *c*-CMC-*g*-PAAm due to non-rigid molecular structure for alginate and pectin. Even between Alg and Pec that function more elastic and higher adhere, *c*-Pec-*g*-PAAm binder led to superior cyclic capacity to *c*-Alg-*g*-PAAm binder. Si/C-*c*-Pec-*g*-PAAm electrode shows significantly improved cycling performance with a specific capacity of 842 mAh g⁻¹ at 0.5 C after 200 cycles compared to same electrode with *c*-Alg-*g*-PAAm (746 mAh g⁻¹) and *c*-CMC-*g*-PAAm (567 mAh g⁻¹). In conclusion, *c*-Pec-*g*-PAAm can be potentially be utilized as a sustainable binder material to realize high-capacity and huge volume exchange Si-based materials. Unfortunately, our developing PS-*g*-PAAm copolymer with branching structured has much higher adhesion strength than pure linear saccharide due to adhere part of polyacrylamide, but it is still limited by the ionic conductive characterization in high-capacity Si-based anode during lithium insertion.

Finally, these finding render than branching designed PS-*g*-PAAm polymers are one of the most promising materials for high-capacity Si based anode. Furthermore, the conjunctivitis of the ionic conductive functionalized part onto pure saccharide backbone to behave ionic conductive properties, then that sulfonated saccharide backbone was grafted with the acrylamide monomer to produce a sulfonate PS-*g*-PAAm (SPS-*g*-PAA). Herein, we significantly examined an ionic conductivity polymeric binder as sulfonated alginate-*g*-polyacrylamide (SAlg-*g*-PAAm) for Si/C electrode. The sulfonated-Alg based copolymer binders found the higher ionic conductivity from impedance analysis, lower sheet resistance form four-proof sheet resistance and higher mechanical performance from peel strength test than non-functionalized Alg and Alg-*g*-PAAm, respectively. Thus, increase of sulfonated conjunction content in SAlg-*g*-PAAm copolymer binder shows the improvement electrochemical performance of the Si/C electrode. As seen as in-situ electrochemical dilatometer analysis, high electrode thickness in the first charging was showed for pure Alg and Alg-*g*-PAAm with 225.0 and 120.0 μm, respectively, but that swelling behavior of Si/C electrodes was became smaller with the SAlg-*g*-PAAm binder due to the aggregate amount of ionic group to form high buffer action on huge volume exchange of Si based electrode. Hence, I conclude modification polysaccharides through grafting material are promising water-treated adhesive binder material for huge volume expansion silicon anode and major interest to comprehensive number of energy source research field.

Reference

- 1 M. Wakihara and O. Yamamoto, *Lithium Ion Batteries: Fundamentals and Performance*, John Wiley & Sons, Incorporated, Berlin, GERMANY, 2008.
- 2 M. Armand and J.-M. Tarascon, *Nature*, 2008, **451**, 652–657.
- 3 R. Van Noorden, *Nat. News*, 2014, **507**, 26.
- 4 M. Endo, C. Kim, K. Nishimura, T. Fujino and K. Miyashita, *Carbon*, 2000, **38**, 183–197.
- 5 B. Scrosati and J. Garche, *J. Power Sources*, 2010, **195**, 2419–2430.
- 6 Y. Nishi, *J. Power Sources*, 2001, **100**, 101–106.
- 7 M. K. Gulbinska, B. Ravdel, F. J. Puglia, S. H. Cohen, S. Santee, J. S. Gnanaraj and W. A. McPhee, *Lithium-Ion Battery Materials and Engineering: Current Topics and Problems from the Manufacturing Perspective*, Springer, London, UNITED KINGDOM, 2014.
- 8 S.-L. Chou, Y. Pan, J.-Z. Wang, H.-K. Liu and S.-X. Dou, *Phys. Chem. Chem. Phys.*, 2014, **16**, 20347–20359.
- 9 M. S. Whittingham, *Chem. Rev.*, 2004, **104**, 4271–4302.
- 10 J.-M. Tarascon and M. Armand, *Nature*, 2001, **414**, 359–367.
- 11 C. Xu, Y. Chen, S. Shi, J. Li, F. Kang and D. Su, *Sci. Rep.*, 2015, **5**, 14120.
- 12 Article Metrics - Lithium batteries, <https://www.nature.com/articles/526S93a/metrics>, (accessed July 14, 2018).
- 13 M. Winter and J. O. Besenhard, *Electrochimica Acta*, 1999, **45**, 31–50.
- 14 F. M. Courtel, S. Niketic, D. Duguay, Y. Abu-Lebdeh and I. J. Davidson, *J. Power Sources*, 2011, **196**, 2128–2134.
- 15 J. Chen, L. Yang, S. Fang, S. Hirano and K. Tachibana, *J. Power Sources*, 2012, **200**, 59–66.
- 16 K. Higa and V. Srinivasan, *J. Electrochem. Soc.*, 2015, **162**, A1111–A1122.
- 17 S. D. Beattie, D. Larcher, M. Morcrette, B. Simon and J.-M. Tarascon, *J. Electrochem. Soc.*, 2008, **155**, A158–A163.
- 18 G. X. Wang, J. H. Ahn, J. Yao, S. Bewlay and H. K. Liu, *Electrochem. Commun.*, 2004, **6**, 689–692.
- 19 C.-M. Park, J.-H. Kim, H. Kim and H.-J. Sohn, *Chem. Soc. Rev.*, 2010, **39**, 3115–3141.
- 20 N. Ding, J. Xu, Y. Yao, G. Wegner, I. Lieberwirth and C. Chen, *J. Power Sources*, 2009, **192**, 644–651.
- 21 H. Wu and Y. Cui, *Nano Today*, 2012, **7**, 414–429.
- 22 A. Urban, D.-H. Seo and G. Ceder, *Npj Comput. Mater.*, 2016, **2**, 16002.
- 23 C. Hwang, S. Joo, N.-R. Kang, U. Lee, T.-H. Kim, Y. Jeon, J. Kim, Y.-J. Kim, J.-Y. Kim, S.-K. Kwak and H.-K. Song, *Sci. Rep.*, 2015, **5**, 14433.
- 24 M. Winter, J. O. Besenhard, M. E. Spahr and P. Novák, *Adv. Mater.*, 1998, **10**, 725–763.
- 25 J. O. Besenhard, J. Yang and M. Winter, *J. Power Sources*, 1997, **68**, 87–90.
- 26 M. Yoshio, R. J. Brodd and A. Kozawa, *Lithium-Ion Batteries: Science and Technologies*, Springer, New York, NY, UNITED STATES, 2010.
- 27 N.-S. Choi, S.-Y. Ha, Y. Lee, J. Y. Jang, M.-H. Jeong, W. C. Shin and M. Ue, *J. Electrochem. Sci. Technol.*, 2015, **6**, 35–49.
- 28 S. Spirk, *Polysaccharides As Battery Components*, Springer, Cham, SWITZERLAND, 2017.
- 29 H. Buqa, M. Holzapfel, F. Krumeich, C. Veit and P. Novák, *J. Power Sources*, 2006, **161**, 617–622.
- 30 J.-S. Bridel, T. Azaïs, M. Morcrette, J.-M. Tarascon and D. Larcher, *Chem. Mater.*, 2010, **22**, 1229–1241.
- 31 J. Li, R. B. Lewis and J. R. Dahn, *Electrochem. Solid-State Lett.*, 2007, **10**, A17–A20.
- 32 M. Yoo, C. W. Frank, S. Mori and S. Yamaguchi, *Chem. Mater.*, 2004, **16**, 1945–1953.
- 33 M. Yoo, C. W. Frank and S. Mori, *Chem. Mater.*, 2003, **15**, 850–861.
- 34 N. Işıklan, F. Kurşun and M. İnal, *Carbohydr. Polym.*, 2010, **79**, 665–672.
- 35 J. Chong, S. Xun, H. Zheng, X. Song, G. Liu, P. Ridgway, J. Q. Wang and V. S. Battaglia, *J. Power Sources*, 2011, **196**, 7707–7714.
- 36 A. Magasinski, B. Zdyrko, I. Kovalenko, B. Hertzberg, R. Burtovyy, C. F. Huebner, T. F. Fuller, I. Luzinov and G. Yushin, *ACS Appl. Mater. Interfaces*, 2010, **2**, 3004–3010.
- 37 Y.-S. Park, E.-S. Oh and S.-M. Lee, *J. Power Sources*, 2014, **248**, 1191–1196.
- 38 C. C. Nguyen, T. Yoon, D. M. Seo, P. Guduru and B. L. Lucht, *ACS Appl. Mater. Interfaces*, 2016, **8**, 12211–12220.
- 39 I. Kovalenko, B. Zdyrko, A. Magasinski, B. Hertzberg, Z. Milicev, R. Burtovyy, I. Luzinov and G. Yushin, *Science*, 2011, **334**, 75–79.
- 40 M.-H. Ryou, J. Kim, I. Lee, S. Kim, Y. K. Jeong, S. Hong, J. H. Ryu, T.-S. Kim, J.-K. Park, H. Lee and J. W. Choi, *Adv. Mater.*, 2013, **25**, 1571–1576.
- 41 J. Liu, Q. Zhang, Z.-Y. Wu, J.-H. Wu, J.-T. Li, L. Huang and S.-G. Sun, *Chem. Commun.*, 2014, **50**, 6386–6389.
- 42 J. Yoon, D. X. Oh, C. Jo, J. Lee and D. S. Hwang, *Phys. Chem. Chem. Phys.*, 2014, **16**, 25628–25635.
- 43 L. Wei, C. Chen, Z. Hou and H. Wei, *Sci. Rep.*, 2016, **6**, 19583.

- 44 Y. Bie, J. Yang, Y. Nuli and J. Wang, *J. Mater. Chem. A*, 2017, **5**, 1919–1924.
- 45 S. Kalia and M. W. Sabaa, *Polysaccharide Based Graft Copolymers*, Springer, Berlin, Heidelberg, GERMANY, 2013.
- 46 R. Geethanjali, A. A. F. Sabirneeza and S. Subhashini, *Indian J. Mater. Sci.*, 2014, **2014**, e356075.
- 47 F. Yang, G. Li, Y.-G. He, F.-X. Ren and G. Wang, *Carbohydr. Polym.*, 2009, **78**, 95–99.
- 48 C. E. Carraher Jr., *Carraher's Polymer Chemistry, Ninth Edition*, CRC Press, Boca Roca, UNITED STATES, 2013.
- 49 W. Wang and A. Wang, *Carbohydr. Polym.*, 2010, **80**, 1028–1036.
- 50 G. S. Chauhan, A. Kumari and R. Sharma, *J. Appl. Polym. Sci.*, 2007, **106**, 2158–2168.
- 51 P. Zhu, M. Hu, Y. Deng and C. Wang, *Adv. Eng. Mater.*, 2016, **18**, 1799–1807.
- 52 K. P. Chandrika, A. Singh, A. Rathore and A. Kumar, *Carbohydr. Polym.*, 2016, **149**, 175–185.
- 53 P. Lanthong, R. Nuisin and S. Kiatkamjornwong, *Carbohydr. Polym.*, 2006, **66**, 229–245.
- 54 D. R. Biswal and R. P. Singh, *Carbohydr. Polym.*, 2004, **57**, 379–387.
- 55 R. O. Muñoz-García, M. E. Hernández, G. G. Ortiz, V. V. A. Fernández, M. R. Arellano, J. C. Sánchez-Díaz, R. O. Muñoz-García, M. E. Hernández, G. G. Ortiz, V. V. A. Fernández, M. R. Arellano and J. C. Sánchez-Díaz, *Quím. Nova*, 2015, **38**, 1031–1036.
- 56 H. Jia, Z. Huang, Z. Fei, P. J. Dyson, Z. Zheng and X. Wang, *ACS Appl. Mater. Interfaces*, 2016, **8**, 31339–31347.
- 57 H. Mittal, R. Jindal, B. S. Kaith, A. Maity and S. S. Ray, *Carbohydr. Polym.*, 2014, **114**, 321–329.
- 58 T. Tripathy and R. P. Singh, *J. Appl. Polym. Sci.*, 2001, **81**, 3296–3308.
- 59 J.-Y. Sun, X. Zhao, W. R. K. Illeperuma, O. Chaudhuri, K. H. Oh, D. J. Mooney, J. J. Vlassak and Z. Suo, *Nature*, 2012, **489**, 133–136.
- 60 A. S. Aricò, P. Bruce, B. Scrosati, J.-M. Tarascon and W. van Schalkwijk, *Nat. Mater.*, 2005, **4**, 366.
- 61 D. Mazouzi, B. Lestriez, L. Roué and D. Guyomard, *Electrochem. Solid-State Lett.*, 2009, **12**, A215–A218.
- 62 Z. Abdollahi and V. G. Gomes, in *Chemeca 2011: Engineering a Better World: Sydney Hilton Hotel, NSW, Australia, 18-21 September 2011*, 2011, p. 2291.
- 63 C. H. Yang, M. X. Wang, H. Haider, J. H. Yang, J.-Y. Sun, Y. M. Chen, J. Zhou and Z. Suo, *ACS Appl. Mater. Interfaces*, 2013, **5**, 10418–10422.
- 64 B. Gendensuren and E.-S. Oh, *J. Power Sources*, 2018, **384**, 379–386.
- 65 J. Shen, H. Wang, Y. Zhou, N. Ye, G. Li and L. Wang, *RSC Adv.*, 2012, **2**, 9173–9178.
- 66 S. Yang, X. Zhou, J. Zhang and Z. Liu, *J. Mater. Chem.*, 2010, **20**, 8086–8091.
- 67 J.-H. Jeong, D. Jung, E. W. Shin and E.-S. Oh, *J. Alloys Compd.*, 2014, **604**, 226–232.
- 68 M. Sun, H. Zhong, S. Jiao, H. Shao and L. Zhang, *Electrochimica Acta*, 2014, **127**, 239–244.
- 69 N. Takami, A. Satoh, M. Hara and T. Ohsaki, *J. Electrochem. Soc.*, 1995, **142**, 371–379.
- 70 C. Lin, X. Fan, Y. Xin, F. Cheng, M. O. Lai, H. Zhou and L. Lu, *J. Mater. Chem. A*, 2014, **2**, 9982–9993.
- 71 B. Koo, H. Kim, Y. Cho, K. T. Lee, N.-S. Choi and J. Cho, *Angew. Chem. Int. Ed Engl.*, 2012, **51**, 8762–8767.
- 72 S. S. Zhang, K. Xu and T. R. Jow, *J. Power Sources*, 2004, **138**, 226–231.
- 73 R. Tripathi and B. Mishra, *AAPS PharmSciTech*, 2012, **13**, 1091–1102.
- 74 J. Li, L. Zhang, J. Gu, Y. Sun and X. Ji, *RSC Adv.*, 2015, **5**, 19859–19864.
- 75 J. N. Hiremath and V. B., *ResearchGate*, 2012, **4**, 946–955.
- 76 L. Zhang, L. Zhang, L. Chai, P. Xue, W. Hao and H. Zheng, *J. Mater. Chem. A*, 2014, **2**, 19036–19045.
- 77 S. Saber-Samandari, M. Gazi and E. Yilmaz, *Polym. Bull.*, 2011, **68**, 1623–1639.
- 78 L. Luo, Y. Xu, H. Zhang, X. Han, H. Dong, X. Xu, C. Chen, Y. Zhang and J. Lin, *ACS Appl. Mater. Interfaces*, 2016, **8**, 8154–8161.
- 79 L. Gong, M. H. T. Nguyen and E.-S. Oh, *Electrochem. Commun.*, 2013, **29**, 45–47.
- 80 M. H. T. Nguyen and E.-S. Oh, *J. Electroanal. Chem.*, 2015, **739**, 111–114.
- 81 B.-R. Lee, S.-j. Kim and E.-S. Oh, *J. Electrochem. Soc.*, 2014, **161**, A2128–A2132.
- 82 S.-W. Han, D.-W. Jung, J.-H. Jeong and E.-S. Oh, *Chem. Eng. J.*, 2014, **254**, 597–604.
- 83 S. Choi, T. Kwon, A. Coskun and J. W. Choi, *Science*, 2017, **357**, 279–283.
- 84 J. S. Kim, W. Choi, K. Y. Cho, D. Byun, J. Lim and J. K. Lee, *J. Power Sources*, 2013, **244**, 521–526.
- 85 J. Kim, M. K. Chung, B. H. Ka, J. H. Ku, S. Park, J. Ryu and S. M. Oh, *J. Electrochem. Soc.*, 2010, **157**, A412–A417.
- 86 Y.-K. Sun, S.-T. Myung, B.-C. Park, J. Prakash, I. Belharouak and K. Amine, *Nat. Mater.*, 2009, **8**, 320–324.
- 87 M. Nie, D. P. Abraham, Y. Chen, A. Bose and B. L. Lucht, *J. Phys. Chem. C*, 2013, **117**, 13403–13412.
- 88 Q. Chen, L. Zhu, H. Chen, H. Yan, L. Huang, J. Yang and J. Zheng, *Adv. Funct. Mater.*, 2015, **25**, 1598–1607.
- 89 Z. Gong, F. Niu, G. Zhang, J. Li, G. Li, W. Huang, H. Deng, R. Sun and C. Wong, *J. Polym. Res.*, 2017, **24**, 127.
- 90 D. Mazouzi, Z. Karkar, C. Reale Hernandez, P. Jimenez Manero, D. Guyomard, L. Roué and B. Lestriez, *J. Power Sources*, 2015, **280**, 533–549.
- 91 S.-W. Han, S.-J. Kim and E.-S. Oh, *J. Electrochem. Soc.*, 2014, **161**, A587–A592.

- 92 X. Zhu, F. Zhang, L. Zhang, L. Zhang, Y. Song, T. Jiang, S. Sayed, C. Lu, X. Wang, J. Sun and Z. Liu, *Adv. Funct. Mater.*, 2018, **28**, 1705015.
- 93 C. Chen, S. H. Lee, M. Cho, J. Kim and Y. Lee, *ACS Appl. Mater. Interfaces*, 2016, **8**, 2658–2665.
- 94 X. Zhao, C.-H. Yim, N. Du and Y. Abu-Lebdeh, *J. Electrochem. Soc.*, 2018, **165**, A1110–A1121.
- 95 X. Duan, Y. Han, Y. Li and Y. Chen, *RSC Adv.*, 2014, **4**, 60995–61000.
- 96 Y. Bie, J. Yang, Y. Nuli and J. Wang, *RSC Adv.*, 2016, **6**, 97084–97088.
- 97 M. Ling, Y. Xu, H. Zhao, X. Gu, J. Qiu, S. Li, M. Wu, X. Song, C. Yan, G. Liu and S. Zhang, *Nano Energy*, 2015, **12**, 178–185.
- 98 M. Murase, N. Yabuuchi, Z.-J. Han, J.-Y. Son, Y.-T. Cui, H. Oji and S. Komaba, *ChemSusChem*, **5**, 2307–2311.
- 99 J. Liu, Q. Zhang, T. Zhang, J.-T. Li, L. Huang and S.-G. Sun, *Adv. Funct. Mater.*, 2015, **25**, 3599–3605.
- 100 D.-E. Yoon, C. Hwang, N.-R. Kang, U. Lee, D. Ahn, J.-Y. Kim and H.-K. Song, *ACS Appl. Mater. Interfaces*, 2016, **8**, 4042–4047.
- 101 G. S. Chauhan, A. Kumari and R. Sharma, *J. Appl. Polym. Sci.*, 2007, **106**, 2158–2168.
- 102 M. A. da Silva, A. C. K. Bierhalz and T. G. Kieckbusch, *Carbohydr. Polym.*, 2009, **77**, 736–742.
- 103 Y. Fang, S. Al-Assaf, G. O. Phillips, K. Nishinari, T. Funami and P. A. Williams, *Carbohydr. Polym.*, 2008, **72**, 334–341.
- 104 J. F. A. S. Maior, A. V. Reis, E. C. Muniz and O. A. Cavalcanti, *Int. J. Pharm.*, 2008, **355**, 184–194.
- 105 X. Guo, H. Duan, C. Wang and X. Huang, *J. Agric. Food Chem.*, 2014, **62**, 6354–6361.
- 106 L. Zhang, L. Zhang, L. Chai, P. Xue, W. Hao and H. Zheng, *J. Mater. Chem. A*, 2014, **2**, 19036–19045.
- 107 J. Liu, Q. Zhang, Z.-Y. Wu, J.-H. Wu, J.-T. Li, L. Huang and S.-G. Sun, *Chem. Commun.*, 2014, **50**, 6386–6389.
- 108 N. S. Hochgatterer, M. R. Schweiger, S. Koller, P. R. Raimann, T. Wöhrle, C. Wurm and M. Winter, *Electrochem. Solid-State Lett.*, 2008, **11**, A76–A80.
- 109 M. H. T. Nguyen and E.-S. Oh, *Electrochem. Commun.*, 2013, **35**, 45–48.
- 110 X. Zhu, F. Zhang, L. Zhang, L. Zhang, Y. Song, T. Jiang, S. Sayed, C. Lu, X. Wang, J. Sun and Z. Liu, *Adv. Funct. Mater.*, 2018, **28**, 1705015.
- 111 M. N. Obrovac and V. L. Chevrier, *Chem. Rev.*, 2014, **114**, 11444–11502.
- 112 W.-J. Zhang, *J. Power Sources*, 2011, **196**, 13–24.
- 113 L. Y. Beaulieu, K. W. Eberman, R. L. Turner, L. J. Krause and J. R. Dahn, *Electrochem. Solid-State Lett.*, 2001, **4**, A137–A140.
- 114 J. M. Tarascon and M. Armand, *Nature*, 2001, **414**, 359–67.
- 115 M. T. McDowell, S. W. Lee, W. D. Nix and Y. Cui, *Adv. Mater.*, 2013, **25**, 4966–4985.
- 116 S. D. Beattie, D. Larcher, M. Morcrette, B. Simon and J.-M. Tarascon, *J. Electrochem. Soc.*, 2008, **155**, A158–A163.
- 117 X. H. Liu, L. Zhong, S. Huang, S. X. Mao, T. Zhu and J. Y. Huang, *ACS Nano*, 2012, **6**, 1522–1531.
- 118 Z. Chen, L. Christensen and J. R. Dahn, *J. Electrochem. Soc.*, 2003, **150**, A1073–A1078.
- 119 Z. Chen, L. Christensen and J. R. Dahn, *Electrochem. Commun.*, 2003, **5**, 919–923.
- 120 Z. Chen, V. Chevrier, L. Christensen and J. R. Dahn, *Electrochem. Solid-State Lett.*, 2004, **7**, A310–A314.
- 121 Z. Chen, L. Christensen and J. R. Dahn, *J. Appl. Polym. Sci.*, 2003, **90**, 1891–1899.
- 122 Z. Chen, L. Christensen and J. R. Dahn, *J. Appl. Polym. Sci.*, 2004, **91**, 2958–2965.
- 123 Z. Chen, L. Christensen and J. R. Dahn, *J. Appl. Polym. Sci.*, 2004, **91**, 2949–2957.
- 124 J. Lopez, Z. Chen, C. Wang, S. C. Andrews, Y. Cui and Z. Bao, *ACS Appl. Mater. Interfaces*, 2016, **8**, 2318–2324.
- 125 C. Wang, H. Wu, Z. Chen, M. T. McDowell, Y. Cui and Z. Bao, *Nat. Chem.*, 2013, **5**, 1042–1048.
- 126 Z. Chen, C. Wang, J. Lopez, Z. Lu, Y. Cui and Z. Bao, *Adv. Energy Mater.*, 2015, **5**, 1401826.
- 127 D. Bresser, D. Buchholz, A. Moretti, A. Varzi and S. Passerini, *Energy Environ. Sci.*, 2018, **11**, 3096–3127.
- 128 P.-F. Cao, M. Naguib, Z. Du, E. Stacy, B. Li, T. Hong, K. Xing, D. N. Voylov, J. Li, D. L. Wood, A. P. Sokolov, J. Nanda and T. Saito, *ACS Appl. Mater. Interfaces*, 2018, **10**, 3470–3478.
- 129 L. Chai, Q. Qu, L. Zhang, M. Shen, L. Zhang and H. Zheng, *Electrochimica Acta*, 2013, **105**, 378–383.
- 130 L. Wei, C. Chen, Z. Hou and H. Wei, *Sci. Rep.*, DOI:10.1038/srep19583.
- 131 D. V. Carvalho, N. Loeffler, M. Hekmatfar, A. Moretti, G.-T. Kim and S. Passerini, *Electrochimica Acta*, 2018, **265**, 89–97.
- 132 V. L. Finkenstadt, *Appl. Microbiol. Biotechnol.*, 2005, **67**, 735–745.
- 133 L. Lü, H. Lou, Y. Xiao, G. Zhang, C. Wang and Y. Deng, *RSC Adv.*, 2018, **8**, 4604–4609.
- 134 W. Zeng, L. Wang, X. Peng, T. Liu, Y. Jiang, F. Qin, L. Hu, P. K. Chu, K. Huo and Y. Zhou, *Adv. Energy Mater.*, 2018, **8**, 1702314.
- 135 M. Ling, J. Qiu, S. Li, C. Yan, M. J. Kiefel, G. Liu and S. Zhang, *Nano Lett.*, 2015, **15**, 4440–4447.
- 136 D. Lee, H. Park, A. Goliaszewski, Y. Byeun, T. Song and U. Paik, *Ind. Eng. Chem. Res.*, 2019, **58**, 8123–8130.

- 137 C.-H. Tsao, C.-H. Hsu and P.-L. Kuo, *Electrochimica Acta*, 2016, **196**, 41–47.
- 138 L. Wei and Z. Hou, *J. Mater. Chem. A*, 2017, **5**, 22156–22162.
- 139 R. Zhou, W. Liu, Y. W. Leong, J. Xu and X. Lu, *ACS Appl. Mater. Interfaces*, 2015, **7**, 16548–16557.
- 140 Y. Liu, Z. Cai, L. Tan and L. Li, *Energy Environ. Sci.*, 2012, **5**, 9007–9013.
- 141 M. Cheng, L. Li, Y. Chen, X. Guo and B. Zhong, *RSC Adv.*, 2016, **6**, 77937–77943.
- 142 Z. Wei, L. Xue, F. Nie, J. Sheng, Q. Shi and X. Zhao, *J. Power Sources*, 2014, **256**, 28–31.
- 143 M. Cheng, Y. Liu, X. Guo, Z. Wu, Y. Chen, J. Li, L. Li and B. Zhong, *Ionics*, 2017, **23**, 2251–2258.
- 144 D. Qin, L. Xue, B. Du, J. Wang, F. Nie and L. Wen, *J. Mater. Chem. A*, 2015, **3**, 10928–10934.
- 145 R. Rohan, Y. Sun, W. Cai, Y. Zhang, K. Pareek, G. Xu and H. Cheng, *Solid State Ion.*, 2014, **268**, 294–299.
- 146 F. Wang, M. Hickner, Y. S. Kim, T. A. Zawodzinski and J. E. McGrath, *J. Membr. Sci.*, 2002, **197**, 231–242.
- 147 C. K. Shin, G. Maier and G. G. Scherer, *J. Membr. Sci.*, 2004, **245**, 163–173.
- 148 S. Liu and T. Chen, *Polymer*, 2001, **42**, 3293–3296.
- 149 B. Hird and A. Eisenberg, *Macromolecules*, 1992, **25**, 6466–6474.
- 150 S. Chauque, F. Y. Oliva, O. R. Cámara and R. M. Torresi, *J. Solid State Electrochem.*, 2018, **22**, 3589–3596.
- 151 J. Pang, H. Zhang, X. Li, D. Ren and Z. Jiang, *Macromol. Rapid Commun.*, 2007, **28**, 2332–2338.
- 152 S. Park, T. Kim and S. M. Oh, *Electrochem. Solid-State Lett.*, 2007, **10**, A142–A145.

List of Publication or Curriculum Vitae

Scientific publications from result in this thesis:

- B Gendensuren, ES Oh, Dual-crosslinked network binder of alginate with polyacrylamide for silicon/graphite anodes of lithium ion battery, Journal of Power Sources 384, 379-386
- B Gendensuren, H Chengxiang, and ES Oh, Preparation pectin based dual-crosslinked network as a newly candidate binder for a high potential Si/C anode in LIBs, Korean Journal of Chemical Engineering, KJCE-D-19-01206R1, (Accepted)
- B Gendensuren, H Chengxiang, and ES Oh, Modification of sodium carboxymethyl cellulose as novel adhesive water-based binder for lithium ion batteries, xxxxxxxx,xx-xx (Publish soon)

Other publication publications:

- S Lee, B Gendensuren, B Kim, S Jeon, YH Cho, T Kim, ES Oh, Effect of emulsified polymer binders on the performance of activated carbon electrochemical double-layer capacitors, Korean Journal of Chemical Engineering 36 (11), 1940-194
- Andrea Miranda,^a Kasturi Sarangb, Bolormaa Gendensurenc, Xiaoyi Lid, Yilin Lid, Eun-Suok Oh,^{*c} Jodie Lutkenhaus,^{*,b} and Rafael Verduzco^{*}, Molecular design principles for polymeric binders in silicon anodes, review (publish soon)
- H Chengxiang, B Gendensuren, and ES Oh, Ionic conductivity and high adhesive polysaccharide binder for lithium ion batteries, xxxxxxxx,xx-xx (Publish soon)

Contribution to conference

Oral Presentations:

- Bolormaa Gendensuren, He Chengxiang and Eun-Souk Oh, Effect of Alginate-polyacrylamide hybrid gel binder on Graphite and Silicon/Graphite anodes of lithium ion battery, 2016 The 11th IFOST (International Forum on Strategic Technology), Novosibirsk, Russia.

Poster Presentations:

- Effects of aniline tetramer-co-acrylic monomer grafted with polysaccharide backbone as a conductive and adhesive binder for high capacity Si/C composite anode in lithium-ion battery, Bolormaa Gendensuren, Chengxiang He, Yanchunxiao Qi, Eun-Suok Oh, 2019, 한국전지학회 2019 _ The Korean Battery Society.
- B Gendensuren, J Kim, ES Oh, Dual-Crosslinked Polyacrylamide Binders with Various Polysaccharides and Their Application to High Capacity Anodes, ECS, Meeting Abstracts-2019, 208-208, Texas, USA.
- Bolormaa Gendensuren, Chengxiang He, Kim Jin Yeong, Yanchunxiao, and Eun-Suok Oh, Modification of Alginate polysaccharide and its application to binder materials for Lithium ion battery anodes, 한국화학공학회 2019.

- Bolormaa Gendensuren , Chengxiang He, Seongdong Seo and Eun-Suok Oh, Crosslinked Poly(acrylamide-co-acrylonitrile) as an efficient binder for Silicon/Graphite anodes of Lithium ion batteries, Recent Progress in Graphene & 2D Materials Research 2017 (RPGR2017_SINGAPORE).
- Bolormaa Gendensuren, Chengxiang He, Seongdong Seo and Eun-Suok Oh, Poly(acrylamide-co-acrylonitrile) grafted Pectin as an efficient binder for Silicon/Graphite anodes of Lithium ion batteries, 2017 The 12th IFOST (International Forum on Strategic Technology).
- Bolormaa Gendensuren, and Eun-Suok Oh, Ionic conductive efficient binder based on poly(acrylamide-co-acrylonitrile) for Silicon/Graphite anodes of Lithium ion batteries, 한국전지학회 2017 추계 학술 대회_ The Korean Battery Society.
- Bolormaa Gendensuren, and Eun-Suok Oh, Study of Pectin and Acrylamide based double crosslinked network binder for Silicon and Graphite electrode of Lithium ion battery, 한국전지학회 2016 추계 학술 대회_ The Korean Battery Society
- BolormaaGendensuren,Kwang-Hyun, Kim and Eun-Suok Oh, Self-healing Hydrogel Polymer for High Capacity Lithium Ion Battery Electrodes, 한국전지학회 2015 추계 학술 대회_ The Korean Battery Society.